The Dissertation Committee for Ashley Purgason

Certifies that this is the approved version of the following Dissertation:

HISTOPATHOLOGICAL AND MOLECULAR CHANGES IN INTESTINAL TISSUE FOLLOWING PROTON EXPOSURE IN VARYING MOUSE MODELS

Committee:

_____
Honglu Wu, Ph.D.   Supervisor

_____
Sherif Abdel-Rahman, Ph.D.

_____
Robert Ullrich, Ph.D.

_____
Yongjia Yu, Ph.D.

_____
Stanley Hamilton, M.D.

_____
Dean, Graduate School of Biomedical Sciences

HISTOPATHOLOGICAL AND MOLECULAR CHANGES IN INTESTINAL TISSUE FOLLOWING PROTON EXPOSURE IN VARYING MOUSE MODELS

by

Ashley Michele Purgason, B.S., M.S.

Dissertation

Presented to the Faculty of the Graduate School of

The University of Texas Medical Branch

in Partial Fulfillment

of the Requirements

for the Degree of

Doctor of Philosophy

The University of Texas Medical Branch

July, 2013

Dedication

This dissertation is dedicated in memoriam to my younger brother, Michael, who was my dearest friend and now serves as my biggest inspiration. He treated everyone with kindness, saw the best sides of us all and believed we all have the ability to achieve greatness, both in our humanity and in our work. I will always try to carry his optimism and generosity with me in scientific endeavors, in my future work as an educator and, most importantly, in all my interactions with my fellow human beings. Thank you for being you, Michael.

Michael Gilles Purgason
December 28, 1990 – July 13, 2012

"Life is too precious to do anything but pour everything we have into the people we love…"

~ Michael, July 11, 2012

Acknowledgements

HISTOPATHOLOGICAL AND MOLECULAR CHANGES

IN INTESTINAL TISSUE FOLLOWING PROTON

EXPOSURE IN VARYING MOUSE MODELS

Publication No._____

Ashley Michele Purgason, Ph.D.

The University of Texas Medical Branch, 2013

Supervisor: Honglu Wu

Abstract: Most people are aware that radiation can have negative health consequences for human beings exposed to the phenomena. These negative outcomes are dependent upon dose, dose rate, the individual's genetic makeup and other factors. Many people do not know, however, that radiation is present constantly in the background of space, posing significant risks for astronauts traveling beyond the low Earth orbit. Protons, one form of charged particle energy, account for the greatest composition of space radiation. Scientists must better understand the aforementioned risks in order to properly counsel astronauts and health care providers about the possibilities of diseases such as cancer following radiation exposure in space flight. Low dose radiation exposure to gamma rays and protons is a much more common exposure in daily life and for astronauts in flight as opposed to high doses like those used in radiation therapy for cancer treatment. The three strategies proposed here utilize an *in vivo* model, specifically

mice, to better extrapolate awareness of the biological consequences of low dose radiation exposure to the space flight setting and determine at the genetic level how low dose exposures differ in the radiosensitive gastrointestinal tract from high dose exposures. The gastrointestinal tract is important to study with regard to space flight for many reasons including the sensitivity of the small intestine to ionizing radiation, the high frequency of colon cancer development in the Western world, and the fact that the brave men and women who don a space suit are typically middle aged and may harbor pre-cancerous lesions even prior to irradiation. Radiation could exacerbate a cancerous event in a cell. Determining exactly which genes are being up- or down-regulated in responses after varying radiation doses and qualities can establish connections between pathways previously unknown and hopefully elucidate molecular insight into the early disease processes associated with irradiation. The significance of this study is provided in that the knowledge obtained here can be used to better select low dose radiation exposure limits, discover effective counter-measures against the harmful effects of radiation, and potentially even discern novel and favorable uses of radiation for humans.

Table of Contents

List of Tables

List of Figures

xiii

List of Abbreviations

AAALAC	Association for Assessment and Accreditation of Laboratory Animal Care
ACF	Animal Care Facility
ANOVA	analysis of variance
ARS	acute radiation syndrome
BALB/c	Bagg Albino color locus genotype *c/c*
BSA	bovine serum albumin
C	Celsius
CCD	charge-coupled device
CCR	Center for Cancer Research
cDNA	complementary DNA
cGy	centigray
cm	centimeter
CO$_2$	carbon dioxide
Cs	cesium
CTFF	corrected total field fluorescence
C57BL/6	C fifty-seven black six
DAPI	4',6-diamidino-2-phenylindole
DNA	deoxyribonucleic acid
DSB	double strand break
g	gram
GI	gastrointestinal

GSBS	Graduate School of Biomedical Sciences
Gy	gray
H2AX	histone 2AX
HDAC	histone deacetylase
H&E	hematoxylin and eosin
H&L	heavy and light chains
HR	homologous recombination
IACUC	Institutional Animal Care and Use Committee
ID	integrated density
IgG	immunoglobulin G
Inc.	incorporated
IPA	Ingenuity® Pathway Analysis
IR	ionizing radiation
JSC	Johnson Space Center
LD50	lethal dose in 50% of sample size
LI	labeling index
LLU	Loma Linda University
LMP	Laboratory of Molecular Pathology
MDA	The University of Texas M.D. Anderson Cancer Center
MeV	megaelectron volt
MGV	mean gray value
min	minute
n	sample size

NASA	National Aeronautics and Space Administration
NBF	neutral buffered formalin
NCI	National Cancer Institute
ng	nanograms
NHEJ	non-homologous end joining
NIH	National Institutes of Health
nm	nanometer
OCT	optimal cutting temperature
OH	hydroxyl
PBS	phosphate buffered saline
PBST	phosphate buffered saline with Tween-20
PCR	polymerase chain reaction
PKcs	protein kinase catalytic subunit
RBE	relative biological effectiveness
RGB	red-green-blue
RIGS	radiation induced gastrointestinal syndrome
RIN	RNA Integrity Number
RNA	ribonucleic acid
RT	room temperature
s	second
SD	standard deviation
SEM	standard error of the mean
SNP	single nucleotide polymorphism

SP	spacer
SPE	solar particle event
SSB	single strand break
TUNEL	terminal deoxynucleotidyl transferase deoxyuridine triphosphate nick end labeling
μL	microliter
μM	micron or micrometer
UT	The University of Texas
UTA	The University of Texas at Arlington
UTMB	University of Texas Medical Branch
X	times, as in magnification
XRCC4	X-ray repair cross-complementing protein 4
WBI	whole body irradiation

Chapter 1: Introduction and Relevant Background Information

1.1   BACKGROUND AND SIGNIFICANCE

Most people are aware that ionizing radiation (IR) can cause negative health consequences for the human species. Chronic exposure to IR has been proven to cause cataracts in astronauts and could even result in carcinogenesis (Langell et al., 2008a; Chylack et al., 2009; Blakely et al., 2010). Acute exposures to IR for the unique population of men and women that brave space flight have the potential for erythema, nausea, vomiting and other physiological insults which may hinder a mission's success due to underperformance (Townsend, 2005; Wilson et al., 2011). Understanding dose and damage effects of radiation is important not only for the health of astronauts, who are continually exposed to radiation while in flight, but also to members of the public who may experience exposure to radiation either occupationally or accidentally (Langell et al., 2008a). Proton radiation is especially concerning with regard to space flight as protons are the most abundant particles in space and are present in highly unpredictable solar particle events (SPE's) (Langell et al., 2008a). Additionally, astronauts as a group are, on the average, middle-aged and consequently at risk to exacerbate a pre-malignant lesion in their colon, for example, upon exposure to the space radiation environment (Roig et al., 2009). It is also well known that the small intestine displays "extreme sensitivity" to IR providing further evidence to make the gastrointestinal system of particular interest when studying radiation and especially the space flight population (Potten, 1977; Potten, 2002).

The linear no threshold model (LNT) states that radiation, even at extremely low doses, is a health risk for individuals undergoing exposure (Higson, 2005). It is becoming

clear that responses such as hormesis and the phenomenon of radio-adaptation pose a challenge to the LNT theory due to their potential benefits to those exposed to any or high doses of radiation, respectively (Brenner et al., 2003; Brenner and Sachs, 2006). To be clear, the phenomenon of radio-adaptation follows a theory in which effects of low dose exposures provide pre-conditioning to provide radio-resistance upon later, high dose exposures (Calabrese et al., 2008; Calabrese, 2009). Hormesis is a response characterized by an exposure reducing natural, background levels of damage and consequently is displayed as a J-shaped curve (Brenner et al., 2003). These are somewhat different than the LNT model which follows a strictly linear dose-response curve (Calabrese, 2009). In order to evaluate the true risks and possible advantages of low dose irradiation the molecular mechanisms underlying such exposures need to be studied further (Brenner et al., 2003).

IR, particularly gamma and X-rays, has been shown to modify the genes being expressed in fibroblast cells and seems to display asymmetry between low and high doses of exposure (Ding et al., 2005; Zhou et al., 2006). DNA damage, signal transduction, apoptosis, and cell-cell signaling pathways were all altered in expression in response to IR-irradiation (Ding et al., 2005). Work completed by Dr. Honglu Wu's laboratory at the NASA Johnson Space Center using RNAi technology identified a group of genes within the DNA damage signaling pathway that undergoes changed expression following low-dose IR-irradiation (Zhang et al., 2008). In the study these genes were similar to those found to be up-regulated after a high dose exposure lending importance to learning more about low dose irradiation and its effects (Zhang et al., 2008).

Little work has been published in the literature at the time of this writing regarding proton exposures and gene expression in the gastrointestinal system. As a reference, however, it has been shown after an exposure of X- or gamma ray-induced apoptosis that p53 is upregulated in a matter of hours after the dose occurs (Merritt et al., 1994; Merritt et al., 1997; Komarova et al., 2000; Inagaki-Ohara et al., 2001). One study did reveal via immunohistochemistry, too, that p53 was highly expressed in the mouse small intestine when exposed to a high dose of 6.4 Gy of protons or a lower dose of 1 Gy of protons (Finnberg et al., 2008). Other work addressing proton exposures to the brain and subsequent gene expression observations have identified antioxidant enzymes, DNA damage response genes and oxidative stress pathways as key players post-irradiation (Baluchamy et al., 2010b, c). One goal of this dissertation is to identify a greater number of genes affected by low and high dose irradiation of both gamma rays and charged particles with regard to the small intestine. It is hoped that a pathway is elucidated which mechanistically explains some of the damage which is observed after radiation exposures.

Some of the current primary literature states that the mechanisms in place to respond to DNA damage which occurs following even low doses of IR may not be able to repair DNA following complex double strand breaks (DSB) making it an important endpoint to factor into a study like this (Jeggo, 2009). It has been well established that cells towards the bottom of the crypts of the small intestine are a stem cell population which turn over every 24 hours (Potten, 1977; Potten, 2002; Harfouche and Martin, 2010). As cells are followed up the crypts approaching the villi, the cells are crypt

3

progenitors or have already differentiated and are somewhat less sensitive to IR; after all it is typically actively proliferating cells which are more sensitive to IR (Harfouche and Martin, 2010). This is simply due to the physics of energy deposition being more likely to damage DNA when it is in a condensed form and packed tightly together. Highly proliferating cells also have less time to repair DNA that is damaged as they move quickly through the cell cycle (Hall and Giaccia, 2006). The colon, however, is more resistant to apoptosis caused by IR and yet cancer is common in this organ; as some authors have very eloquently pointed out, cellular resistance to IR may actually be linked to an unstable genome and apoptosis may be protective rather than harmful in the long run (Harfouche and Martin, 2010). Colon cancer is a common form of carcinogenesis and charged particle exposures have been shown to cause persistent unrepaired DNA damage marked by foci 24 hours post-irradiation which could lead to genomic instability (Roig et al., 2009). We wish to fill gaps in the literature which do not discuss differences in DNA repair between the small intestine and colon after low AND high doses of radiation exposure. What we are particularly interested in with regard to DNA repair is the potential for the presence of different pathways (non-homologous end joining (NHEJ) vs. homologous recombination (HR)) to be at work in different compartments of each organ. For example, in the highly proliferative crypt a hypothesis is that HR is used in the stem cell compartment while NHEJ is used as the predominant repair mechanism in those cells which are higher and transient. Conversely, in the quiescent stromal parts of the colon you may see less active DNA repair and it may be of the NHEJ type. Epigenetics is also thought to play a strong role in the carcinogenic process. To our knowledge, there has not been a study yet using an *in vivo* model to observe epigenetic endogenous alterations in

the colon, only colon cancer cell lines, following proton exposures making such an experiment of interest in this work (Goetz et al., 2011).

Although many, many studies have been published with results of apoptosis, mitotic changes and morphometric analysis following X- or gamma rays, there has been a sparse amount of research performed for these endpoints following charged particle exposures like that of protons. Treatment of cancer is beginning to utilize proton exposures more and more and this therapy and its results have been characterized in the primary literature (Brada et al., 2009; Merchant, 2009; Schulz-Ertner, 2009; Terasawa et al., 2009; Weber and Kraft, 2009). An advantage of proton therapy is that it can be localized to the tumor or interest; unfortunately, those tissues which are healthy may still receive a substantial dose if they are along the particles' path of trajectory. The Bragg Peak-induction of particle radiation does prevent those tissues past the tumor from receiving any dose and that is beneficial in comparison to gamma rays. There is little published work on total body irradiation with regard to charged particle exposures, however. This is another void in science which this research should work to address in part.

Astronauts traveling on long duration missions will be at risk of exposure to SPE's containing high doses of protons and, consequently, increased risk for negative health effects. Researching high and low dose proton-mediated effects on the radiosensitive GI tract and their underlying molecular mechanisms can potentially reduce the biological threats of these unpredictable exposures by aiding in risk assessment and

providing insight into the complexity of responses to low-dose exposures. Determining which genes are being up- or down-regulated in such responses can be used to demonstrate intricate interactions occurring between pathways. In completing analysis of all of the sacrificial time points it is hoped a set of genes was identified across parts of the GI tract that seem to experience altered expression, especially in the low-dose response. The long-term hope is that, after many future studies by others in this field in addition to this one, eventually the work will impact public health with this knowledge by establishing more appropriate risk assessments, developing countermeasures against the harmful effects of radiation, and even discern ways in which low-dose irradiation may be beneficial.

It is widely accepted that apoptosis is an important mode of death for cells whose integrity has been damaged beyond repair. One such damaging mechanism is that of IR exposure. Radiation-induced apoptosis has been heavily studied and can be defined as death of a cell occurring before the first mitosis post-irradiation and following classical signs of damage like nuclear condensation (pyknosis) and fragmentation (karyorrhexis) (Hendry and West, 1997; Meyn et al., 2009). In highly proliferative organs that are considered to be radio-sensitive, such as the blood forming organs and small intestine, this radiation-induced apoptosis can be dangerous for an organism as the cell population of these organs become largely depleted following acute whole-body radiation exposure. Astronauts on long-term missions beyond the low Earth orbit are at risk from chronic exposure to heavy ions present in galactic cosmic radiation as well as acute exposure to protons from solar particle events (Langell et al., 2008b). Acute whole-body exposure to a high dose of radiation usually results in acute radiation syndrome (ARS) characterized

by symptoms such as nausea, vomiting, and fatigue (Donnelly et al., 2010). If the absorbed radiation dose is high enough the organism can also experience the gastrointestinal (GI) syndrome in which a majority of the mucosal surface area is damaged (Dörr and Meineke, 2011). This condition can be very fatal (Dörr and Meineke, 2011). These physical ailments would no doubt cause potential complications on a mission. Better risk assessment for the health of astronauts generates a need for an understanding of the consequences associated with the space radiation environment which is abundant in high energy protons.

It is important to consider surviving cells in the crypts, the highly proliferative, organizational units of the small intestine, as well as it has been established that only one cell is needed to regenerate the crypt (Schuller et al., 2006). Withers and Elkind established the microcolony survival assay to assess surviving crypts following insults to the intestine in 1970 and it has become a gold standard for intestinal damage studies involving radiation exposures (Withers and Elkind, 1970). The assay provides an assessment which does not account for dose to surrounding tissues making it highly favorable (Schuller et al., 2006). There has been little work assessing microcolony survival following proton exposures, except to determine the RBE of therapeutic proton beams. In such studies mouse models have been used and revealed a range of RBE's from 1.07-1.18 (Mason et al., 2007). A similar result for RBE of protons was found to be approximately 1.1 according to multiple studies looking at endpoints not assessing therapeutic beams (Gerweck and Kozin, 1999; Sorokina et al., 2013). The literature shows that most all of the stem cells of the crypts of Lieberkuhn will be killed after doses of approximately 15 Gy of gamma irradiation and the population can be scarce after

doses lower than this (Hornsey, 1973; Potten, 2004). Death of an organism from the GI syndrome is likely ultimately due to a loss of proper functioning of the intestine (Schuller et al., 2006). The aforementioned death of the stem cells causes a subsequent reduction of the differentiated cells and eventually the villi, which play an important role in nutrient uptake, and this cell loss results in the dysfunction of the intestine (Schuller et al., 2006). Changes in the mucosal surface area are also a measure that should be taken into account when observing intestinal morphology. The small intestine is responsible for 95% of nutrient uptake in the body and a larger, or smaller, surface area of this organ likely results in more, or less, efficient function (Vereecke et al., 2011).

Many different mouse models have been used for radiation studies. BALB/c mice are considered to be radio-sensitive and were chosen as a counter to C57BL/6, which are considered radio-resistant, for this reason (Roderick, 1963; Fabre et al., 2011). Our focus was on the duodenum of the small intestine due to the well-documented radiosensitivity of and apoptosis occurring in the organ after whole-body gamma-irradiation (Potten, 1977). While very few studies of proton-induced apoptosis have been reported, apoptosis induced by X- or gamma rays in the intestines of animals has been investigated in the past 30 years. In an early study of apoptosis in the small intestinal crypt cells of mice following whole-body exposure to X- and gamma rays, Potten reported that the apoptotic lesions peaked between 3-6 hours post-irradiation and the yield of apoptosis was higher than would have been predicted based on a linear dose response relationship (Potten, 1977). Delayed apoptosis that peaked after 24 hours of exposure has also been observed (Merritt et al., 1997; Miyoshi-Imamura et al., 2010). While the delayed apoptosis was suggested to be P53-independent (Merritt et al., 1997), this document is focused on

8

apoptosis detected at both 4 hours post-irradiation and longer time points. Finnberg et al., using that same 4 hour time point and 1 Gy or 6.4 Gy proton exposure, showed a dose-dependent increase in apoptotic cells in the small intestines of ICR mice when observing whole fields of vision under the light microscope (Finnberg et al., 2008).

Cell proliferation following whole-body gamma irradiation to restore crypt cell number has also been studied previously. This is significant as newer cells, even in unirradiated tissues, have to be created to replace the transient cells which move up the villous structures and eventually slough off into the intestinal lumen (Potten, 1991). Replacement of damaged cells following irradiation is likely determined by a relationship between apoptosis, cell proliferation and time and is important to study with regard to crypt and villous function. It was shown following a relatively high dose of 8 Gy of gamma rays that in the mouse small intestine the labeling index (LI), or percentage of cells labeled as being in the S phase of the cell cycle, decreased quite quickly until 15 hours post-exposure (Potten, 1991). Return to control levels of the LI took approximately 3 days after the dose of 8 Gy (Morris, 1996). Cell proliferation in the intestinal crypts did not reach an initial peak until 10-12 hours after irradiation, but did begin as early as 3 hours following the insult (Potten, 1991). Furthermore, an increase in LI beyond control levels multiple days after doses of both 3 and 8 Gy of gamma irradiation has been observed (Morris, 1996). These studies are important to understand with regard to the replacement of apoptotic cells in the small intestine.

In this dissertation, the results of the expression of genes involved in the apoptotic pathways in the small intestine post-irradiation are also reported. P53 is known to play an important role in apoptosis induced by X- or gamma rays that occurs within several hours

post-irradiation (Merritt et al., 1994; Merritt et al., 1997; Komarova et al., 2000; Inagaki-Ohara et al., 2001). Up-regulation of p53 using immunohistochemical analysis has also been observed in the small intestine of mice post proton-irradiation of the small intestine following 1 Gy or 6.4 Gy of proton exposures (Finnberg et al., 2008)

1.2   STUDY OBJECTIVES

1.2.1   Rationale for Study

This research investigated the gastrointestinal (GI) tract after varying acute doses and types of ionizing radiation (IR) exposure following several time points. Work done using animal models in this area of research is particularly sparse.

1.2.2   Overview of Study

The research was conducted using C57BL/6 and BALB/c male mouse models experiencing whole body irradiation (WBI) of varying doses sacrificed at differing time points. The bulk of this work was focused on the small intestine and, more specifically, the duodenum. Endpoints to determine the presence and extent of damage included apoptotic lesions, with further breakdown by regions of crypts, villous morphometry, and stereological assessment. Gene expression alterations of oxidative stress and apoptotic pathways were researched to learn more about the mechanistic process of GI responses following low and high doses of exposure to different qualities of ionizing radiation, gamma rays and protons. Additionally, DNA repair proteins in both the HR and NHEJ

pathways were studied. Finally, a small-scale analysis was performed to observe endogenous histone deacetlyase (HDAC) levels in the colon after proton exposure.

1.2.3 Hypotheses and Associated Aims of Study

In this study, C57BL/6 male mice were exposed to IR, specifically ^{137}Cs gamma rays, and sacrificed 4 hours post-exposure in order to examine the presence or absence of acute morphological effects and changes in gene expression profiles in the gastrointestinal tract as they differ between low and high doses. Controls were mice experiencing sham radiation only.

Hypothesis 1. Animals receiving the high dose would display significantly greater acute morphological effects and differences in gene expression profiles than those receiving the low dose.

Aim 1.1. Acute morphological effects in the crypts and villi of the small intestines of mice receiving low or high doses of IR exposure were confirmed by observing and characterizing apoptotic lesions and morphometric changes.

Aim 1.2. Genes important in the response to IR were identified by studying gene expression profiles of oxidative stress pathways in the small intestines of mice exposed to low or high doses of gamma rays.

In order to differentiate between responses in the GI tract of animals following gamma ray exposure based upon time post-irradiation, groups of mice were next sacrificed 24 hours, 3 days, 7 days or 21 days after receiving the same high or low exposure doses as in experiment 1. Mice were also weighed daily for the longer time points to scrutinize any changes in body weight after irradiation. GI tissues were immediately collected after sacrifice using appropriate methods.

Hypothesis 2. The degree of damaging, acute morphological effects would decrease with increased time intervals between exposure and sacrifice. It was also hypothesized that the tissue environments would be different at each time point for potential gene expression changes. Lastly, mice exposed to higher doses of radiation would weigh less at the time of sacrifice as compared to their low dose counterparts.

Aim 2.1. The presence or absence of acute morphological effects in the crypts and villi of the small intestines of mice receiving low or high doses of ionizing radiation exposure were characterized by observing apoptotic lesions and morphometric changes. Groups were then compared across time points to determine if a greater amount of recovery took place at longer sacrificial time points as compared to the earlier sacrificial time points.

Aim 2.2. Genes important in the response to IR were identified by studying gene expression profiles of oxidative stress pathways in the small intestines of mice exposed to

low or high doses of gamma rays. Groups were compared across time points to determine if there were any differences present in the gene expression profiles present in tissue.

Aim 2.3. Mice were weighed daily after IR dosage for the 7 day and 21 day sacrificial time points to discern any alterations in body weight.

The final experiment was modeled after experiments 1 and 2. However, proton irradiation was substituted in place of ^{137}Cs gamma rays in order to characterize the response of both BALB/c and C57BL/6 gastrointestinal tracts to charged particle exposures. Time points of 4 hours and 24 hours were used for C57BL/6 mice and 4 hours was used for BALB/c mice.

Hypothesis 3. The degree of damaging, acute morphological effects would differ between strains of mice. It was also hypothesized that the tissue environments would be different between doses and strains for DNA repair proteins, potential gene expression changes and epigenetic alterations. Finally, it is hypothesized that damage and molecular profiles will differ between strains of mice and radiation qualities compared between C57BL/6 mice.

Aim 3.1. The presence or absence of acute morphological effects in the crypts and villi of the small intestines of mice receiving low or high doses of proton exposure were characterized by observing apoptotic lesions and morphometric changes. Dosage groups

were compared across strains to determine if differing amounts of damage occurred between strains.

Aim 3.2. Any differences in the types and/or amounts of DNA repair proteins expressed in the crypts and villi of the small intestines and colons of mice receiving low or high doses of proton exposure were characterized by detection of proteins of both the non-homologous end joining (NHEJ) and homologous recombination (HR) repair pathways. Groups were compared across strains and doses to determine if there are any differences present in the types and/or amounts of DNA repair proteins present in tissue.

Aim 3.3. Genes important in the response to IR were identified by studying gene expression profiles of oxidative stress and apoptotic pathways in the small intestines of mice exposed to low or high doses of protons. Groups were compared across strains and radiation qualities to determine if there were any differences present in the gene expression profiles present in tissue.

Aim 3.4. The colons of C57BL/6 mice exposed to low or high doses of proton exposure were investigated with regard to epigenetic changes, specifically changes in histone deacetylase enzyme activity. Groups were compared across time points and doses to observe if there were any differences present in the epigenetic status of the tissue.

In summary, it was hypothesized that low dose exposure groups will show a reduction in negative outcomes as compared to their high dose counterparts and that each

will show a different gene profile from the other, especially with differing sacrificial time points. Additionally, it was also hypothesized that low and high dose charged particle exposures and varying mouse strains will mediate diverging responses in the GI tract.

Chapter 2: Materials and Methods

2.1   FACILITIES

The experiments conducted for this work were completed at the National

Aeronautics and Space Administration (NASA) Johnson Space Center (JSC) in Houston,

Texas unless stated otherwise elsewhere in this document. The Core Laboratories and

Facilities as well as the Radiation Biophysics Laboratories at NASA-JSC provided bench

space, materials, instrumentation, chemicals, storage and consultation upon request for

the execution of experimental studies. The Animal Care Facility (ACF) at NASA-JSC

was used to receive, house and sacrifice mice and harvest tissue during each study unless

stated otherwise. The ACF at JSC is fully accredited by the Association for Assessment

and Accreditation of Laboratory Animal Care (AAALAC) and provides a full-time

employee serving as a facility manager. The facility manager functioned to maintain the

animals' quarters, to preserve the animals' health through daily observation and

intervention if necessary and to advocate for the animals' well-being through assurance

that scientists adhered to the utmost standards of care when conducting experimentation.

The ACF also has a consulting veterinarian who assisted with questions on the animals'

behavior and health when necessary. An irradiator on-site at NASA-JSC was used to

expose animals to radiation for each major study unless stated otherwise. For security

purposes, exact specifications and other details of the irradiator will not be provided.

2.2   ANIMAL MODELS

2.2.1   Selection and Ethical Standards

The results presented in this document are all from *in vivo* work. Not every experiment described in this chapter was done on every group of mice obtained. Depending on funding, time and adaptability of the project based upon results, assays were prioritized by dose and time point. Mouse strain, time points and doses are pointed out in specific mentions of work. All animal work was approved by the NASA-JSC Institutional Animal Care and Use Committee (IACUC) before the animals were ordered (IACUC #09-01). In addition, for animal studies involving proton exposures (2.2.3.2), studies were approved by the Loma Linda University (LLU) IACUC in Loma Linda, California (IACUC #8110044). Each person who handled the animals received proper training and certification to do so before studies began. My own certificates were obtained from The University of Texas Medical Branch (UTMB) and The University of Texas Health Science Center at Houston (UT Health). The animal models used in these studies were of the order Rodentia (rodents), the family Muridae and the subfamily Murinae. More specifically we chose to use *Mus musculus*, the common mouse. (rodents common, mouse common in rad) It is more appropriate to refer to the specific strains of laboratory mouse models chosen as they are typically thought to have originally been bred from two different subspecies, *Mus musculus musculus* and *Mus musculus domesticus*. Two strains of mice were utilized in our studies: BALB/c and C57BL/6. The two strains differ genetically as well as phenotypically. BALB/c mice resemble the common idea of a research mouse model to the lay person as they are albino, giving them white fur and red eyes (Figure 1a). This is a slight misconception, however, as the

17

Figure 1:	Example photographs of the two strains of mice used in this study. Notice the phenotypic differences between a) BALB/c and b) C57BL/6. Photographs were provided by the creative director at Charles River Laboratories, Inc. where mice were purchased and are used with permission.

C57BL/6 strain, which has very dark brown or black fur and dark eyes, is actually the

most commonly cited species and strain of laboratory animal when performing literature

searches on most scientific databases (Figure 1b). The photographs shown in Figure 1

were provided by the creative director at Charles River Laboratories, Inc. and are used with permission. Again, BALB/c mice have been shown to be radio-sensitive when compared to C57BL/6, generally deemed radio-resistant, when observing many different biological endpoints (Ponnaiya et al., 1997; Rodgers et al., 2001; Hamasaki et al., 2007). It was determined that this is due to two single nucleotide polymorphisms (SNPs) in BALB/c mice which encode a gene responsible for DNA-dependent protein kinase catalytic subunits (DNA-PKcs) involved in DNA repair processes (Fabre et al., 2011). This makes the BALB/c strain naturally deficient in NHEJ (Fabre et al., 2011). Due to the use of male mice in the studies published in the literature concerning proton exposure and time points we wished to model, male mice were also employed in this work (Ito et al., 2007; Finnberg et al., 2008; Finnberg et al., 2013). The efforts published here were primarily done in the interest of assessing risk for those persons traveling to space beyond the low Earth orbit. Astronauts are mostly middle-aged and considered healthy on the average and so it was appropriate that we chose adult, 6-8 weeks old, mice of normal body weight (approximately 20-25 g) for our work.

2.2.1.1 Power Analysis

In order to determine the proper sample size for our animal studies, a power analysis was conducted based on short-term end points (< 1 month) resulting from a small pilot study we conducted using only 12 mice in total. In observing percent viability of bone marrow cells in C57BL/6 mice irradiated and sacrificed 3 days later, the standard deviation within groups was 4.0%. It was determined that with statistical assumptions being satisfied, a power of 97% could be achieved with n=6 per group. This would allow

for the rejection of the null hypothesis that no difference between means exists when using a student's t-test when there is a real difference of 10%. For this dissertation, n=6 in experimental results unless stated otherwise in this document.

2.2.2 Animal Care

Mice were ordered, purchased and shipped from Charles River Laboratories International, Incorporated (Inc.) (Wilmington, MA) to the NASA-JSC ACF (Houston, TX). For the studies involving proton exposures, animals were ordered from Harlan Laboratories (Placentia, CA) and shipped to and housed in the fully AAALAC accredited LLU vivarium (Loma Linda, CA). Similar to the above mentioned staff for NASA-JSC, animals were properly cared for by full-time employees at the LLU vivarium. At both animal facilities, mice were housed 6 to a cage and given standard laboratory chow and water *ad libitum*. The vivariums were kept on 12 hour light and dark cycles. Mice were given at least one full week in their new setting to acclimate before any handling or experimentation occurred. Animals were observed daily for signs of distress, discomfort and pain using a chart provided by the NASA-JSC ACF (Figure 2). For post-irradiation time points (see 2.2.4) studied that exceeded three days, mice were weighed individually every day using an electronic scale. The veterinarian recommended placing a single, moistened food pellet on the floor of the cage in a small petri dish to counteract fatigue and weight loss that is common in mice post-irradiation. In following best practices, we did as the veterinarian ordered and did this for all the animals whose sacrificial time point post-irradiation exceeded 24 hours. For the sacrificial time points post-irradiation which

20

exceeded 3 days, animals were housed 1 to a cage following irradiation at the

veterinarian's request so that they might receive better rest to recover.

| Date: | Protocol #: | | | Cage ID# |
| Time: | Date of exposure: | | | |

SIGNS OF PAIN, DISTRESS AND DISCOMFORT IN RODENTS

APPEARANCE:					
Coat	loss of sheen		**Digestive**	altered feces	
	loss of hair			diarrhea	
	starey coat			blood	
	failure to groom			mucus	
	soiled perineum			color	
				consistency	
Discharge	ocular			volume	
	nasal				
	urogenital		**Cardiovascular**	cyanosis	
	rectal			extremities cold and blue	
				skin tinting	
Eyes	black around eyes			dark claws and feet	
	sunken eyes				
	glazed eyes			**Musculoskeletal**	
				lameness	
	eyes partly closed			arthritis	
	eyes bulging				
			Nervous	convulsions	
Body	hunched up			twitching	
	backbone prominent			ataxia	
	pinched abdomen				
CLINICAL SIGNS:			BEHAVIORAL:		
	poor growth rate			isolated from cagemates	
				Dormouse posture	
Respiration	rapid			unaware of extraneous activities	
	labored			no response when blown on	
	pneumonia			self mutilation	
	pleurisy			restlessness	
	grunting before expiration or grinding teeth			reluctance to move	
	panting			vocalization, especially when provoked	
	strong pulse			recumbent	
	weak pulse			excessive licking or scratching	
				writhing (abdominal pain)	
FOOD AND WATER INTAKE					
	water intake reduced			no water intake	
	food intake reduced			no food intake	
	reduced feces			no feces	
	reduced urine output			no urine output	

This animal should be referred to the Veterinarian for examination   Yes _____   No _____

Inspecting Veterinarian's signature: _____

Figure 2:   Chart used to monitor animals daily for signs of distress, discomfort and pain. Upon observation of the completed chart, the veterinarian would provide instructions to prevent further complications and death and to mitigate symptoms.

2.2.3 Radiation Exposures

2.2.3.1 Gamma Irradiation

Before radiation exposures, mice were assigned in a random fashion to an experimental or control group. Mice were placed in plastic mouse restrainers and positioned inside the irradiator. The on-site irradiator at NASA JSC provides ^{137}Cs gamma radiation. For low dose exposures of 0.05 gray (Gy), or 5 centigray (cGy), animals were exposed vertically from both the front (top of the mouse) and back (the bottom of the mouse) sides. The dose rate was 0.072 Gy/minute (min) without shielding at the center of the holder. The exposure time was 25 seconds (s) to the front and 25 s to the back and the dose was 0.06 Gy without shielding. The center of the mouse was expected to receive 0.05 Gy.

For high dose exposures of 6 Gy, the same style of plastic restrainers and the same irradiator were used. The dose rate at the center of the holder without shielding was 0.444 Gy/min. The exposure was 425 s on one side and 425 s on the opposite side with a total exposure duration of 850 s. The total dose at the center of the holder without shielding was 6.3 Gy. Taking into account the attenuation in the mouse body, the dose at the center of the mouse was expected to be 6 Gy. Dosimetry was provided by the manufacturer of the irradiator. All irradiated groups regardless of dose received whole body irradiation (WBI).

This work was originally planned to explore the radio-adaptive response, but eventually became more focused on discerning differences between low and high doses of irradiation between mouse strains and qualities. This is important to mention for the experimental set-up of the radiation exposures using gamma rays. Exposure groups received either the low dose of 5 cGy, the high dose of 6 Gy or a combination dose consisting of a 5cGy priming dose with a 6 Gy challenge dose 24 hours later. One sacrificial time point was set up differently and that was the 21 day time point. For this time point, there was no 5 cGy group. Instead there was a 6 Gy group and two combination dose groups. The combination dose groups differed in the time between priming dose and challenge dose. One had the previously used time between doses of 24 hours and the other was 7 days. All sacrifice time points are applicable after the challenge dose in the combination groups.

The group of mice assigned as the control group for every time point studied underwent sham radiation in which the animals were placed in the plastic restrainer the same length of time that irradiated mice were in order to mimic the stress generated from being confined. Therefore, their dose received was 0 Gy. The control groups are referred to in this document as control(s), sham or 0 Gy.

2.2.3.2 Charged Particle Exposures

The work described in this dissertation involves the application of two different types of ionizing radiation, gamma rays and protons. Protons are also sometimes referred to as charged particles. Radiation is not present in doses relevant to the background of

space or radiotherapy in the typical surrounding environments we live in on Earth. Therefore, man-made devices are used to generate radiation fields or beams that replicate in part the space radiation environment or are used in radiotherapy. There are few facilities on Earth which will generate mixed-field radiation of more than one particle type. Although more common than mixed-field beams, proton accelerators are still rare as compared to their gamma radiation source counterparts. In order to achieve the proton exposures necessary to complete this work, a collaboration with LLU scientists was capitalized upon in order to utilize the proton accelerator on-site at that institution since JSC is not home to one. Animals were placed in plastic mouse restrainers and exposed to 250 MeV protons at plateau phase in the late hours of the night and the early hours of the morning when the accelerator was not being used for patient therapy. 250 MeV protons have a residual range of approximately 31 cm in water. Dosimetry was provided by the radiation physicist on-site. Mice received doses of 0 Gy (sham radiation), 0.05 Gy, 0.1 Gy, 2 Gy or 6 Gy at dose rates ranging from 0.46-0.64 Gy/min, with an average dose rate of 0.56 Gy/min. The exposure times varied from 0.25-9.68 min with an average exposure time of 3.52 min. All irradiated groups regardless of dose received whole body irradiation (WBI).

2.2.4   Sacrifice and Tissue Harvesting

Animals were sacrificed at varying time points following irradiation: 4 hours, 24 hours, 3 days, 7 days or 21 days. A plastic chamber was used to expose the animals to carbon dioxide (CO_2) until they were adequately sedated. Afterwards, the mice were

decapitated using a guillotine. Animals experiencing severe weight loss, illness or other conditions recommended for euthanasia by the veterinarian were sacrificed using CO_2 sedation followed by cervical dislocation. The duodenum of the small intestine was excised from the animal. The piece of intestine was flushed with phosphate buffered saline (PBS) to clean and rid the inside of feces. It was then cut into four equal pieces. Two pieces were immediately placed in a cryotube and snap frozen in liquid nitrogen and eventual storage in -80° Celsius (C). Next, the two remaining pieces of tissue were cut open and laid flat so that the interior of the small intestine was facing upward. One piece was placed in a cassette, secure between two small squares of blue foam, which went into a 10% neutral buffered formalin (NBF) solution kept at room temperature (RT). The last piece was placed in optimal cutting temperature (OCT) gel (Sakura Finetek USA, Inc., Torrance, CA) in a small cryomold, frozen on dry ice and stored at -80°C. For the proton-based work, mice were sacrificed and their tissues harvested in a laboratory on-site at LLU. Colon samples were also collected as part of those studies. The colon was fixed in a manner similar to the fixation of the intestinal samples mentioned previously. Tissue samples were packed or stored on dry ice and shipped to NASA-JSC within one to two days of harvesting and subsequently stored at appropriate temperatures (-80°C or RT) until further processing.

2.2.4.1 Tissue Processing

Samples which were snap-frozen in cryotubes and stored in -80°C remained there until experimentation was conducted with them. Tissue which was placed in cassettes in the 10% NBF was subsequently handled and processed 48 hours later by the

Histotechnology Core Laboratories at either UTMB or The University of Texas M.D. Anderson Cancer Center (MDA) (Houston, TX). Briefly, the samples were dehydrated using an automated process which places the tissues in consecutive and ordered ethanol washes and then they were perfused with paraffin wax. The samples were then embedded into metal blocks filled with paraffin and placed permanently back into their original cassette. In order to achieve paraffin sectioning on glass slides, the paraffin blocks were mounted on a microtome chuck and then cut at a setting of 5 microns (μM). Sectioning was put onto glass slides and stored permanently at RT.

The Histotechnology Core Laboratories also stained many of the paraffin sections with hematoxylin and eosin (H&E) for purposes of viewing nuclear matter apart from other cellular and tissue components. Slides were deparaffinzed using a series of xylene washes and then hydrated using multiple grades of ethanol. After rinsing in water, sections were stained with hematoxylin for several minutes and then rinsed again thoroughly in tap water. Differentiation, or removal of excess hematoxylin, was then completed using an extremely short rinse of acid alcohol followed by water once again. The so-called bluing procedure, or conversion of hematoxylin from a red to a blue color, was done using lithium carbonate and a final rinse in water. The eosin counterstain was applied next and the slides were dehydrated afterwards using increasing concentrations of ethanol. Finally, the slides were cleared with xylene in order to keep light diffraction to a minimum and sealed with a coverslip.

Intestinal samples which were placed in OCT gel in cryomolds were mounted on a cryotome chuck on-site at NASA JSC and then cut with the cryotome in 5 μM sections. The optimal temperature for both the cryotome box and the chuck was approximately -23°C. Sections were kept flat using a roll out bar inside the cryotome. The sections were picked up with and placed on glass slides coated in gelatin, which helps keep the sections attached, using a roll-of-the-hand and wrist technique. Slides were then stored at -20°C until further processing.

2.3   MICROSCOPY

2.3.1   Bright Field Microscopy

Bright field microscopy, a form of light microscopy, was used to view and photograph tissue samples stained with H&E. Simple two-dimensional (2D), still images were captured using a video camera attached to the microscope and the Linksys 32 software system (Linkam Scientific Instruments, Surrey, United Kingdom). Images were captured with a range of magnifications depending on the assay being used (see 2.4.1-2.4.3). The magnification provided in this document is the objective magnification multiplied by the eyepiece magnification (10 times (X)).

2.3.2   Fluorescence Microscopy

There are many fluorescence microscopy systems available at NASA JSC. In an attempt to view and analyze paraffin and frozen sections of GI tissues that were immunohistochemically stained using fluorescently tagged antibodies (see 2.5), a Zeiss Axioplan (Zeiss, Oberkochen, Germany) fluorescent microscope was employed which

had electronic image capture capability. A Sensys charge-coupled device (CCD) camera (Photometrics, Ltd., Tucson, AZ) was part of the microscope system and that together with the CytoVision® software (Leica Biosystems, Buffalo Grove, IL) provided the ability to capture 2D images of our immunofluorescence work. The filters on the microscope system allowed viewing and image capture of the wavelengths of emission of our fluorescent antibody tags. Images were captured with a range of magnifications depending on the region of interest in the tissue.

2.4   HISTOPATHOLOGIC ANALYSES

2.4.1   Apoptotic Lesions

After standard H&E staining, tissue was evaluated for any obvious morphologic changes using bright field microscopy. A numeric system was used by a colleague in advance of slide observation in order to provide a blinded analysis. Standard definitions were used to determine which cells were apoptotic: those presenting pyknosis or karyorrhexis (Kerr et al., 1972; Ijiri, 1989; Wyllie, 1997). Pyknosis can be explained as the genetic material of the nucleus appearing to be condensed. Karyorrhexis usually follows making fragments of the nuclear material appear to be broken away from the rest. Condensed and fragmented nuclei were obvious in the lesions identified in this work. These quintessential indications of damage needed to be easily recognized among healthy cells to be included in quantification. Cells which appeared unhealthy but did not clearly display pyknosis or karryorhexis were not included in our analyses. More than 40 crypts selected at random on varying regions of tissue sections were quantified for apoptotic lesions. The details of this assay are published in the literature (Ijiri and Potten, 1983). In

28

brief, the tissue was observed for both the stem cell region of the crypts (cell positions 1-6) and the upper region of the crypts (defined in this work as cell positions 7-20) in order to quantify dying cells. Intact Paneth cells had to be present at the base of a crypt to be considered for quantification. Finally, crypts had to have a minimum of 20 cells between their base and villous junction to be analyzed for apoptosis. Magnifications of both 500X and 1000X were used to complete this work.

Pathologists at MDA confirmed the presence of apoptotic lesions before quantification and sometimes provided short reports grading the severity and extent of apoptosis based upon a small subset of the samples. These confirmations and reports provided scientific assurance that I was appropriately screening and quantifying the tissue sections for apoptotic lesions although I had not been formally trained as a pathologist. Dr. Stanley Hamilton provided confirmation of apoptosis on the samples exposed to protons. Veterinary pathologists in the MDA Histotechnology Core Laboratories provided the above mentioned reports for samples exposed to both gamma rays and protons.

2.4.2   Villous Morphometry

The villi of the small intestine were analyzed for any morphometric changes following irradiation. Specifically, the area of villi were measured and compared. Villi were photographed under the microscope as described above (see 2.3.1) at a magnification of 200X. Later, the images were opened using the freely downloadable software, ImageJ, from the National Institutes of Health (NIH) (Bethesda, MD). A

photograph taken under the microscope of a µM scale at 200X magnification was used in

ImageJ to calibrate pixels to µM and set scale bars onto images. Using the polygonal

drawing tool in the ImageJ program, lines were superimposed onto the photographs as if

the villi were being traced. ImageJ then used each completed polygon to generate an area

calculation of an individually traced villous in units of $µM^2$. An example of a

superimposed image is provided in Figure 3.
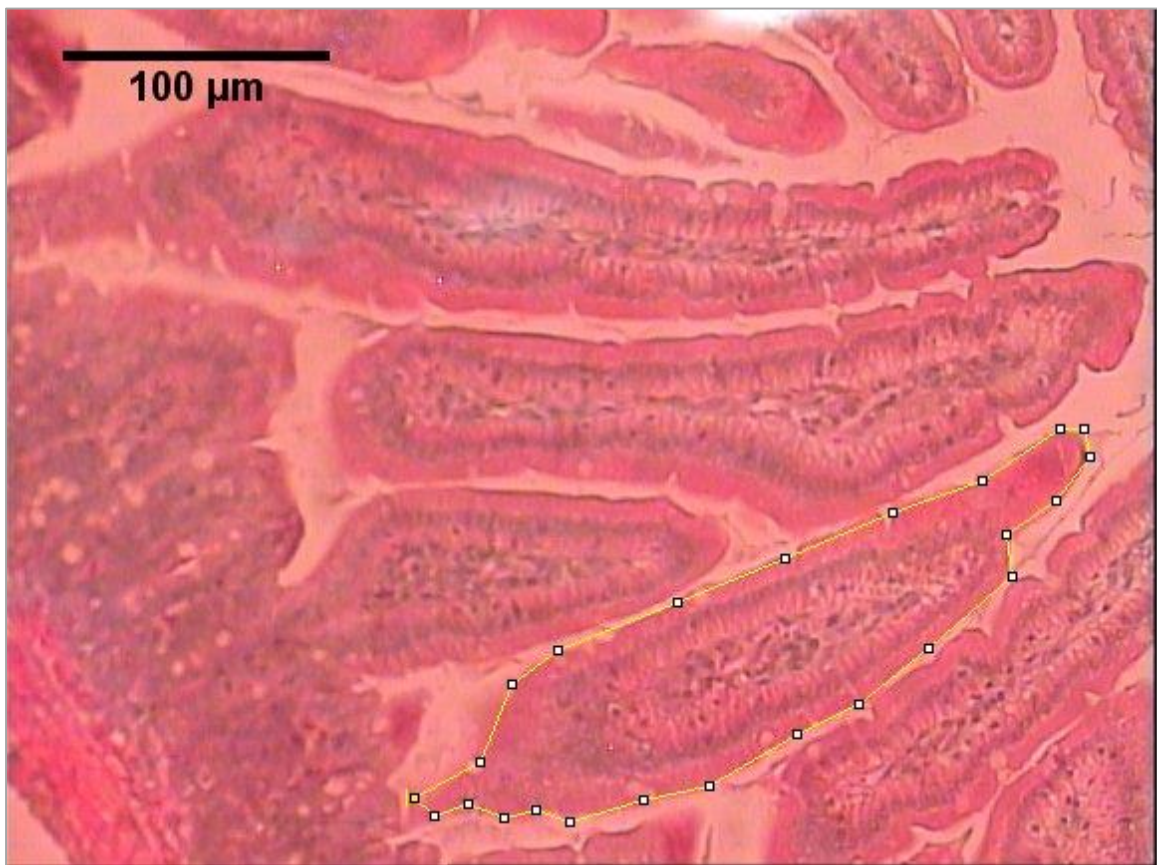
Figure 3:   Example of a photograph opened and analyzed using the NIH's ImageJ
software. The polygonal drawing tool in the program was used to assess the area of
intestinal villi after radiation exposures. The tissue pictured is from a mouse duodenum
and viewed at 200X magnification.

2.4.3 Stereological Assessment

An assay to look at and quantify mucosal surface was completed only for the BALB/c mice exposed to protons. This work was done at the request of an editor following the submission of a manuscript. It is included in this dissertation to point out another endpoint of significant damage in the small intestine following radiation exposure in mice.

Using H&E-stained slides containing both transverse (5X magnification) and longitudinally (10X magnification) cut sections of small intestine, images were captured of tissue and opened using ImageJ. Briefly, the first step is to estimate the volume of each intestinal segment. The methodology begins with a uniform grid of points overlaid onto an image of a transversely cut intestine displaying the entire circumference (Figure 4a). Each point on the grid is representative of the center of a fixed, square area. That area's value is provided to the user by the software. The points "touching" the intestinal tissue were quantified and the total area was determined by multiplying that number of points by the area around one point. The volume was calculated for each animal by summing the areas of each section collected (n=2 per animal) and then multiplying that sum by the distance between collected sections (approximately 3 mm).

The next step involves surface area estimation and utilizes longitudinally cut sections of the intestine. The long sections of intestinal tissue were photographed and a cycloidal grid of arcs was overlaid onto the images (Figure 4b). The places at which the grid intersects with the surface, and the surface only, were quantified (Figure 4b, black dots). Then, the points where the grid intersects with any other parts of the tissue were also quantified (Figure 4b, grey dots). A ratio of surface interactions to tissue interactions was calculated and this value represented the surface density. Finally, the surface density was multiplied by the previously calculated intestinal volume to obtain the surface area estimation (Casteleyn et al., 2007; Casteleyn et al., 2010).

2.5   IMMUNOHISTOCHEMICAL STUDIES

2.5.1   ApopTag® Red *In Situ* Apoptosis Detection Kit

The ApopTag® Red *In Situ* Apoptosis Detection Kit (Chemicon/Millipore International, Billerica, MA) was used to immunohistochemically stain paraffin sections of select intestinal samples in order to confirm findings observed in histopathologic quantification of apoptosis. Slides were first deparaffinized using xylene, ethanol and PBS washes in coplin jars and were then treated with proteinase K. The rest of the procedure was completed according to the manufacturer's instructions. Slides were stored long-term in the dark to avoid photobleaching at -20°C.

The terminal deoxynucleotidyl transferase deoxyuridine triphosphate nick end labeling (TUNEL) method is the scientific basis of this kit. Free 3'-hydroxyl (OH) termini in DNA are labeled with the kit indicating the presence of both single-strand breaks (SSBs) and double strand breaks (DSBs) in DNA. An anti-digoxigenin-rhodamine
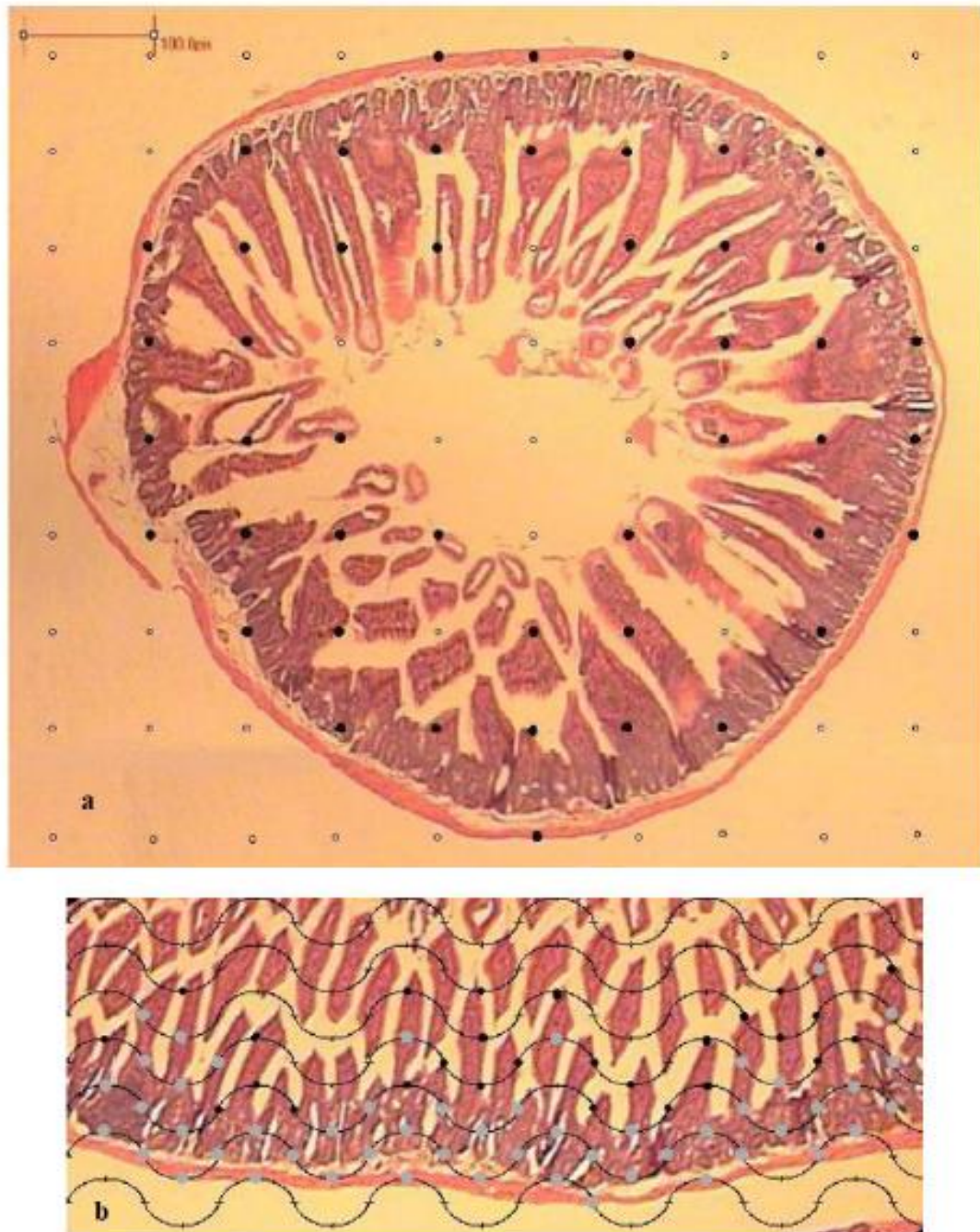
Figure 4:   Mucosal surface area assay. Example images of a) area grid and b) grid cycloid arc overlays provided by ImageJ in order to condcut stereological analysis on transverse and longitudinal intestinal sections, respectively. The tissue pictured here is from BALB/c mouse duodenum and viewed at a) 50X and b) 100X magnification.

antibody (sheep, polyclonal) allows for detection (excitation wavelength of 540 nanometers (nm), emission wavelength of 550 nm) of the labeled ends using fluorescence microscopy (see 2.3.2). A 4',6-diamidino-2-phenylindole (DAPI) nuclear counterstain with antifade was used alongside this assay (excitation wavelength of 365 nm, emission wavelength of 480 nm). The apoptotic cells fluoresce bright red against the blue nuclear counterstain.

2.5.1.1 Quantification of Fluorescence for Apoptosis

Slides were next observed in a blinded fashion using fluorescent microscopy (see 2.3.2). 40 or more whole crypts selected at random on varying regions of tissue sections were quantified visually for apoptotic lesions as indicated by concentrated red fluorescence at 1000X magnification.

A second method was used to quantify the fluorescence indicating apoptotic cells in the intestinal tissue. ImageJ was applied once again to images in this analysis. The use of a software program such as ImageJ eliminates human bias in the quantification process. It also provided the advantage continuous data of fluorescence rather than discrete numbers of apoptotic lesions. Nonetheless, due to the expensive nature of the ApopTag® kit, analysis and quantification of fluoresce were primarily employed to verify the accuracy of the methodology of visual findings of apoptotic lesions in H&E-stained slides. Red-green-blue (RGB) images of fluorescently stained tissues were opened with ImageJ and immediately split by color channel into three single images separately showing red, green and blue channels by gray intensity. Measurements of area,

mean gray value (MGV) and integrated density (ID) were taken first of three regions of

background near and around bright gray areas. Next the same measurements were taken

for the entire visual field of the image. An example of this process is provided

photographically in Figure 5. Corrected total field fluorescence (CTFF) was calculated by

subtracting the product of the field area and average background MGV from the field ID.

A minimum of six images were used for every dose point.
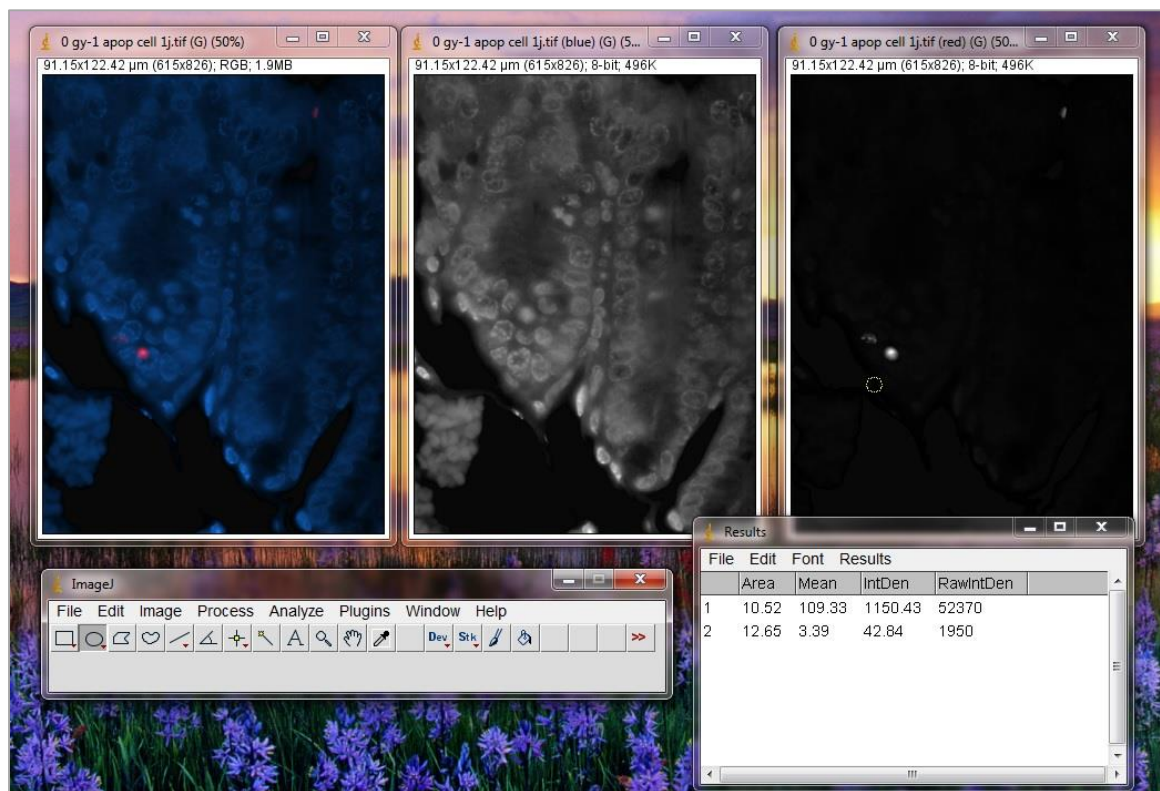
Figure 5:   Fluorescence quantification in ImageJ. Screen shot from a computer
showing the process of fluorescent quantification using ImageJ. A single, color RGB
image has been split by the software into gray-based images displaying red and blue
channels individually. Background can be subtracted based on area from other measures
generated like integrated density to ensure accurate quantification.

2.5.2 Ki67 as a Cell Proliferation Marker

This assay is relevant only to the group of BALB/c animals exposed to protons. It was completed at the request of editors following the submission of a manuscript. It has been included in this dissertation as the data raises interesting questions.

All anitbodies were purchased from Chemicon/Millipore International (Billerica, MA). Slides were deparaffinized by warming them for an hour at 65°C and then using xylene, ethanol and PBS washes in coplin jars as mentioned above. Antigen retrieval was achieved with the use of a sodium citrate buffer made in house and a water bath set to 98°C. Slides were blocked in 10% normal goat serum with 1% bovine serum albumin (BSA) in PBS to prevent non-specific binding of antibodies. The primary antibody, a rabbit-raised anti-Ki67, was applied to tissues in PBS with 1% BSA at a dilution of 1/1000 and the sections were incubated overnight in a humidified chamber at 4°C. The next morning, slides were rinsed in PBS with Tween-20 (PBST) and incubated with the fluorophore-conjugated secondary antibody, a goat anti-rabbit immunoglobulin G (IgG) conjugated with a biotin spacer (biotin-SP), at a dilution of 1/500 in PBS with 1% BSA for 1 hour. To achieve fluorescence and increase the sensitivity of the assay, a streptavidin-fluorescein conjugate (diluted 1:100) from Chemicon/Milliopore (Billerica, MA) as well as an endogenous Avidin+Biotin blocking system from Abcam (Cambridge, MA) were used. Slides were then rinsed in PBS, counterstained with DAPI with antifade and stored at -20°C in the dark with a sealed coverslip until further use. Fluorescein has excitation and emission wavelengths of 494 nm and 521 nm and appears green.

2.5.2.1 Quantification of Ki67 Fluorescence

Proliferating cells in the intestinal tissues were quantified visually in a blinded fashion using fluorescent microscopy (see 2.3.2) at 1000X magnification for each animal in 20 crypts selected randomly as depicted by bright green, concentrated fluorescence against the blue nuclear DAPI stain.

A second method of quantification was used as well and followed the process described in 2.5.1.1 with the exception that the green channel was analyzed and not the red.

2.5.3   DNA Repair Proteins

Another immunohistochemical experiment performed was the staining of intestinal tissues with antibodies specific to DNA repair proteins. Paraffin sections were stained as described above in 2.5.2 with the exception that two primary and two secondary antibodies were used to complete a double stain. Frozen sections were also double stained. Frozen sections had to be warmed to room temperature for approximately 30 minutes and then fixed in ice cold acetone for 5 minutes. Sections were allowed to air dry for 30 minutes and then washed in PBS. From there, blocking of non-specific binding was performed and the protocol followed the subsequent steps described in 2.5.2. Due to the double staining, both a 10% normal donkey serum and 10% normal goat serum block were performed in PBS with 1% BSA. All antibodies were ordered and purchased from Abcam (Cambridge, MA). The primaries were ab3669 and ab97351, antibodies specific to Rad51 and X-ray repair cross-complementing protein 4 (XRCC4), respectively, and were used with dilutions of 1/100 and 1/200. The XRCC4 antibody was rabbit polyclonal

while the Rad51 antibody was goat polyclonal. The secondary antibody for XRCC4, ab96885, was a goat polyclonal to rabbit IgG-H&L (DyLight 594) and a dilution of 1/150 was found to be best for this work. A donkey polyclonal secondary antibody to goat IgG-heavy and light chains (H&L) (DyLight 488), ab96931, was used to tag the primary antibody to Rad51 at a dilution of 1/250. DyLight 594 has excitation and emission wavelengths of 593 nm and 618 nm and appears orange to red-orange. DyLight 488 has excitation and emission wavelengths of 493 nm and 518 nm and appears green.

2.5.3.1 Quantification of Fluorescence for DNA Repair

Images of DNA repair proteins present in intestinal tissue and the colon were captured using fluorescent microscopy (see 2.3.2). Fluorescence was quantified using ImageJ as described above in 2.5.1.1 and 2.5.2.1. Crypts in the small intestine were divided into lower and upper regions and the two were quantified separately.

2.6   MOLECULAR ASSAYS

2.6.1   RNA Isolation

Total ribonucleic acid (RNA) was isolated from small intestinal tissue using the Qiagen RNeasy Mini Kit (Qiagen, Valencia, CA) according to the manufacturer's protocol. Snap-frozen intestinal tissue was homogenized completely before isolation using an electric homogenizer and approximately 50 strokes. The optional DNase treatment mentioned in the instructions from the manufacturer was performed in order to eliminate genomic DNA contamination. Samples and reagents were kept on ice throughout the process and RNA was stored in -80°C until further use.

2.6.1.1 RNA Concentration Quantification

In order to determine the concentration of RNA achieved after isolation, a Spectramax® Plus 384 instrument and SoftMax® Pro Software (both from Molecular Devices, Inc., Sunnyvale, CA) with cuvette were used to attain absorption amount in a mixture of the RNA with water at wavelengths of 260 and 280 nm. These wavelengths are indicative of RNA and DNA presence, respectively. The resulting absorptions were used to ensure there was an acceptable ratio of RNA to DNA and to calculate RNA concentration. The absorption at 260 nm was multiplied by 50 to represent the 1/50 dilution in water for measurement. That product was then multiplied by 40 to normalize to the expected concentration for a 1 cm pathlength. The resulting product provided the RNA concentration in nanograms (ng)/microliter (μL). Concentrations as low as 25 ng/μL were acceptable in order to perform subsequent experiments, but ideal concentrations were upwards of 200 ng/μL.

2.6.1.2 RNA Quality Analysis

An Agilent 2100 Bioanalyzer and Agilent RNA 6000 Nano Kit (Agilent Technologies, Inc., Santa Clara, CA) were used to test the quality of the isolated RNA according to instructions provided by the manufacturer. As little as 5 ng of RNA was used per sample in some cases. Agilent's patented RNA Integrity Number (RIN) value was the endpoint used to determine RNA quality (1-10). RIN values of 8-10 were considered extremely high quality, but any value of 5 or greater was consider acceptable according to the manufacturer to move forward with subsequent experimentation.

2.6.2   First-Strand cDNA Synthesis

Qiagen's RT² First Strand Kit (Qiagen, Valencia, CA) was the methodology of choice to synthesize complementary DNA (cDNA) from isolated RNA. The kit uses a cocktail of reverse transcriptase, primers, genomic DNA elimination reagents and RNA to create a first strand of cDNA after being placed in a thermocycler and heated to 42°C and then 95°C. The cDNA was held at -20°C until further use.

2.6.3   Quantitative Real-Time PCR

Quantitative real-time polymerase chain reaction (PCR) was used substantially throughout the process of completing the work described in this dissertation. RT² Profiler PCR Arrays were used in combination with RT² SYBR Green quantitative PCR (qPCR) mastermixes (both from Qiagen, Valencia, CA) and cDNA to study gene expression after irradiation. The arrays are 96 well plates which come equipped with primer assays specific to a set of genes related to similar signaling pathways. We employed both the Mouse Oxidative Stress and Mouse Apoptosis arrays. The plates also have built-in housekeeping genes, genomic DNA contamination detection and positive controls for the PCR process itself. qPCR was completed using the CFX96 Real-Time PCR Detection System from Bio-Rad (Hercules, CA).

2.6.3.1 Analysis of Gene Expression and Pathways

An Excel-based document was provided by Qiagen that was used to analyze the results of qPCR. It is based upon cycle number for both control and test samples and

normalization to housekeeping genes. In order to further confirm qPCR results, a more stringent statistical analysis method was applied to the data in which the cycle numbers were normalized to each other within the data set even after normalization with housekeeping genes. This double normalization allowed for more confidence in the qPCR results. Genes were only considered significantly different in expression from control samples if both normalization procedures had been performed and they had an up or down fold change exceeding 2 and a p-value of less than 0.05 after a student's t-test.

To provide potential mechanisms using qPCR data, Ingenuity® Pathway Analysis (IPA) (Ingenuity® Systems, Inc., Qiagen, Redwood City, CA) was used to generate pathways. The program uses data from the literature and inputs from the user in order to provide real network relationships between molecules. Only genes with significant fold changes as described above were used an inputs in the program. The confidence level chosen to build the networks was "experimentally proven" only (the highest level of confidence query) (Ingenuity Systems, 2013). The illustrations in the document were created by the author personally using the IPA program.

Finally, to further understand differences between the large gene expression data sets, so-called heat maps were generated using an online program known as CIMminer (Genomics and Bioinformatics Group, Laboratory of Molecular Pharmacology (LMP), Center for Cancer Research (CCR), National Cancer Institute (NCI), Bethesda, MD) (Group, 1997-present). This tool is freely accessible to the public. Gross differences in the colors on the heat maps between time points, strains or radiation qualities were

observed and the individual genes at those points were teased out. Next, those genes were compared for significance and inputted into the IPA system mentioned above to observe possible molecular networks responsible for changes in the samples.

2.6.4   Histone Deacetylase Assessment

Histone deacetylase (HDAC) activity and inhibition were assessed in colon samples in C57BL/6 mice exposed to protons. The Epigenase™ HDAC Activity/Inhibition Direct Assay Kit (Colorimetric) (Epigentek, Farmingdale, NY) was used and executed according to the manufacturer's protocol. The kit measures the total inhibition and/or activity of HDAC enzymes using proteins extracted from nuclei. The kit also provides internal controls in the form of a histone standard which is deacetylated. Proteins were extracted from the nuclei of snap-frozen colon tissues using the EpiQuik™ Nuclear Extraction Kit I (Epigentek, Farmingdale, NY). The instructions provided by Epigentek were used to complete that work. Next, a serious of reactions were performed in a 48 well plate according to Epigentek's protocol. HDAC activity was measured colorimetrically using a Tecan Safire Absorbance and Luminescence reader and Magellan software (Tecan Group Ltd., Mannedorf, Switzerland). Absorbance was measured at 450 nm with a reference wavelength absorbtion of 655 nm. Final activity or inhibition of HDAC was calculated by subtracting the average absorbance readings of blank wells from average readings of sample wells and then dividing that difference by the product of nuclear extracts inputted and incubation time with HDAC substrate. A standard curve of the deacetylated histone standards was also used in calculations.

2.7 STATISTICAL ANALYSES

Statistical analysis was completed using Excel or SPSS which was freely downloadable from UTMB. Statistical consulting was provided when necessary by the JSC Statistical Consulting group. Student's t-test was used to assess statistical differences in experiments which had only two groups or when two groups needed to be assessed for differences. Analysis of variance (ANOVA) was used to observe statistical differences in experiments which had three or more groups. Tukey's test was used for post-hoc analysis of ANOVA when necessary in order to determine differences between specific groups. Groups were assessed for equality of variance. Data sets which did not exhibit a normal distribution were assessed using a parametric t-test or ANOVA after transformation. An alpha level of 0.05 was set as the significance standard for all statistical testing. Therefore, a p-value of less than 0.05 was considered significant for these studies and when encountered merited rejecting the null hypothesis that no difference existed between groups. P-values of less than 0.05 are portrayed throughout this dissertation in various forms: asterisks (*), pound signs (#) and percent signs (%) depending on the level of significance. Please refer to the individual figure captions for explanations. When possible dependent upon visual aesthetics, it was attempted to easily depict significant differences between groups with adjoining line segments. Most results of this experimental work were displayed graphically as means with error bars representative of either the standard deviation (SD) or the standard error of the mean (SEM).

Chapter 3: Assessment of Histopathologic Alterations in the Gastrointestinal Tract after Radiation Exposures of Varying Doses and Qualities

3.1 ADDITIONAL EXPERIMENTAL RATIONALE

All of the work presented in this dissertation was performed *in vivo*. Originally a study was funded with plans to assess the radio-adaptive response in animal models with gamma rays (and not protons). Experiments were therefore performed involving an additional group receiving a priming and challenge dose of irradiation rather than a single dose alone. In order to provide a study more meaningful for the space flight environment and due to an interest in characterization of intestinal affects after charged particle exposures, another set of experiments were performed using simple, single-dose proton exposures. For purposes of this dissertation, differences between low and high dose exposures are addressed across varying strains of mice using both proton and gamma ray data. Any protection afforded to animals due to the combination priming and challenge dose, or so-called radio-adaptive response, will be reported though as to provide a more comprehensive numerical and informational report.

Weight loss in mice following radiation exposures has been well characterized in the primary literature and is mostly thought to be an effect of acute enteritis or the more serious radiation induced gastrointestinal syndrome (RIGS) in the case of high dose irradiations (Bhanja et al., 2009). It can occur following both exposures limited to the abdominal area or when using WBI (Jia et al., 2010). It was decided that weight loss would be an excellent first endpoint to measure for this work for multiple reasons.

Tracking the mice's weight would provide early indicators that the irradiation procedure had taken place as planned and that animals were exhibiting a typical physiologic response. It was also used as an assessment to ensure that the animals were not too ill after the radiation exposures to allow for the best care that could be given. Weight loss was written into the IACUC protocol as a required measurement and imposed limits upon how much weight was acceptable for an individual mouse to lose without intervention from a veterinarian and possibly subsequent euthanasia. It was also felt that by measuring weight daily, the ability to pinpoint on which days after irradiation weight loss was occurring may offer insight into future experimental data, objectives or chosen time points.

Apoptosis is quite prevalent in the intestine after radiation exposures, both high- and low-LET, of high end even low doses (Potten et al., 1994; Hendry et al., 1995). The time course and quantification of gamma ray-induced apoptosis in the intestine has been known for some time, but much work remains to be done to characterize the effects of protons and other radiation qualities. As apoptosis is a major pathway of cellular death and the small intestine turns over daily in humans, it was chosen for this work because cellular death and eventual replacement proliferation is an important component in acute enteritis and/or ARS following irradiation (Ramachandran et al., 2000). In other words, apoptosis is an important regulator of maintaining intestinal function both normally and following an insult such as radiation, partly because of the rapid turnover rate of the organ (Ramachandran et al., 2000). In this manner, apoptosis can be thought of as both a protective measure and a damage marker, a double-edged sword. Therefore, although it

does not persist for extremely long periods of time, apoptosis is an extremely important homeostatic process (Potten et al., 1994).

Astronauts who may receive a large radiation dose (such as from a solar particle event (SPE)) in space flight and experience acute enteritis can experience symptoms such as vomiting, diarrhea and weight loss which can hinder their performance and potentially be detrimental to the mission (Shadad et al., 2013). Learning more about this topic to prevent such a state in space flight is critical. Additionally, it is known that cell death in the intestine when apoptosis is blocked, thought to be due to a lack of p53, is marked by persistent DNA damage, unchecked cell proliferation and other hallmarks of carcinogenesis (Leibowitz et al., 2011). Therefore, delineating relationships between apoptosis, its mechanism and cell survival or other endpoints after varying radiation qualities can also potentially provide some important information relevant to cancer and the possibilities of persistent DNA damage (Leibowitz et al., 2011). This work attempts to do just that. Apoptosis was quantified and mechanistic possibilities are addressed in gene expression studies (see Chapter 4). Although small intestinal cancer is rare in human beings with regard to cancer incidence, colon cancer is not. The age-adjusted incidence rate of colon cancer in 2009 was 42.5 per 100,000 men and women (Group., 2013). Learning if and how apoptosis is related to persistent DNA damage or the lack thereof in either the small intestine or the colon may be helpful for those studying the colon and carcinogenesis, which is a concern for our middle-aged astronauts. This work observed a four hour time point to study the presence of DNA repair proteins in the intestine and colon after proton radiation to help with that discovery. Four hours may not fit some

definitions of persistent DNA damage. It was considered an appropriate time point for this work because apoptosis peaks in the small intestine at four hours after gamma ray exposure and due to the complex relationship that apoptosis likely has with the presence and absence of DNA damage, it was thought that observation of both apoptosis and DNA repair at the same and pertinent time point could be very relevant (Potten, 1977).

The ApopTag® kit (see 2.5.1) was used a chemical means of quantifying our findings of visual apoptotic analysis in order to verify the accuracy of the visual analysis. The kit provides a fluorescent stain which can easily provide continuous data, void of human bias.

Villous morphometric analysis represents an assay with easily quantifiable data making it an obvious advantage (see 2.4.3). Its biological relevance lies in the function of intestinal villi and the effects on their structure and function following radiation exposure. Villous structures project like fingers into the lumen of the intestine and function to maintain intestinal homeostasis with specialized, differentiated cells as their make-up (Sarna and Otterson, 1989). Their primary role is in nutrient absorption following food digestion (Sarna and Otterson, 1989). Enteritis from causes other than raditation is characterized by flattening and atrophy of the intestinal villi (shrinking), which disrupts nutrient absorption and is one of the main causal agents of enteritis symptoms (Cummins et al., 2011; Kim et al., 2012). ARS syndrome shares many symptoms with acute and even chronic enteritis, yet only some of the literature makes the connection that villous atrophy is a likely underlying factor in ARS, or focuses on the fact

47

that villous atrophy may be caused by other processes in the gut like the neuromuscular system and not necessarily radiation (Somosy et al., 2002; MacVittie et al., 2012). Upon reviewing the literature, it was determined this disease process should be studied further as it does not matter exactly what causes a symptom if the negative outcome happens following radiation for purposes of space flight success. This assay once again correlates nicely with quantification of apoptosis because maintenance of villi structure and prevention of flattening is *dependent* upon crypt survival and regeneration (Kim et al., 2012). As crypt stem cells proliferate the tissue with new cells, they move up the villi in a highly strategized fashion and replace cells at the tip of villi which slough off into the intestine (Potten, 1991; Kim et al., 2012).

Finally, mucosal surface area analysis, though not a commonly used technique, provides an idea of morphology changes in the intestine very much related to the villi, which again are dependent on crypt survival (see 2.4.4). This assay is related to the villi because it functions to determine changes in surface area and villi have evolved in order to increase the surface area of the intestine, in turn increasing absorption of nutrients (Sarna and Otterson, 1989). This assay is indeed pertinent to radiation insult since it is directly related to the villi which are commonly affected in radiological exposures; however it was not a priority over the villous morphometric analysis due to its extensive time required for completion and the fact that it is not as well published in the literature compared to villous morhpometry with regard to radiation (Kim et al., 2012). This assay was suggested to us by an editor after submission of a manuscript and we have included it

because it provides significant data. This assay was only used on BALB/c mice exposed to protons and sacrificed four hours after irradiation.

3.2 RESULTS

3.2.1 Animal Body Weights

Mice were weighed beginning the day of radiation exposure and everyday afterwards until the animals were sacrificed. Only groups assigned to sacrificial time points exceeding three days were weighed as weight loss over a shorter time span is unlikely. For our work this comprised of a 7 day time post-IR time point and a 21 day post-IR time point. Significant differences were observed across multiple groups and this is comparable to what has been reported in the literature (Bhanja et al., 2009; Oh et al., 2010; Kim et al., 2012).

Over a one week time period after irradiation, all three experimental groups (5 cGy, 6 Gy and 5cGy+6Gy) exhibited a body weight significantly different than that of the control group (0 Gy) (p-value < 0.001) (Figure 6). The high dose and combination dose groups also significantly differed from the low dose group (p-value < 0.005) (Figure 6).

This is suggestive of a true dose response in body weight after irradiation. No difference of significance was observed between the 6 Gy and 5 cGy+6Gy group, however, which do have a difference, though small, in dose. The priming dose did not provide any radio-adaptive response for the 7 day time point concerning body weight. Furthermore, the visual appearance of the graph reveals that the high and combination dose groups lost more weight the day after irradiation while the low and control dose

49
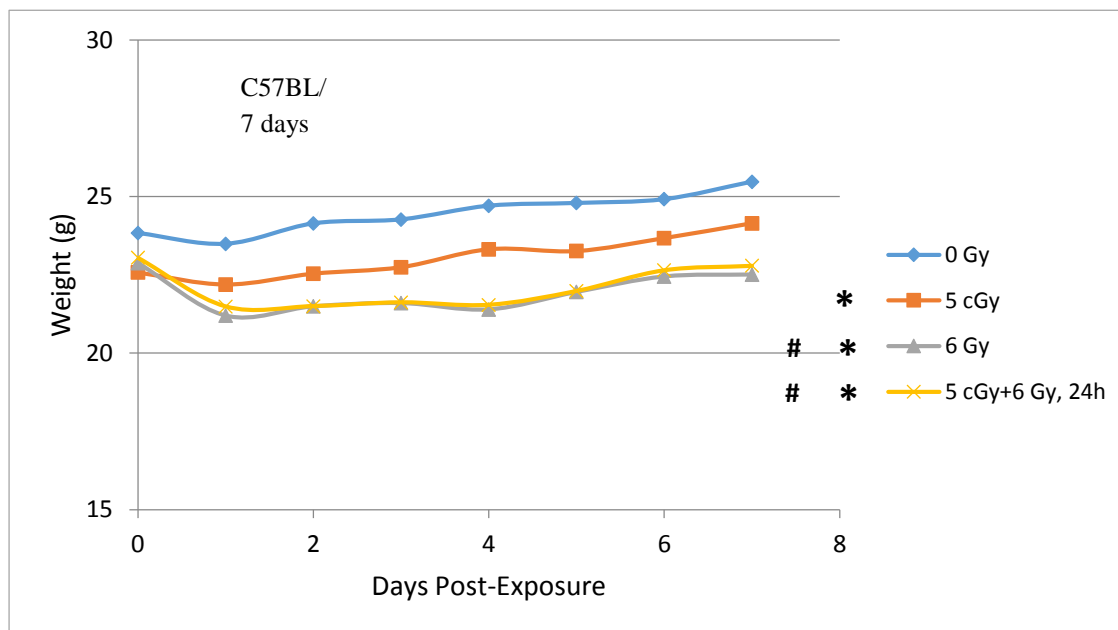
Figure 6: Mean body weights in C57BL/6 mice after exposure to gamma rays. Mice were sacrificed 7 days after IR. Significant differences between groups are noted with: * p-value < 0.001 as compared to 0 Gy and # p-value < 0.005 as compared to 5cGy.

groups seem to have gained weight over the week long period. Indeed both these observations were confirmed when assessed mathematically. A student's t-test showed for each individual group compared to their day 0 original weight, the control and low groups were significantly different (p-value < 0.05) on the last day while the high and combination groups were significantly different (p-value < 0.05) on day 1 (data not shown). This caused us to reject the hypotheses that animals would lose weight throughout the experimental time point.

21 days after IR exposure all animals had started gaining weight again and both combination dose groups, 5 cGy+6Gy, 24h and 5 cGy+6Gy, 7d, were found to be significantly different (p-value < 0.005) from the high dose of 6 Gy for the overall 3

week period (Figure 7). For the endpoint of body weight then, the priming dose provided a protective effect against weight loss whether it was administered one week or 24 hours before the challenge dose. When compared to the 7 day weight data, which only had the 5 cGy+6 Gy, 24h group and not the 5 cGy+6 Gy, 7d group, one can infer that perhaps with regard to mechanisms affecting body weight a radio-adaptive response takes longer than one week to occur. Longer time points between priming and challenge exposures that induce radio-adaptive responses have been observed before (Horie et al., 2002).

3.2.2   Intestinal Apoptotic Lesions

Apoptotic lesions including time course and other measures have been documented in the literature for gamma ray exposure in the intestine. However, several doses in different mouse strains have yet to be reported such as those in this document. Starting with a paper in 1977 that turned into a seminal work for this field, C. Potten has become the authority on radiation and intestinal damage (Potten, 1977). Potten has shown that apoptosis peaks in the small intestine at approximately 4 hours after gamma ray exposure (Potten, 1977). Conversely, very little work has been published regarding proton exposures, particularly with regard to *in vivo* work and the intestine. Radio-adaptation is also quite limited in current knowledge when speaking specifically of intestinal apoptosis.

Photographic images of affected intestine after irradiation are provided in Figure 8. The photographs have been labeled to identify apoptotic lesions and depict the types of lesions that were quantified in this work. This particular set of photographs are from
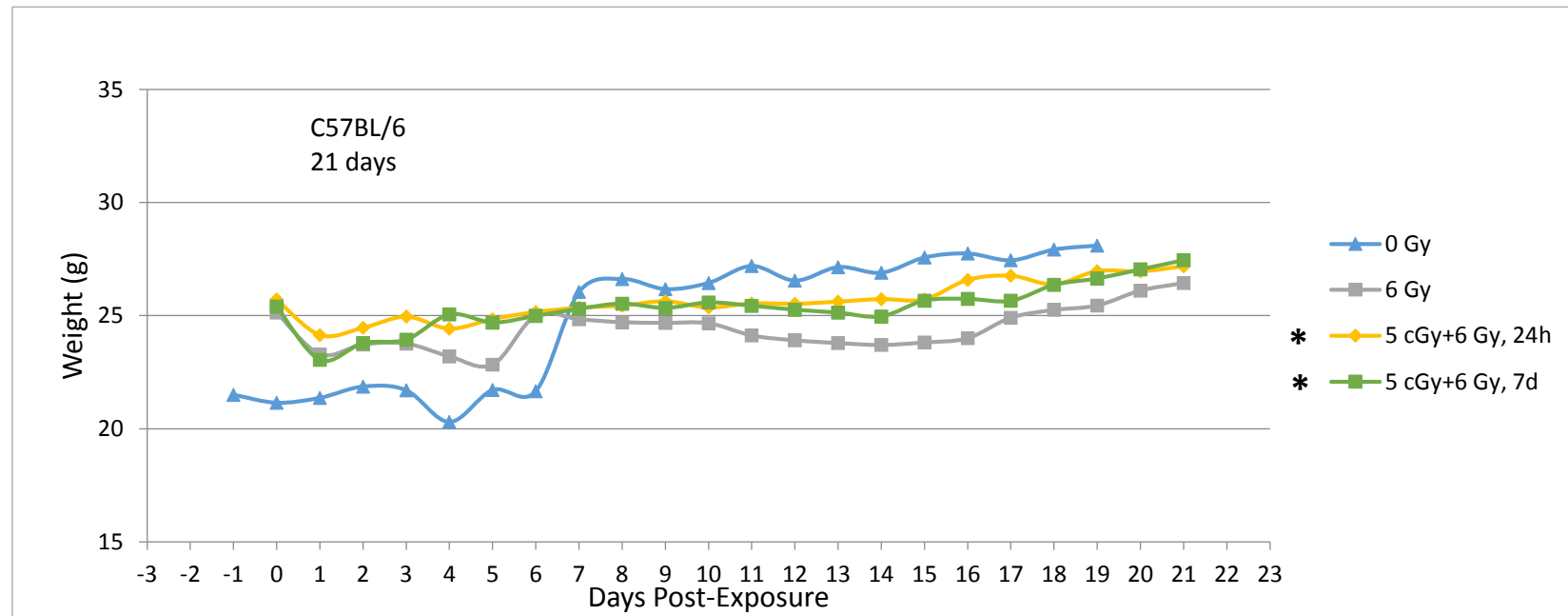
Figure 7: Mouse weights 21 days following radiation exposures. Both C57BL/6 priming dose groups were significantly different from the 6 Gy group over the three week period (* p-value < 0.005).

BALB/c mice following varying doses of proton irradiation and sacrificed four hours post-exposure. The images beautifully display

what appears to the trained eye to be a likely linear dose-response of apoptotic lesions in the intestinal crypts.

3.2.2.1 Gamma Ray Time Course

Time points of 4 hours, 3 days and 21 days were studied. The first time point for our observations of apoptotic lesions was 4 hours post-irradiation. C57BL/6 mice exhibited significantly increased means of lesions for every dose when compared to their control counterparts (*p-value < 0.05). The high and combination dose groups were also altered from the low dose mice in mean number of lesions by a factor of more than 10 (Figure 9). High dose and combination groups were not significantly different. It is possible based on means that the combination dose group did provide an adaptive response indicating protection from apoptosis, but this was not proven statistically. In order to display the greater sensitivity often shown at low doses due to IR in the small intestine, the mean number of apoptotic lesions was also plotted on a logarithmic scale (Figure 10). It is important to notice the extreme difference in rise on the logarithmic scale between the 5 cGy group and the control group as compared to the rise between 5 cGy and the higher doses or even 0 Gy to the higher doses. This rapid rise in the mean number of lesions is indicative of a damage response that is higher than the expected amount of lesions would be proportionate to the higher radiation doses in linear dose response. However, this is consistent with what has previously been published in other mouse strains, doses, dose rates and radiation qualities (Potten, 1977; Potten et al., 1994). Also displayed on this figure is quantification of apoptotic lesions in just the basal region of the intestinal crypts. The literature consistently shows that the lower half of intestinal crypts are far more sensitive to IR as measured by cell death than the upper regions (Ijiri and Potten, 1983; Potten, 1991). This is primarily because the lower region of the crypts contain the stem cells which are continuously repopulating the upper half of the crypt and

53
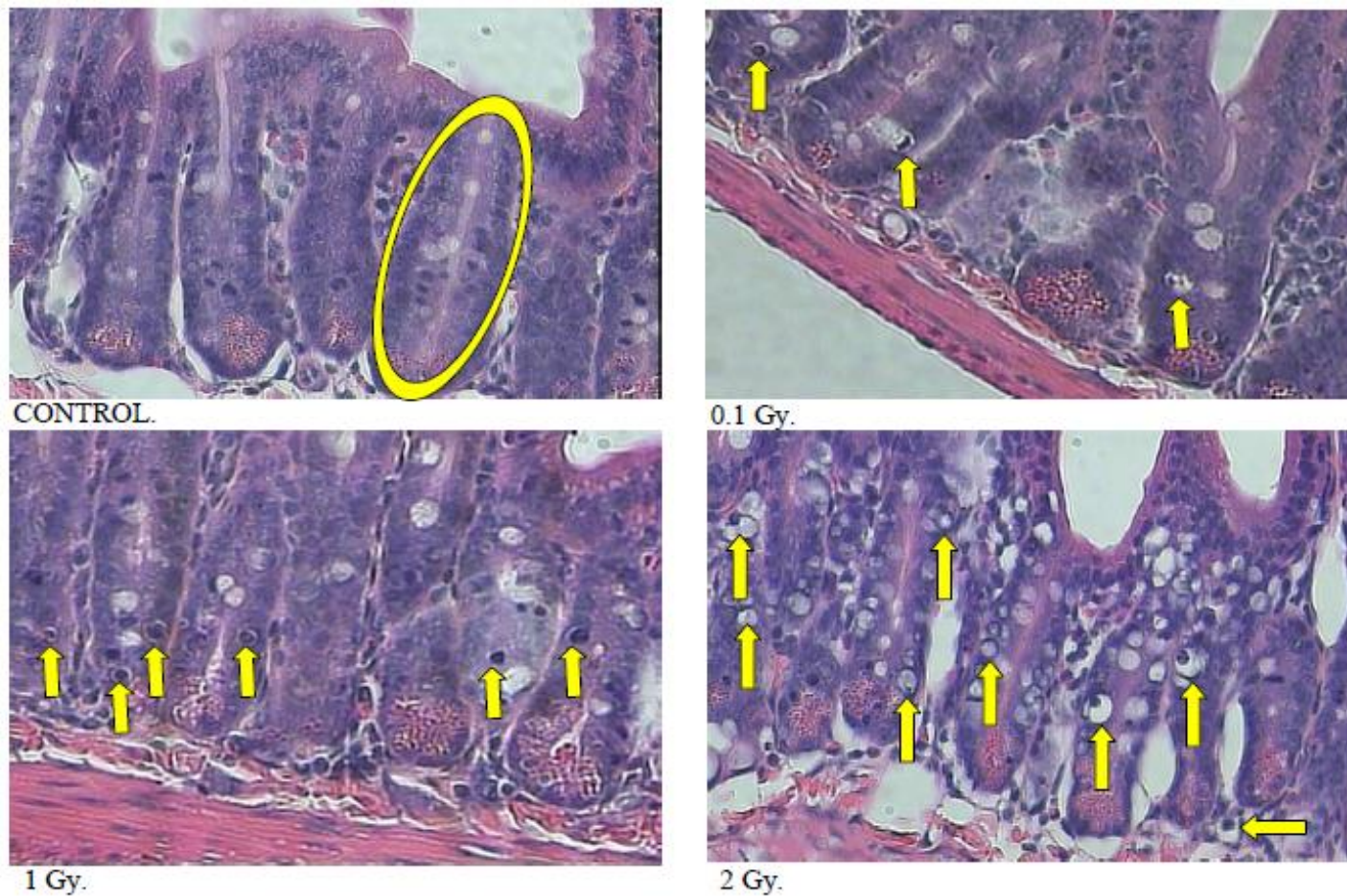
Figure 8:   H&E-stained tissue sections displaying apoptosis. The duodenum shows lesions (identified by yellow arrows) after proton exposure of varying doses in BALB/c mice. A yellow circle overlaid on the control image familiarizes the viewer with one crypt in the tissue.
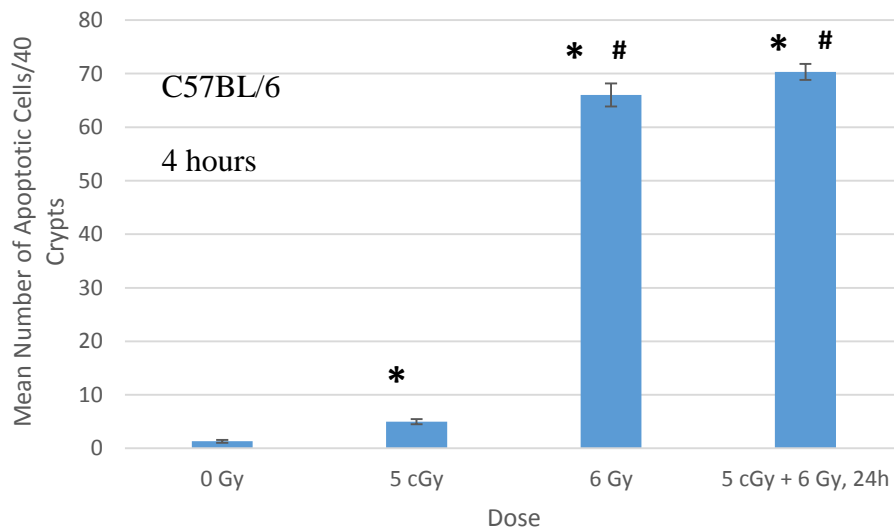
Figure 9: C57BL/6 mice 4 hours after IR exposure exhibit significant apoptotic lesions. * p-value < 0.05 as compared to 0 Gy. # p-value < 0.001 as compared to 5 cGy.
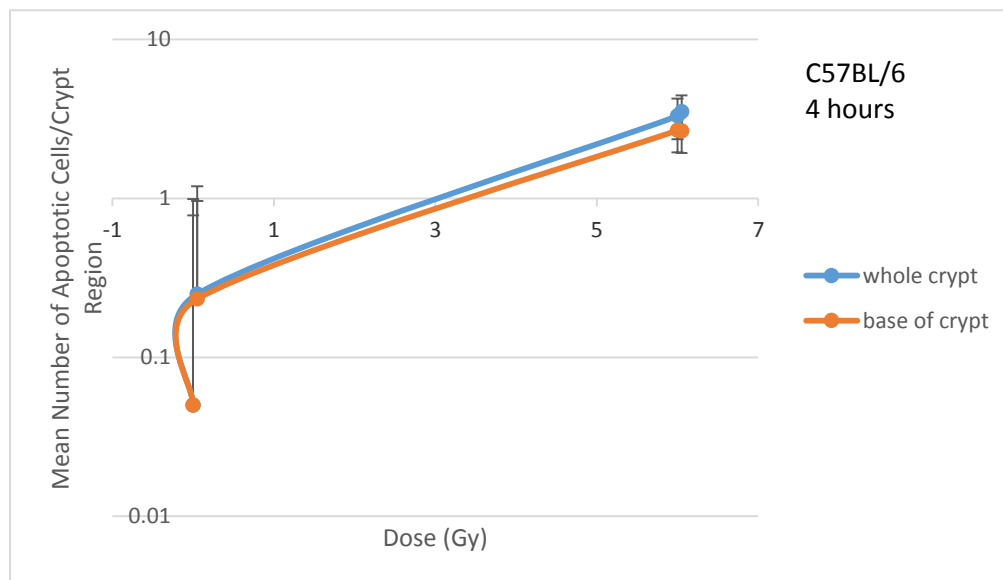
Figure 10:   Sensitivity of low dose and basal crypt responses 4 hours after IR in C57BL/6 mice. The base of the crypt is responsible for almost all of the mean cell death. The low dose of 5 cGy appears to generate an apoptotic response greater than that of a linear dose response.

villi above it. Why are stem cells more sensitive to radiation? The physics of radiation commands that it deposits energy in a given space and time. When cells' genetic material is tightly packed and organized for replication, and doubled in amount, too, it is more likely to undergo multiple ionizations as they occur together closely in time and space (Hall and Giaccia, 2006). Therefore, cell cycle is an important factor to consider in assessing damage caused by radiation (Hall and Giaccia, 2006). Secondly, a faster rate of cell cycle automatically means that there is less time for DNA repair to occur which can lead to mutation or apoptosis (Hall and Giaccia, 2006). Finally, Figure 11 has been presented on a linear scale so that the curvature between high dose and combination dose groups can be observed (Figure 11). There was not a significant statistical difference between the two groups, indicating that the priming dose of the combination group did not provide a protective effect or undergo an adaptive response.

Similar figures are provided next for the measurement and display of apoptotic lesions in C57BL/6 mice after gamma ray exposure for sacrificial time points of 3 days and 21 days.

The same strain and doses as in the 4 hour sample just discussed were used for the 3 day time point shown next. For this group of mice, each irradiated group still had a significant amount (p-value < 0.05) of apoptotic lesions as compared to their control counterparts 3 days after exposure (Figure 12). However, there were no differences at this time between irradiated groups of significance. At four hours, that was not the case- the higher dosage groups had a significantly greater number of apoptoses than the low dose set of mice. This indicates that by three days after radiation exposure, the environment
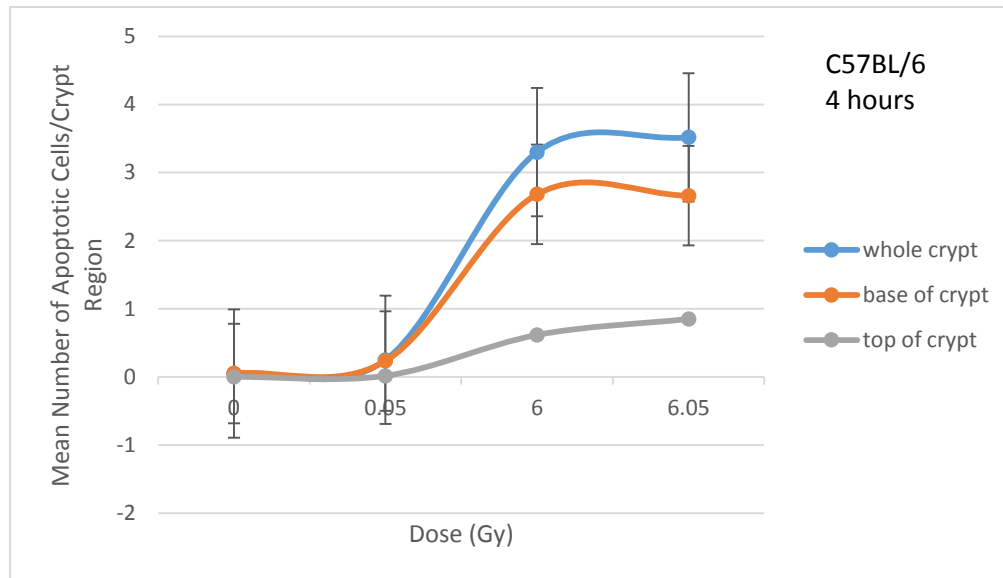
Figure 11: Lack of protection by priming dose as measured by cell death. C57BL/6 mice exposed to gamma rays and sacrificed four hours later appear to have no difference in apoptotic cells in the combination dose when compared to the high dose indicating that no radioadaptive response took place.

and cells of the crypts function similarly no matter if they were exposed to a high or low dose prior. Furthermore, at shorter time points like 4 hours and at low dose irradiations there may be a mechanistic response which maintains lower levels of apoptosis when proportionately compared to the higher doses. The mean number of lesions present for each dose at 3 days is far lower than the means at 4 hours which supports the idea that apoptosis in the intestinal crypts peaks before 3 days post-IR treatment. Again, this is supported in the literature as it is published to be 4 hours following IR insult in other strains of mice (Potten, 2002). It also begs the question how much do the separate doses continue to produce lesions over time in proportion to their original lesion numbers at 4 hours? For example, the 3 day 5 cGy average of lesions was not statistically significant from the 4 hour 5 cGy average (5 to 6.33). The high and combination doses, however, dropped approximately 87% and 84%, respectively between time points (66 to 9 and
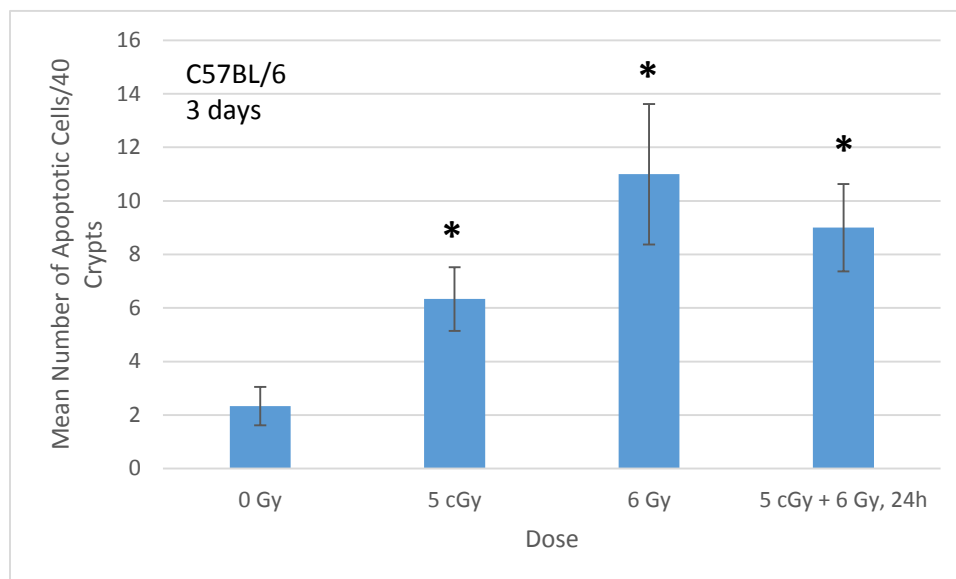
Figure 12:   Mean apoptotic lesions 3 days post-IR insult in C57BL/6 mice. All three experimental groups are sigificantly different than 0 Gy (*p-value < 0.05).

70.33 to 11). With such a substantial difference in how many less lesions are formed over time between the groups proportional to one another, it is likely that there are mechanistic and molecular signaling differences occurring with regard to apoptotic induction over time between the low and high doses. A simpler explanation may be that the higher doses killed much of the crypt cell population leaving fewer cells to still undergo apoptosis between 4 hours and 3 days. Figures 13 and 14 are similar to Figures 10 and 11. Figure 13 represents the supra-linear dose response seen with the 5 cGy points. Figure 14 is provided to show that, again while not statistically significant from one another, the mean number of apoptotic lesions between the high and combination dose groups does appear to trend to a protective effect by the combination group's priming dose. The "top crypt" portion of these graphs have been removed as there were 0 lesions present in the top half of the crypts quantified. Therefore, the basal region of the crypt was responsible for all

58
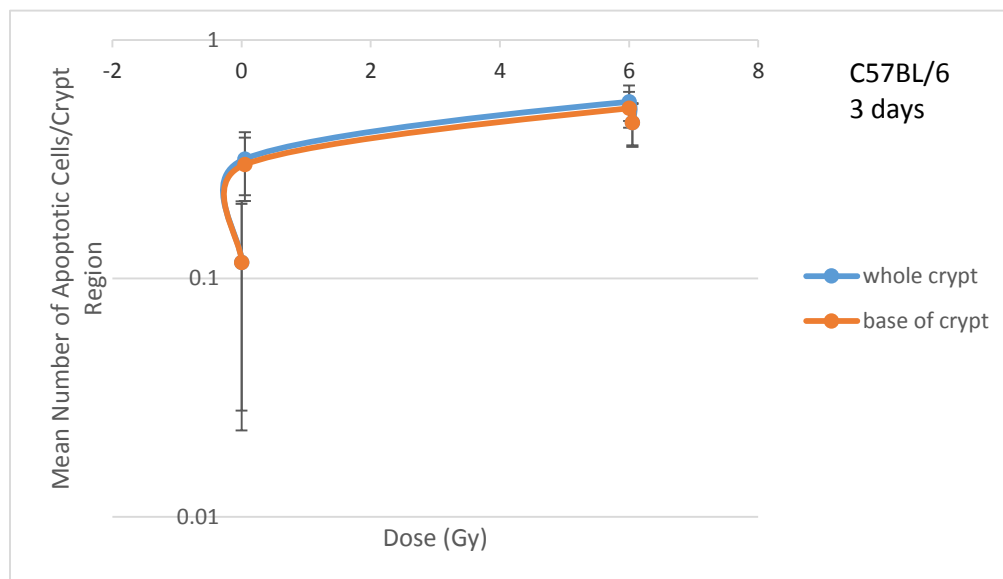
Figure 13: Logarithmic dose-response of apoptotic lesions in C57BL/6 mice 3 days after IR treatment. The dose-response curve displays a supralinear behavior at the lowest dose of 5 cGy.

the apoptotic lesions quantified for the 3 day time point.

21 days after gamma ray exposure, another group of animals was sacrificed. This group demonstrated no significant differences between any of the dosage groups in apoptotic lesions (Figure 15), indicating that by three weeks' time post-irradiation, initiation of apoptoses following exposure had probably stopped (Figure 15). Mean apoptotic damage was also plotted as a line graph in order for the viewer to discern differences more clearly between the two combination dose groups (Figure 16). Once again, although not statistically significant, there was a trend towards a protective effect for the combination dose group with 7 days between priming and challenge doses. There did not appear to be a protective trend at 21 days for the combination group of 24 hours
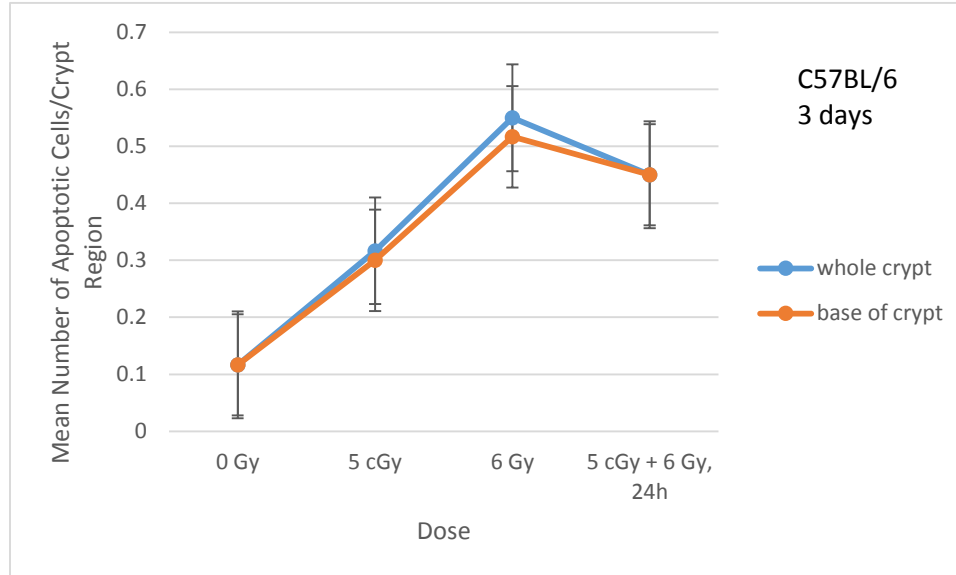
Figure 14:   Apoptotic lesions identified by region of crypt. This group is C57BL/6 mice sacrificed 3 days post-IR exposure. Notice that there are less lesions in the combination dose group of 6.05 Gy than the high dose group of 6 Gy.
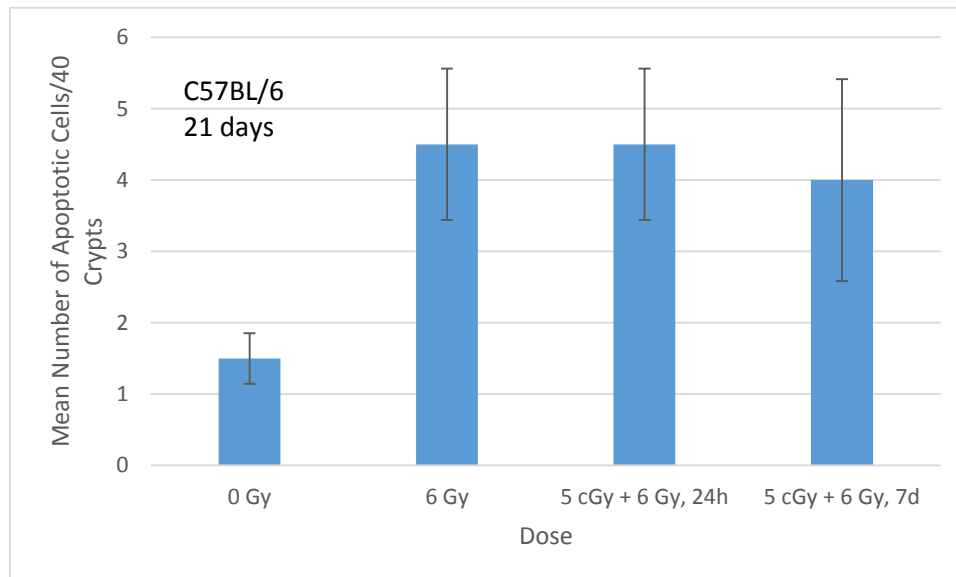
Figure 15:   Mean apoptotic lesions in C57BL/6 mice 21 days after IR-treatment. There were no significant differences between any of the groups.
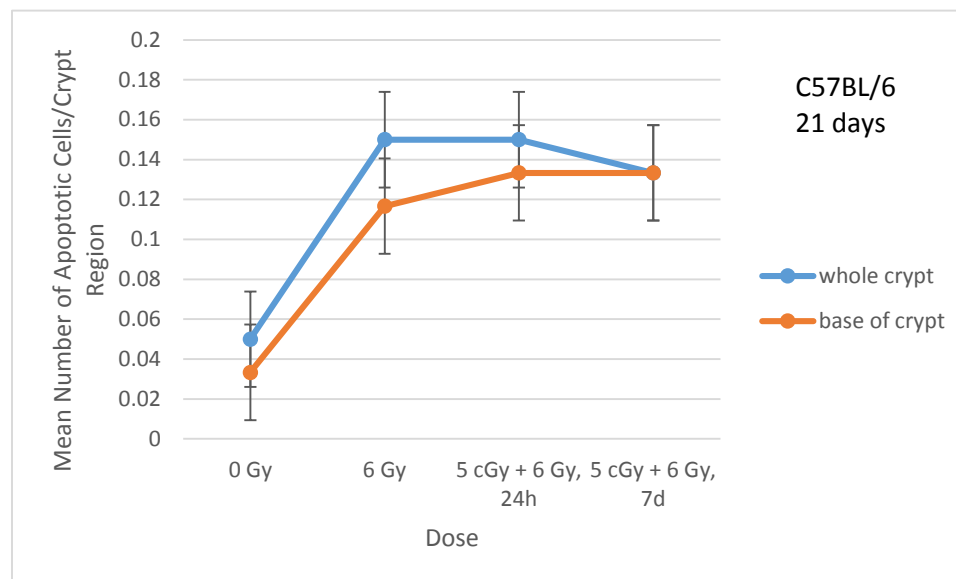
Figure 16: Mean apoptotic lesions after 21 days in crypt regions. Notice the potential protective effect provided between the 7 day combination group and the high dose group of 6 Gy.

between doses. At 3 days, the 24 hour combination did appear to trend towards protection. If a potential for protection with 24 hours between doses disappears between 3 days and 21days, but a longer time between priming and challenge dose may provide potential protection at 21 days, perhaps longer periods of protection require longer time between priming and challenge exposures. The literature does not discount or support this theory. Most of the studies available on radio-adaptation employ the use of shorter (usually 4 or 24 hours) time points between priming and challenge doses (Wolff, 1998). Indeed they rule out longer time periods between the two doses, but none of the endpoints measured involved the small intestine. The top region of the crypt was not provided in Figure 16 as there were no lesions present there. A logarithmic plot was not provided as

the hypersensitivity at low dose cannot be viewed for this group as there was no 5 cGy

dose point.

      A time course of apoptotic lesions for C57BL/6 mice at the doses of 5 cGy, 6 Gy

and the combination groups was established after completion of this work (Figure 17).

When making comparisons between similar doses across time points, both the 6 Gy

group and the 5 cGy+6Gy, 24h group at 3 days were significantly smaller in number of

lesions than their 4 hour counterparts (p-value < 0.001). This same finding was true for

the 21 day time point in these two higher dosage groups, too (p-value < 0.001). No

significant differences were found between the 3 day and 21 day group. In observing

Figure 17, one immediately notices the marked difference in lesions present at 4 hours

compared to the other time points. The extremely significant drop in lesions across

irradiated groups between 4 hours and 3 days indicates that there is a significant decrease
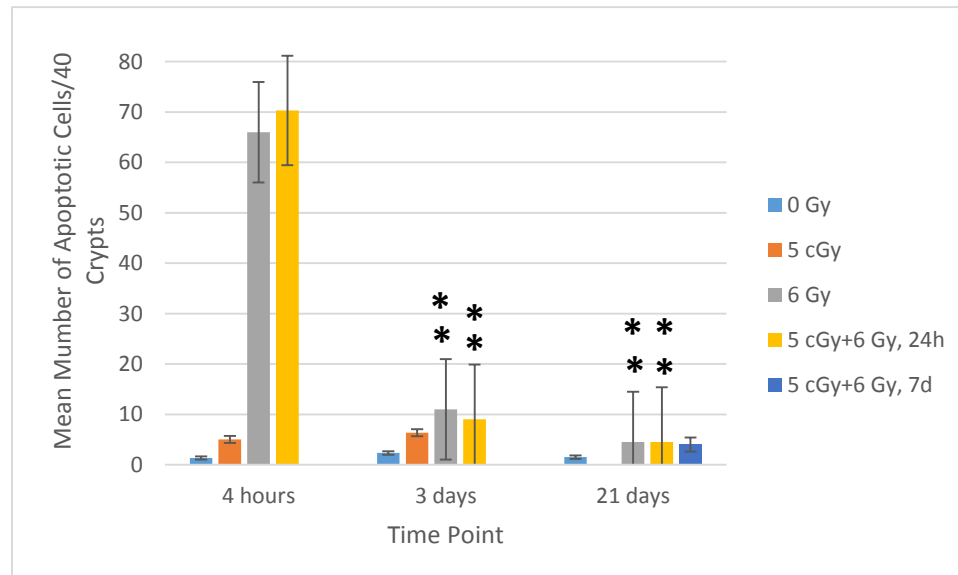
Figure 17:   Time course of apoptotic lesions in C57BL/6 mice. Animals were exposed
to gamma rays. Significant differences displayed are between similar doses of the labeled
group and its 4 hour counterpart (**p-value < 0.001).

in apoptotic induction in these mice between 4 hours and 3 days post-IR insult.

3.2.2.2 Inter-Strain Comparison Following Proton Exposure

We also observed BALB/c mice exposed to protons. As part of a pilot study, we received samples of intestine from these mice exposed to 0 Gy, 0.1 Gy, 1 Gy and 2 Gy protons and sacrificed 4 hours after irradiation. BALB/c mice are considered to be a radio-sensitive strain in comparison to C57BL/6 mice for multiple endpoints including LD50, mammary tumors and micronuclei (Ponnaiya et al., 1997; Rodgers et al., 2001; Hamasaki et al., 2007).

The average apoptotic lesions for each dose of proton exposure at the 4 hour time point for BALB/c is given in Figure 18. Only the two higher doses of 1 and 2 Gy differed significantly from the control group (p-value < 0.05) and there was no inter-group significance between the low and higher doses between one another. However, the data did display a dose-response in apoptotic lesions. A logarithmic plot of lesions based upon crypt region reveals once again a hypersensitivity to radiation exposure at the low dose of 0.1 Gy (Figure 19). Similar to the gamma ray data in C57BL/6, the top region of the crypt makes little contribution toward the lesion total and instead the basal region is the location of most of the damage as measured by apoptotic cells. In an effort to reaffirm this important concept, the average number of lesions per crypt quantified versus location (cell position) within the crypt are plotted below (Figure 20). For reference, cell positions1-6 are considered to be the stem cell region of the crypt in which a high amount
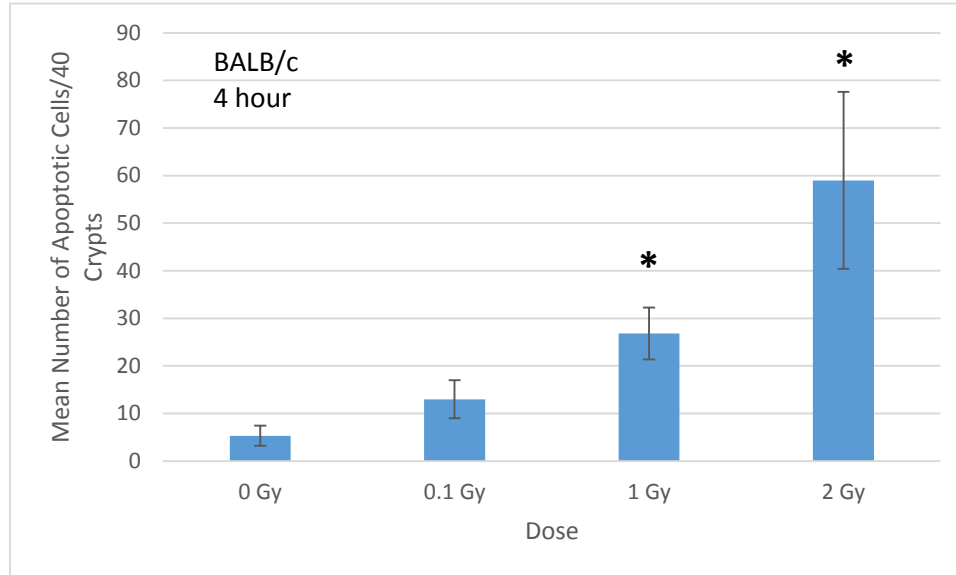
Figure 18:   BALB/c mice demonstrate significant apoptotic lesions after proton exposure. Mice were sacrificed four hours after exposure. 1 Gy and 2 Gy groups were statistically distinct from controls (*p-value < 0.05).

of cell proliferation occurs.

The number of apoptotic lesions was compared between both experimental strains of mouse, C57BL/6 and BALB/c, after whole-body irradiation with protons (Figure 21). Although no differences were observed between strains, a greater number of lesions was observed in BALB/c mice, the typically radiosensitive strain, at every dose point when comparing to C57BL/6. A comparison between C57BL/6 gamma and proton exposures revealed a RBE of approximately 1 which is consistent with the literature when observing apoptoses and numerous other endpoints.
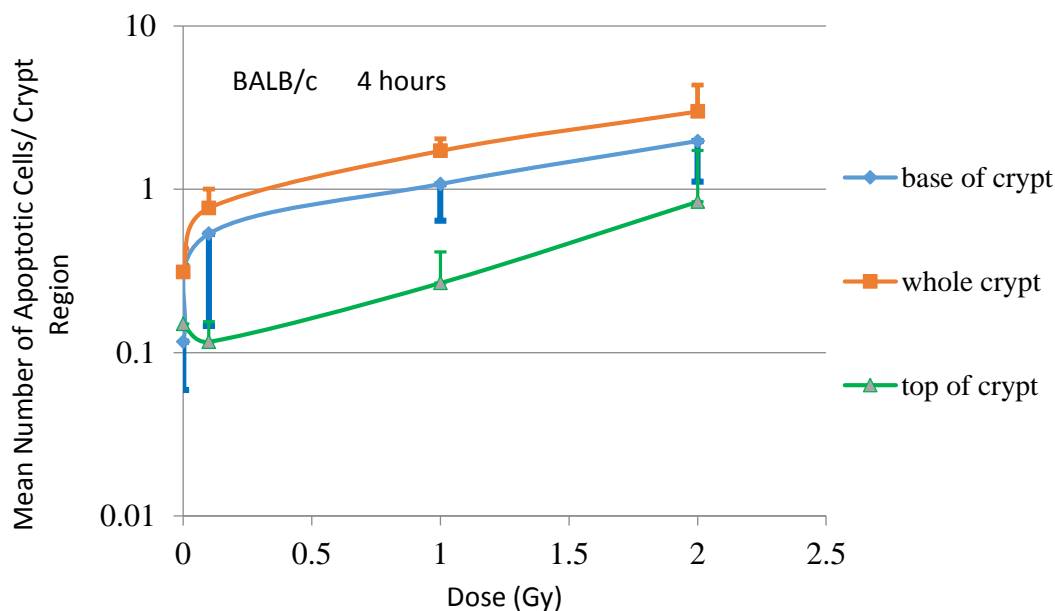
Figure 19:   Apoptotic dose-response by crypt region in BALB/c mice. A greater than expected number of lesions for the low dose of 0.1 Gy are observed. Notice also the small contribution of the top region to total lesions as compared to the basal region.
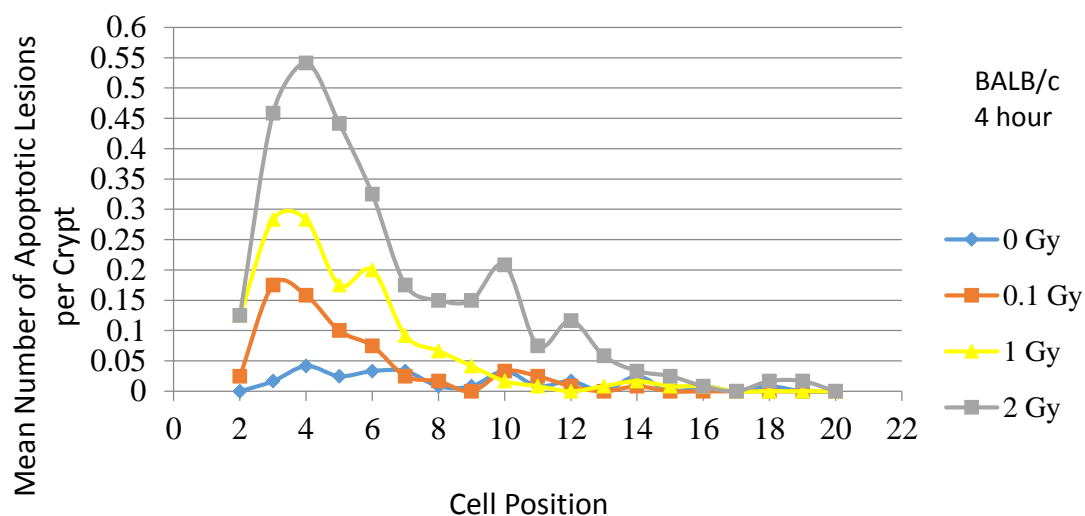
Figure 20:   Cell position in intesinal crypts of apoptotic lesions. This is four hours post-exposure in BALB/c mice. Most apoptoses occur in cell positions 1-6, the stem cell region of the crypt.

In order to provide an indirect comparison for the reader between different doses in BALB/c mice which underwent proton exposure and C57BL/6 that experienced gamma rays (both a 4 hour time point), calculations of the percentage of crypts
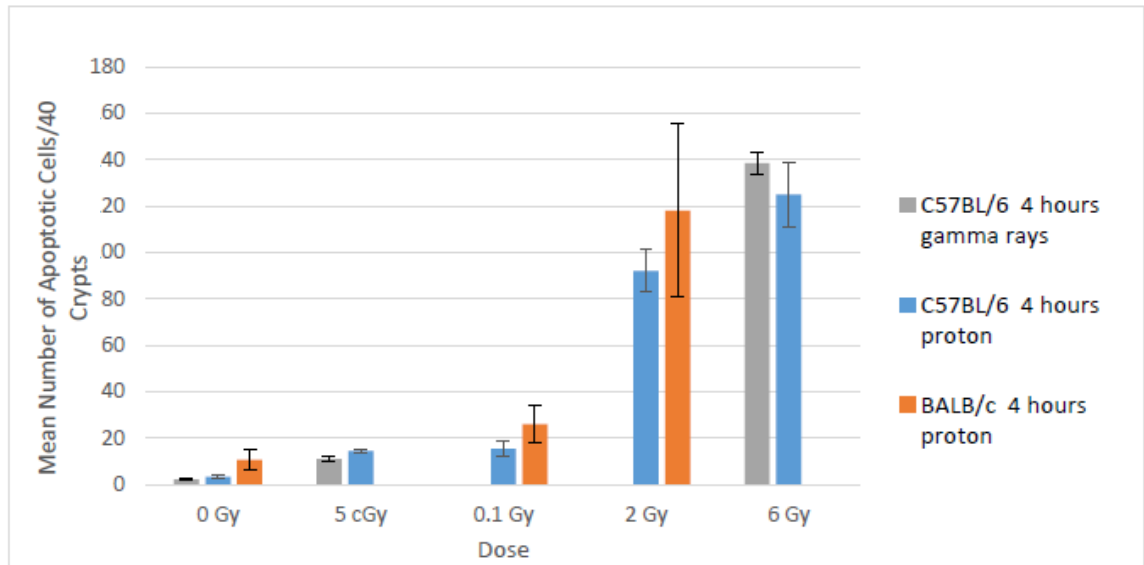
Figure 21:   Inter-strain comparison of apoptoses after proton exposure.

expressing different frequencies of lesions (0, 1-2, 3-5 or 6+ lesions in a single crypt) were made (Figure 22). Each strain of mouse follows a stair step dose-response in this figure showing that at higher doses it is not only the total or mean apoptotic lesions which increase; it is also the mean lesions per crypt. It is important to note that there are not simply a few crypts with many lesions that skew the data. Instead this figure displays that as the dose increases the uniformity of multiple lesions is real in the intestine after WBI and this can have implications for the health of the organ as a whole and not simply one or two damaged areas. This data is difficult to directly draw conclusions from as the doses are different in each group. Speculations can be made on the potential mechanisms

66

underlying the different extents of damage based upon the unique properties of each experiment, however, to further review the literature (see Discussion).

3.2.2.3 Immunohistochemical Confirmation of Apoptotic Findings

The ApopTag® kit was used as described previously to immunohistochemically confirm our quantification of apoptotic lesions in BALB/c mice mentioned above. The TUNEL-based kit reveals cells likely undergoing apoptosis as bright red against a blue DAPI nuclear stain (Figure 23). Representative images of this work at each dose point are shown and staining was quantified using the ImageJ software.

The quantification of fluorescence confirmed our findings in Figure 18 of significant differences in apoptotic lesions between the 1 Gy and 2 Gy groups from controls when quantified visually using H&E-stained sections. Those same groups were significantly different (p-value < 0.05) from 0 Gy in terms of CTFF and there was in fact a stronger statistical difference between the 2 Gy group and the controls when measured this way (p-value < 0.001) (Figure 24). Furthermore, 2 Gy was also found to be significantly different from both the 0.1 and 1 Gy groups (p-value < 0.05). One can infer from this data when compared to Figure 18 that our visual estimates of apoptosis are conservatively accurate. Because the blinded visual quantification method was accurate and did not overestimate damages to the intestine (it actually underestimated them), the methodology was continued to be used for other strains and time points of samples.
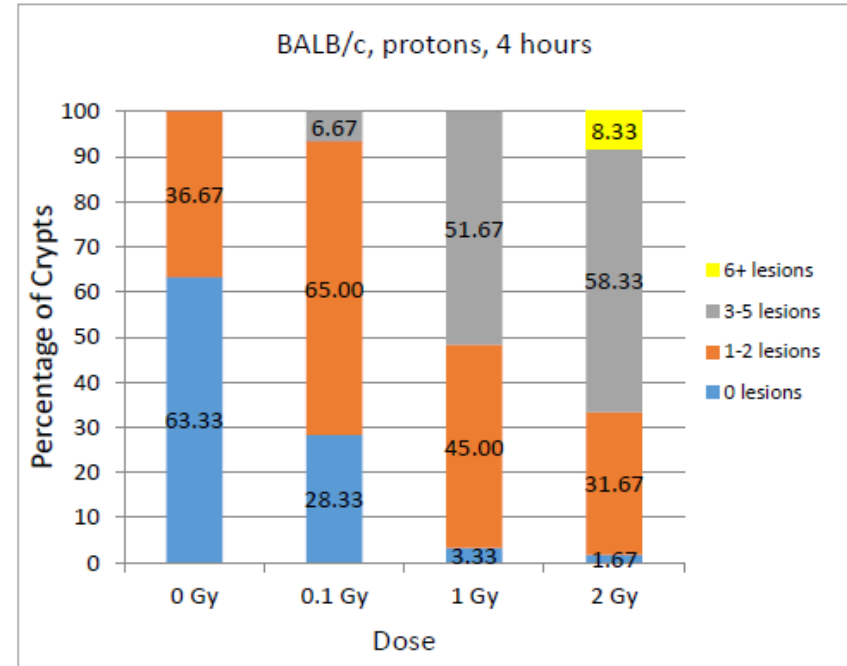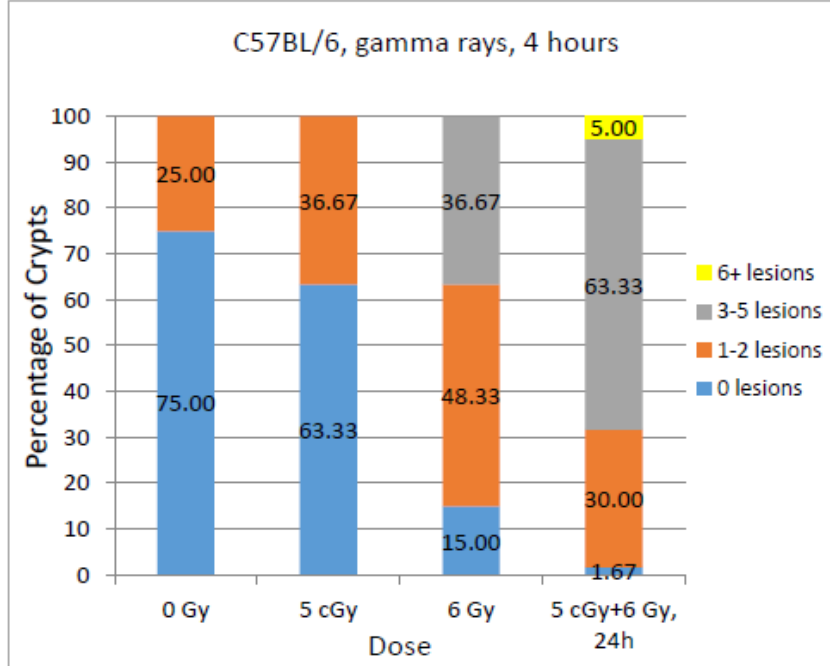
Figure 22:   Apoptotic lesions compared in C57BL/6 and BALB/c after varying radiation qualities. Lesions are shown as a frequency of increasing count in percentages of the total crypts measured.
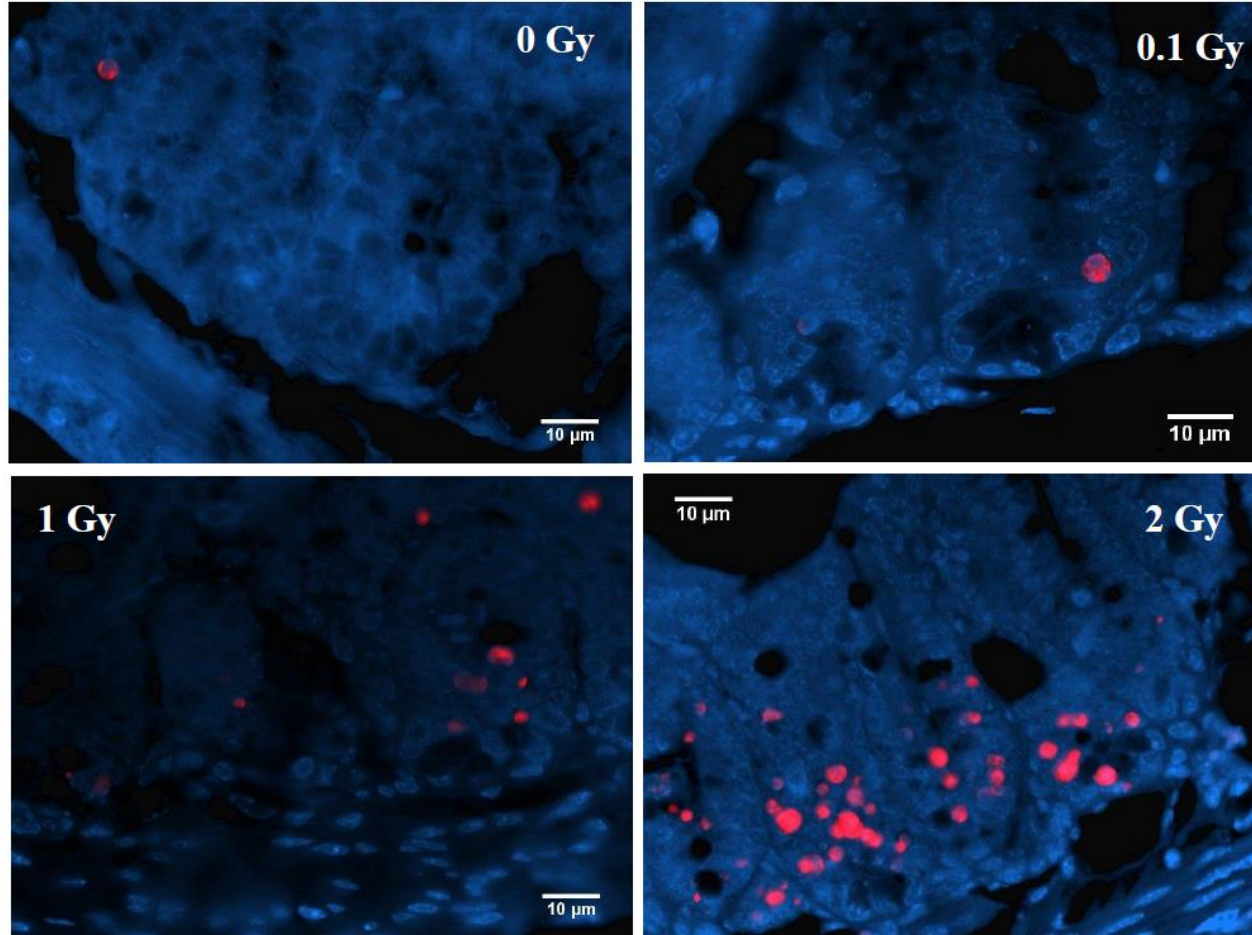
Figure 23: Fluorescence of apoptotic cells. Images captured of apoptotic lesions in BALB/c mouse intestine following varying doses of proton exposure using fluorescent microscopy. The red is indicative of damaged DNA, staining free 3'-OH ends of DNA. The blue is a DAPI nuclear stain. Notice the marked, dose-dependent difference in the presence of apoptosis between low and high doses.
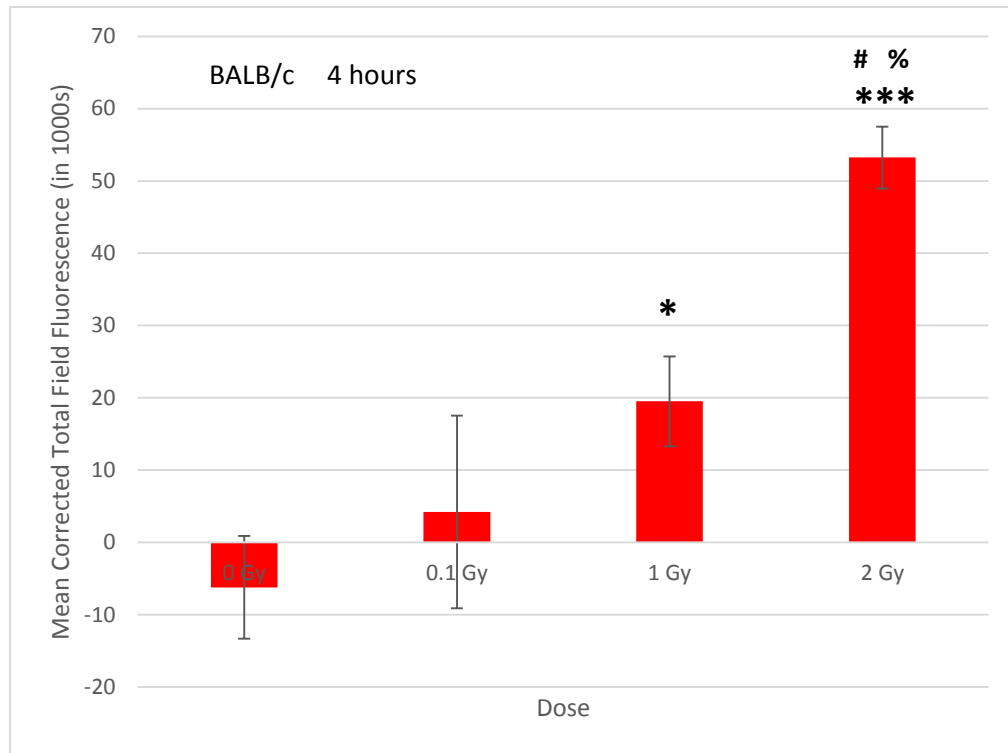
Figure 24: Mean fluorescense of apoptotic lesions. This methodology confirms our findings using H&E staining. *p-value < 0.05 as compared to 0 Gy. ***p-value < 0.001 as compared to 0 Gy. #p-value < 0.05 as compared to 0.01 Gy. %p-value < 0.05 as compared to 1 Gy.

3.2.3 Alterations in Villous Area

Daughter cells from crypt stem cells require 3-5 days to proliferate and move up to the villous tip and be sloughed away as waste (Somosy et al., 2002). This time frame is important when studying acute intestinal damages and, more importantly, subsequent recoveries. When irradiation kills stem cells and some differentiated cells in the intestine, these cells never move up the villous length to replace that vital micro-organ. Cells will continue to slough off of the villi, however, into the lumen of the intestine causing the villi to become flattened and dysfunctional (Morris, 1996). The villi of the intestine are critical to a human being's everyday health as they absorb nutrients and maintain the

70

actual interaction of the small intestine with the rest of the body (Sarna and Otterson, 1989). The crypts maintain the villi, but the villi maintain the human body's nutrients. There is a reason that one of the major pathways in which radiation is lethal is through the GI system. The higher portion of the GI tract is required for energy (nutrient absorption) and the lower portion of the GI tract is required for hydration (water retainment in the colon in proper balance). Death of an organism from the GI syndrome is likely ultimately due to a loss of proper functioning of the intestine (Schuller et al., 2006). We therefore decided to observe the small intestinal villi for shrinking after radiation exposures in this work as it has not been well-characterized shorter time points, low doses or for protons.

The first time point, 4 hours, seemed to have an effect on villous area for the high dose of 6 Gy (Figure 25). Each dosage group and the controls were significantly different from this one (p-value < 0.05). However, this data is not necessarily what has been shown before in the literature. Other studies have typically observed the villi at 3 days, but there was one observation with a shorter time point of 6 hours. In this study, villi did not measure as atrophied until the 3 day time point after 5 cGy of gamma radiation in C57BL/6 mice (Brennan et al., 1998). That study did not provide a high dose observation, however. Another study using in rats did show villous atrophy at 24 hours after irradiation (Karatzas et al., 1991). 4 hours is a short time point and it is doubtful that the villous would shrink by that time. Considering the fact that the GI syndrome takes a matter of weeks to develop and kill someone after radiation exposure, and the fact that the intestine requires 24 hours to turn over, these numbers should be carefully considered

71

when drawing conclusions. The BALB/c mice exposed to protons and sacrificed four hours later did not exhibit any differences in villous morphometry (Figure 26). Although we cannot compare this side by side with the C57BL/6, gamma data, it is an example that 4 hours may be too soon for villi to be changing.

The longer time points of 3 days and 21 days had significant changes in villous area after irradiation. This certainly is a possibility as both of these time points are
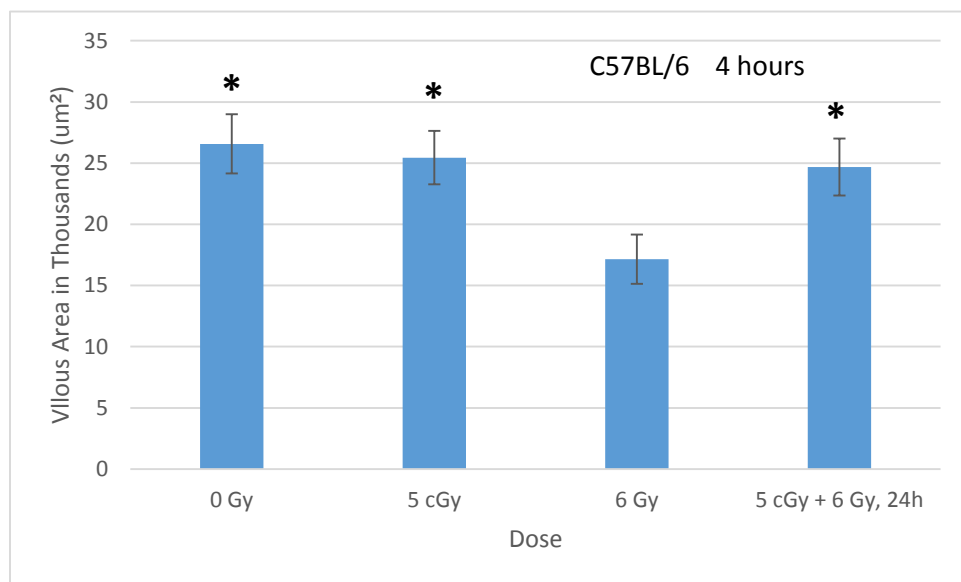
Figure 25:   High dose decreases villous area 4 hours post-IR treatment. *p-value < 0.05 when compared with the 6 Gy group.

beyond the 24 hour turnover cycle. In fact, most of the literature states that villous damage reaches a peak in mouse intestine at 3 days after high doses of x- or gamma rays of approximately 10 Gy (Kamel et al., 1988; Brennan et al., 1998; Kim et al., 2012). It is alarming to see villous atrophy at just three days and then see it prolonged to 21 days in the data presented here. Prolonged villous atrophy does not peak past 7 days according to

the literature, but our weight loss data for the 21 day group do correspond with this data as the high dose group continued to lose weight from day to 11 to day 16 post-irradiation (Carr and Toner, 1972; Rao and Fritz-Niggli, 1988). As stated previously, villous atrophy is not always recognized enough in discussion of ARS, but it is known from other diseases like celiac disease that the changes in villi like those observed here cause chronic abdominal pain, weight loss and diarrhea (Cummins et al., 2011). It must be said again
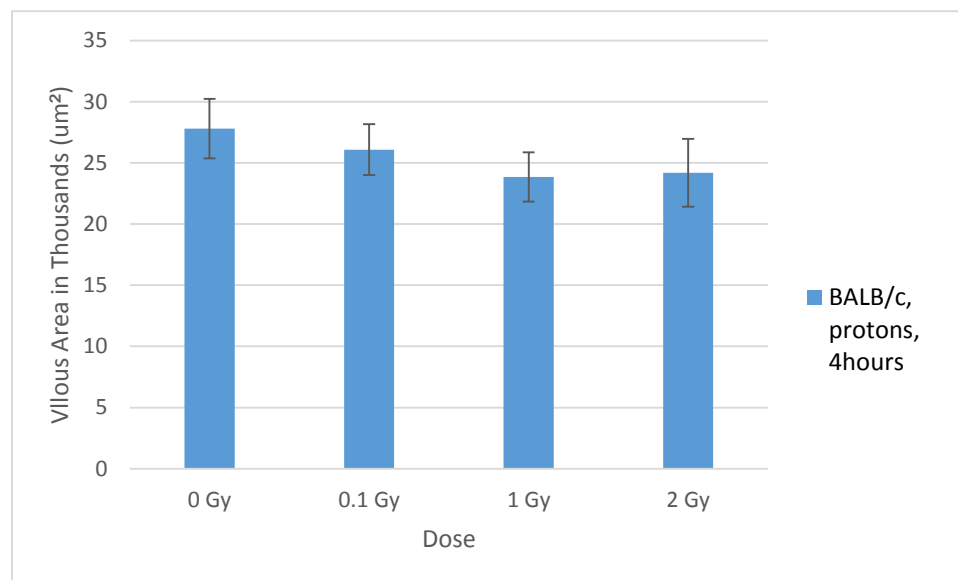
Figure 26: Proton irradiation in BALB/c mice does not elicit villous area changes.

that these can harm an astronaut's performance, especially if symptoms last for multiple weeks or days. Figure 27 reveals the significant differences at 3 days between both irradiated and control groups as well as the low and high dose. Figure 28 is representative of the 21 day time point. Each irradiated group experienced a significant decrease in villous area at three weeks post-exposure. Interestingly, the high dose group was also different than the 7 day combination group indicating a protective effect of the priming
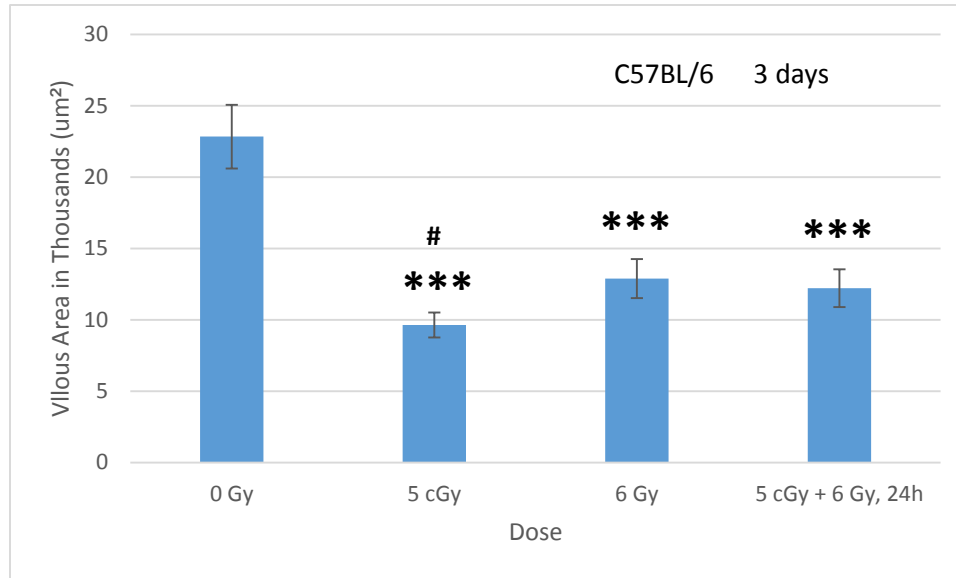
Figure 27: C57BL/6 experience smaller villous structures three days after exposure to IR. ***p-value < 0.001 as compared to 0 Gy. #p-value < 0.05 as compared to 6 Gy.
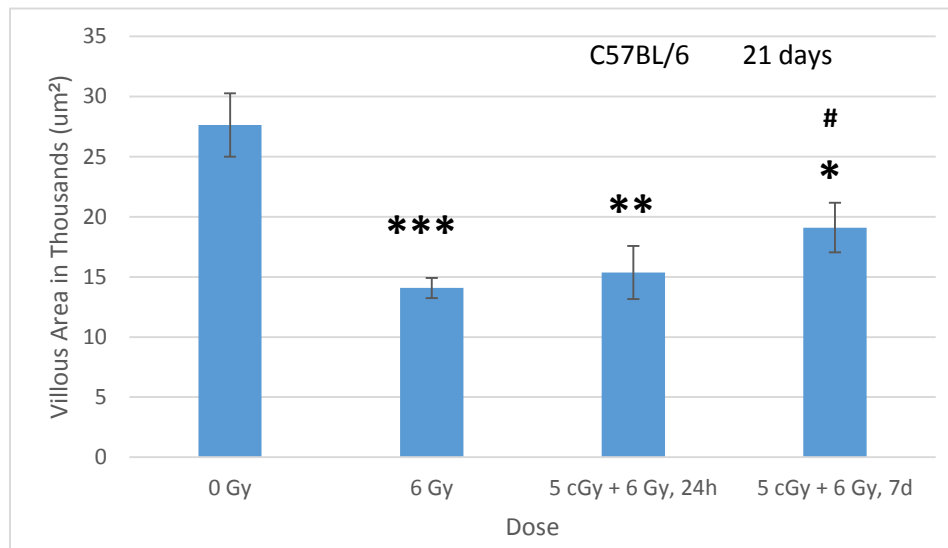
Figure 28:   Villi significantly shrink in total area three weeks post-treatment with gamma rays. ***p-value < 0.001 as compared to 0 Gy, **p-value < 0.01 as compared to 0 Gy, *p-value < 0.05 as compared to 0 Gy, #p-value < 0.05 as compared to 6 Gy.

dose (p-value < 0.05). A figure of combined findings of villous changes is given in

Figure 29.
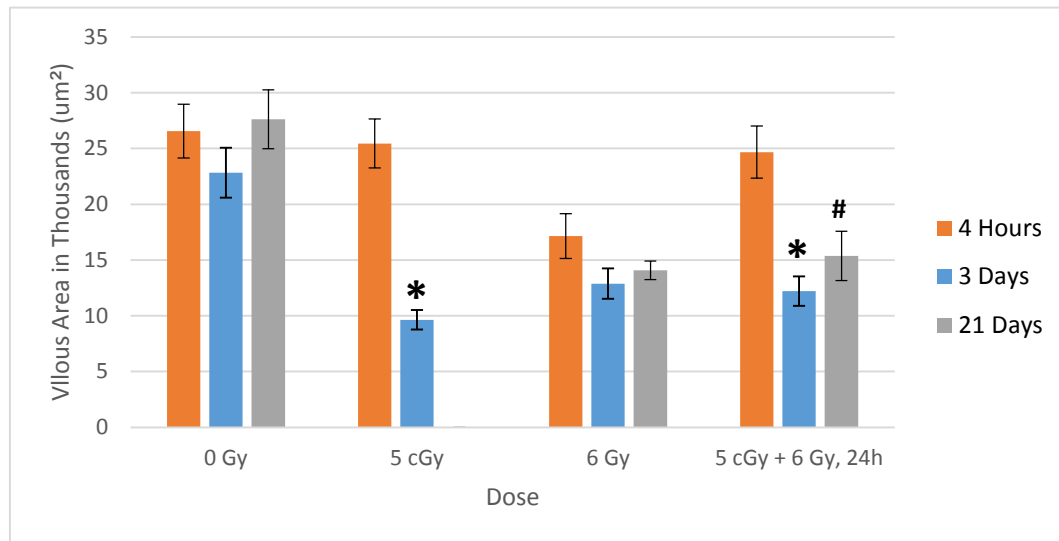
Figure 29:   Villous area grouped by dose for varying time points. *p-value < 0.005 as compared to 4 hours for the same dose. #p-value < 0.05 as compared to 4 hours for the same dose.

This data has interesting implications to consider in regards to the villi's

dependence upon crypt survival and regeneration in order to maintain their function. A

comparison of crypt apoptosis and microcolony survival tracked against delayed villous

atrophy could provide interesting indicators of long-term villous shrinking. The

significant loss of villous area after the 5 cGy dose at only 3 days post-exposure is

certainly concerning for astronauts in space-flight. This dose would be on the low end of

what could be received in a SPE and could be very harmful to a mission's success

(Wilson et al., 2011). Although experimentally it can be said that radiation caused the

observed villous atrophy seen here, other physiological processes must be considered

when explaining a potential cause for the prolonged atrophy at 3 weeks post-irradiation (see Discussion).

3.2.4 Protons Affect Mucosal Surface Area in BALB/c Mice

Mucosal surface area analysis, or stereological analysis, is very much related to the villous morphometry inquiry above. When discussing the mucosal surface area you are addressing the villi as they exist to increase surface area of the intestine. A stereological analysis was conducted on our BALB/c mouse samples. The extremely long-natured work of this assay makes the villous morphometry assay a more logical choice and so it was not performed on our other samples. The comparability of these two assays to one another is unknown; but below demonstrates data that was not observed in the villous morphometry data which implies that the two should not be considered replacement assays for one another. BALB/c mice showed a significant decrease in mucosal surface area as compared to control animals after proton irradiation (p-value < 0.05) (Figure 30). How can the same animal samples show no change in the area of their villi, which make up most of the surface area in the intestine, but display significant changes when measuring mucosal surface area? The answer most likely lies in the assays themselves. The mucosal surface area analysis involves a series of calculations which give small measurements and encompass the structure as whole, making it well-suited to discover even small changes. Measuring villous area, however, is a very finite process observing only one structure on the tissue that may not change at a 4 hour time point based upon the physiology of the mouse intestine and the 3-5 period needed to replace cells at the villous tip (Somosy et al., 2002).
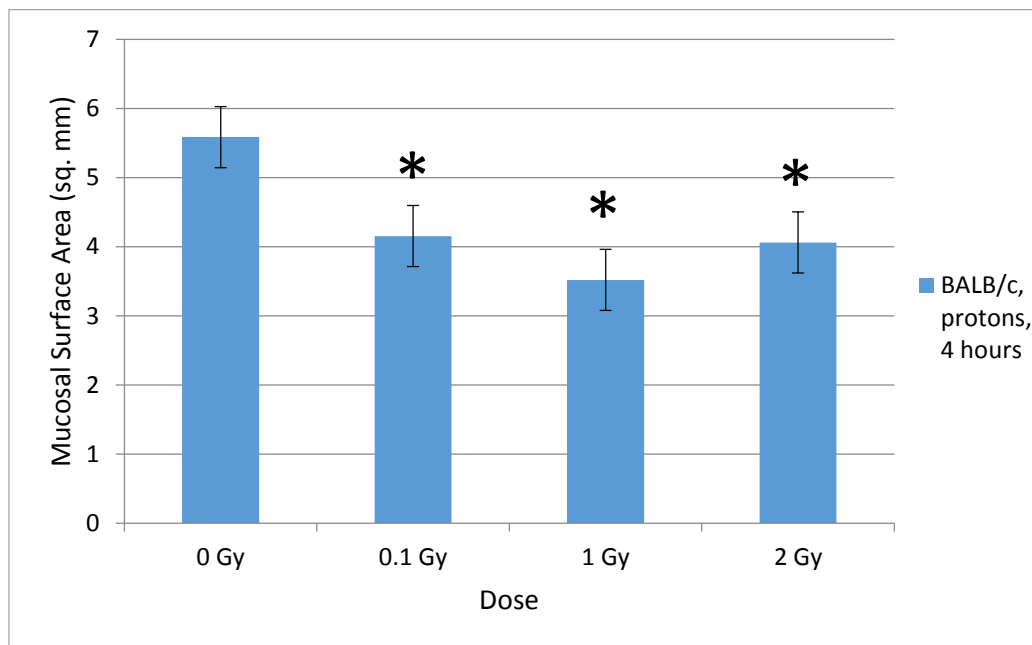
Figure 30: BALB/c mice show decreased surface area of the intestine following proton exposure. *p-value < 0.05 as compared to 0 Gy.

3.3   DISCUSSION

Villous area in this work was likely the result that was the most unexpected. The significant shrinking of villi persisted for 3 weeks after irradiation and was significantly changed in all 3 irradiation doses by 3 days post-exposure. Even the high dose of 6 Gy was found to be altered significantly at only 4 hours post-irradiation. The significant change at only 4 hours post-irradiation does not match the findings of the literature and should likely be investigated again. The 3 day and 21 day alterations are certainly possible after irradiation exposure, however. Of particular concern was the large decrease in villous area after the low dose of 5 cGy at the 3 day time point. The area shrank a

77

substantial amount just between 4 hours and 3 days and a rapid change like that can cause the symptoms of ARS (Sarna and Otterson, 1989). Villi atrophy is not a disease process limited to radiation exposures and causes similar physical problems no matter its origin (Cummins et al., 2011). It has even been suggested after radiation exposures that changes to villous structures long term, after an initial radiation response that is primarily cell or molecular based, become due to other organ systems and processes (Somosy et al., 2002). One such potential controlling organ system is the neuromuscular system which operates the smooth muscle of the intestine (Somosy et al., 2002). This idea should be entertained based upon the data presented here. At 21 days post-irradiation, there was not any more apoptosis occurring. This implies that cell proliferation has been restored to their normal levels and this process is responsible in normal intestinal physiology for replacing cells in the villous that were being lost (Potten, 1991). Yet, changes in villous area were still being seen. One should consider the measurement of area: it encompasses length, width and all sides when measuring an oddly-shaped structure such as a villous. A measurement such as this will detect changes that are related to the cell replacement in the tissue, but not limited to it. Indeed other studies have shown villous changes in multiple parameters, not just length or area (Somosy et al., 2002). Further support for this theory lies in the fact that hyperthermia produces similar effects to intestinal villous structures and is known to be caused by alterations in the neuromuscular areas of the intestinal wall (Indran et al., 1991). Moreover, one study using both gamma radiation and a drug which adjusts the activity in the mucosal wall due to neuromuscular function found that villous atrophy was present after both conditions as well as injured intestinal muscle (Indran et al., 1991). Another study explored the use of a therapeutic drug known

to mildly inhibit the smooth muscle function of the gut in conjunction with radiation and found that attenuation of villous atrophy was achieved (Carr et al., 1991). A literature search did not produce any relevant information on this topic, but the potential neuromuscular involvement in ARS pertaining to the gut should be studied further in the future due to the promising data and published work shown here.

In analyzing our results, overall we found that apoptosis in the intestine of C57BL/6 mice after gamma irradiation decreased over an extended time period from 4 hours to 21 days and this was not surprising. What was intriguing about the apoptosis data was the rapid recovery that took place between the 4 hour and 3 day time point between doses. The low dose of 5cGy did not induce any more damage at 4 hours than it did at 3 days while the two higher doses of 6 Gy and 5 cGy+6 Gy induced a considerable amount more of damage at 4 hours versus their 3 day counterparts. What's important about this statement is that the higher doses, even with their disparate outcomes in damage at 4 hours, were not significantly more damaging at 3 days than the 5 cGy dose in terms of apoptotic lesions. This means three things: that a substantial amount of clearing of apoptotic cells must occur for high doses between the 4 hour and 3 day marks (which is obvious), that apoptotic induction likely stops between the 4 hour and 3 day marks (obvious according to the literature) and, less obvious, a molecular distinction must be taking place between low and high dose responses in the intestine after irradiation which maintains apoptotic cells at relatively low numbers after low doses as compared to high doses during the initial storm of cell killing and keeps the low dose levels fairly constant into the 3 day time point (Potten, 2002). Further complicating this

difference in initial response is the hypersensitivity displayed by the stem cells in the

crypts to low doses. The dose response of apoptosis follows a logarithmic curve in which

more damage is observed at the low dose of 5 cGy than is expected for a normal linear

response.

The hypersensitivity at low dose can be explained as mentioned previously

regarding rapidly proliferating cells being more susceptible to radiation killing due to the

increased likelihood their genetic material will be hit close together in time and space

with radiation. These cells also have less time to undergo DNA repair between cell cycles

(Hall and Giaccia, 2006). It was also discussed that the lower regions of the crypts, where

the stem cells are, is where most of the apoptosis occurs. It is important to mention a

basic principle of radiation biology for the reader to ensure the use of best practices that

radiation scientists prefer to describe cell killing: the linear-quadratic model. In simplified

terms, this model places cell killing into a mathematical model in which there are two

components in an equation, $S=e^{-\alpha D - \beta D2}$, where αD and βD^2 can best be described in lay

terms as the portions of cell killing that occur. S is cell survival, D is dose, α and β are

constants and e is the natural log (Hall and Giaccia, 2006). The αD component can be

thought of as killing based upon the intrinsic radio-sensitivity of a cell population, or the

hits to a cell that cause irreparable damage initially. This is independent of dose rate. The

βD^2 component can be thought of as cell killing which is secondary damage that can

potentially be repaired. This is dependent on dose rate. The ratio of α to β is useful for

mentally comparing doses between cells. For example, a slowly dividing cell population

receiving the same dose as a rapidly proliferating one will have a smaller α/β (meaning a

smaller α and a bigger β). A rapidly dividing cell will have a larger α as there will be

fewer damages that have a chance to be repaired compared to the slower cells. Therefore, the rapidly proliferating cells' α contribution to cell killing is larger than their β. Intestinal stem cells are examples of cells which have a large αD component in the linear-quadratic model. What about the high dose of 6 Gy? Higher doses will eventually saturate the cell population in a way with cell killing that a plateau of damage is reached in which increasing dose will not induce many more apoptotic lesions.

In returning to the question at hand, why do the levels of apoptosis after high dose drop so drastically indicating recovery of a greater percentage after the 4 hour peak but the 5 cGy levels seem to remain somewhat constant at both 4 hours and 3 days? Perhaps there is a mechanistic explanation for this phenomenon of differential dose responses at the molecular level. It may be a simple explanation that after a greater amount of apoptosis occurs, a greater amount of subsequent cell proliferation occurs. It is found in the literature that there is a rapid upswing in cell proliferation after apoptosis in the intestine (Potten, 1991). This makes sense as to how the 6 Gy samples would have such a small percentage of apoptotic induction at 3 days compared to 4 hours. It could be possible that the 5 cGy-exposed tissues spare more cells from radiation-induced apoptosis through other cellular pathways than death as some damage may be on the cusp of being irreparable versus repairable. If this is the case, cells may linger that would have undergone greater damage in high dose and been killed. Over time, the cells may eventually need to undergo apoptosis anyway which could explain the lasting effect of apoptosis seen at 3 days in this work. DNA repair is one possible pathway which could differ between low and high doses in intestinal crypts. Furthermore, why are the stem

cells in positions 1-6 of a crypt so much more sensitive than the few above them that are still differentiating and also relatively radio-sensitive compared to most tissues? Cell cycle kinetics and the lack of time for DNA repair is again likely the cause whereas the higher, transient cells either do not leave G1 or enter S, G2 and M much slower and less often. It is plausible that DNA repair responses differ between the lower and higher regions of the crypts. The higher regions may utilize NHEJ more than the lower regions simply because of their transient versus stem cell designations as NHEJ is performed in G1 and HR requires a sister chromatid. HR is a more elegant DNA repair pathway than NHEJ, which can be error-prone simply joining broken ends of DNA together (Hartlerode and Scully, 2009). Although the lower regions may have the HR capabilities present, the damage from radiation may just be too great to overcome. The upper transient cells, however, some of which are known to become stem cells upon death of current stem cells, may be able to repair damage as they are currently in a G1 state. If the damage is not properly repaired, however, or if it is repaired incorrectly as it can be in NHEJ, and one of these cells must now become a stem cell or tries to enter one more division, apoptosis can then occur at a later time. This is a possible explanation for the later induction of apoptosis seen here at 3 days. At higher doses, the damage is likely too much to overcome for both the stem cells and some of the transient cells and so no cells attempt repair with NHEJ but instead apotose.

If the linear no threshold model (LNT) is followed, which states that radiation, even at extremely low doses, is a health risk for individuals undergoing exposure, then the possibility of the questions above must be considered (Higson, 2005). For purposes of

space flight and the occupational nature of the endeavor, the LNT model must be appreciated in some capacity in order to protect astronauts from harm in radiation exposures. To explore the idea of differing DNA repair or other responses in the crypts of the small intestine by region or by dose, it must first be established what is known already. Only recently has knowledge emerged regarding DNA repair pathways and their specific functions in intestinal crypt cells. It was actually shown very recently that in the small intestines of mice after radiation exposure, stem cells in positions 1-3, some of the more sensitive cells to likely undergo apoptosis, do indeed utilize HR and more so than the differentiating and transit cells above them (Hua et al., 2012). This implies that these lower region cells do not undergo apoptosis after radiation exposure more frequently than do the cells above them due to an inability to utilize HR or a predisposition to use NHEJ. A different reason for these cells' tendency towards apoptosis must be the cause of their demise. It should be noted, however, that some of the literature states that radiation-induced apoptosis more often occurs in cell positions 4-5 (Potten and Booth, 1997).

There is a school of thought that excessive apoptosis is actually a protective measure in the small intestine, utilized by low dose-exposed cells as much or more than cells undergoing high dose exposures. One can observe basic properties and happenings in the colon and small intestine to become a believer of this theory. The small intestine is much more sensitive to IR than the colon when observing apoptosis (Potten and Booth, 1997). Some of this is a matter of physics and DNA repair times. Again, small intestinal stem cells divide every 24 hours while the colon only turns over approximately every 7 days (Potten and Booth, 1997). This apoptosis is usually viewed as a damage marker, but

the colon has far greater rates of cancer than the small intestine (Potten and Booth, 1997). Apoptosis is actually a spontaneous process in the small intestine, protecting itself from an excess of as many as 120 cells produced per stem cell, and occurs normally and absent of p53 (Potten et al., 1994). This process is not observed in the colon (Potten and Booth, 1997). Upon radiation exposures, p53 is found to be increased in both organs, but is not located near the stem cells in the colon, further explaining why the same radio-sensitivity is not observed between the two tissues (Potten and Booth, 1997). The increase in p53 in the small intestine holds some of the cells at G1 in the cell cycle (Potten, 2002). It is plausible to think that this G1 hold is why 3 days after irradiation, the data presented here shows apoptotic induction continuing after 3 days at the low dose of irradiation. Those cells which were not damaged as severely are held and may still undergo apoptosis later.

With regard to low doses, there is certainly evidence for different pathway or gene expression responses when compared to high doses of radiation. X-rays and gamma rays have both been shown to induce gene expression of profiles that vary considerably between low and high doses of IR (Ding et al., 2005; Zhou et al., 2006; Zhang et al., 2008). There is also evidence which shows varying gene expression after charged particle exposures in organs such as the brain (Baluchamy et al., 2010a; Baluchamy et al., 2010b, c). There is little published work, however, regarding charged particle exposures and gene expression in the intestine. DNA repair proteins have been profiled after proton exposure as well, but I have not been able to find any work that is both *in vivo* and relating to intestinal tissues (Roig et al., 2009; Tariq et al., 2011). Taken together, this evidence and follow-up hypotheses provide the basis for the work shown in Chapter 4.

Chapter 4: The Effect of Gamma Ray and Charged Particle Exposures on Intestinal Gene Expression and Other Molecular Endpoints

4.1   INTRODUCTION

For purposes of this work, intestinal responses to radiation exposures are extremely important to characterize, discover and mitigate when possible due to two important health outcomes: acute radiation enteritis and carcinogenesis. The first is characterized by symptoms such as fatigue, nausea and vomiting. The underlying cause of this condition is dysfunction of the intestinal villi which is caused by a general break down of the small intestinal structures on a microscopic level (Cummins et al., 2011). In turn, this too likely has a cause beginning at the intestinal crypts whose stem cell function feeds the daily replacement of villous cells. If the crypts are dying or delayed in proliferating the differentiated cells around them, the villi begin to break down at the tip and are unable to replace the normal, daily loss of cells (Potten et al., 1994). Radiation exposure happens to express the most damage concerning the intestine in the basal region of the crypts following the standard dogma of being the most effective where the stem cells are (Potten, 2002). The phenomenon of apoptosis occurring primarily in the basal region of the crypts after radiation exposure became a primary focus of this work after the first samples studied here followed that same process.

Many questions are asked when learning about the process above and studying intestinal radiation exposures such as: 1) what molecular mechanisms are taking place to heal or mitigate damages between peak apoptosis times and later time points so quickly? 2) Is there an immediate difference in gene expression responses to radiation insults

between low and high doses? Or is that brought on over a period of time? 3) Are there other reasons why the crypts are more radio-sensitive than their surrounding tissues besides cell cycle such as DNA repair profiles? 4) How does the complex relationship of apoptosis and cell proliferation after exposure differ between low and high doses? 5) How does the colon differ from the small intestine in these processes and what specifically within them makes the colon susceptible to cancer in some way that the small intestine is not? 6) How do protons vary from gamma rays in all of these same inquiries? It is precisely these questions we were asking when formulating a plan for the next step of this project.

In studying apoptosis, it was obviously important to characterize the samples for the different damage endpoints to gain more knowledge about the C57BL/6 and BALB/c strains and provide new hypotheses and directions of study. All the work described in Chapter 3 provided the framework to try to answer the question that is so difficult in science: why is this happening? In moving into the molecular biology arena to focus on the mechanistic causes of the data, there were specific things that were hoped to be addressed.

DNA repair is largely studied pertaining to differences between two pathways: NHEJ and HR. In thinking about radiation as it is received by a tissue, especially in the case of whole body irradiation like our study, the tissue is bombarded fairly uniformly with ionizing tracks. These tracks will deposit energy uniquely, but indeed the seemingly radio-resistant top half of crypts, as has been discussed in Chapter 3, receive a dose

similar to that of the basal or stem cell region of the crypt. In Chapter 3 the point was made that rapidly proliferating cells are often more sensitive to cell killing by IR because of the availability of the genetic material to be ionized close together in time and space and the lack of time for DNA repair (Hall and Giaccia, 2006). Both of these are due to fast cell cycle time and the crypts are a hallmark example of this model of sensitivity to radiation exposure. It is conceivable that other mechanistic differences, not exclusive of but in addition to cell cycle kinetics, exist for the extreme sensitivity seen in the lower stem cells of the intestine. Perhaps in addition to a lack of time for DNA repair, different pathways of DNA repair are being utilized in different regions of the crypts. A similar question can be asked for the some of the unique responses observed in Chapter 3 between doses and time points in the assays described: what unique pathways due to gene expression are occurring between low and high doses, between radiation qualities and between mouse strains that may underlie some of the results observed in Chapter 3? These curiosities bring us to the next set of results.

4.2   RESULTS

4.2.1   DNA Repair Proteins

We chose to observe a protein from each of the DSB repair pathways as these are the most important DNA repair pathways when radiation is concerned. This is because radiation is most effective at cell killing when DSBs are caused (Hall and Giaccia, 2006). An example image of DNA repair staining with antibodies bound to XRCC4 (orange/red), a protein active in NHEJ, and Rad51 (green), which is active in HR, in the intestine is shown below (Figure 31). The small intestine in both C57BL/6 and BALB/c

mice were observed after exposures to 0 Gy and 2 Gy proton radiation. BALB/c was also

observed after 0.1 Gy proton radiation. Samples of colon were also obtained from

C57BL/6 mice and these samples were analyzed for the presence of XRCC4 and Rad51

as well at doses of 0 Gy and 2 Gy proton exposure. Small intestinal samples were

compared across doses within strain and between mouse strains. The samples were also

compared by crypt region, in which separate images were taken by the region dividing

the crypts in half longitudinally, across doses within strain and between mouse strains.

Lastly, the colon samples were compared across doses and against the small intestine of

the same mouse strain.
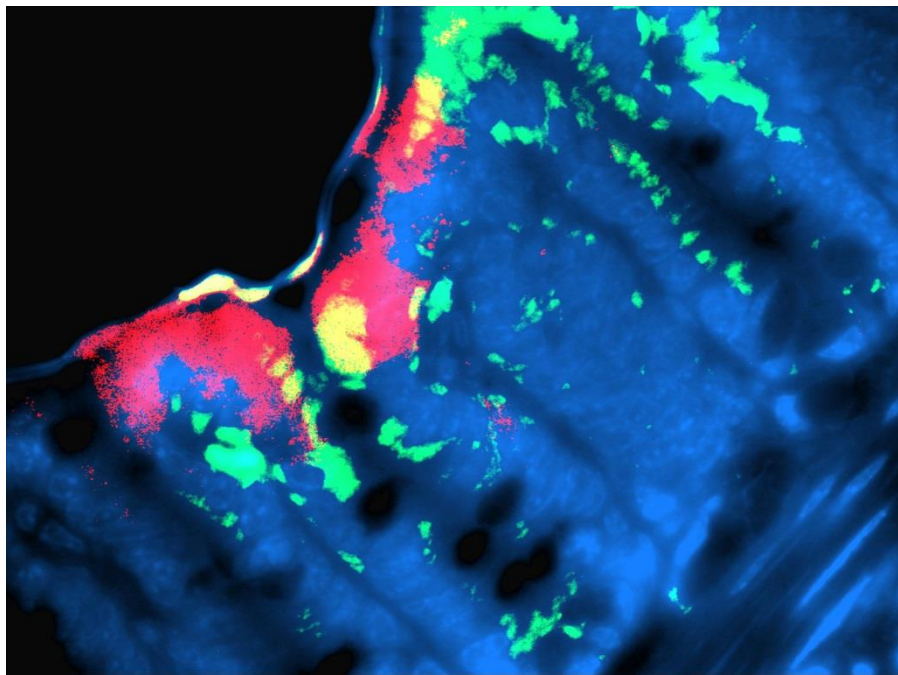
Figure 31:   Image of DNA repair proteins using fluorescent microscopy. The sample
shown is a BALB/c mouse small intestine after exposure to 0.1 Gy of protons.

The first figure displays the results for C57BL/6 mice (Figure 32). No significant differences were observed between doses of exposure. Figure 33 shows DNA repair
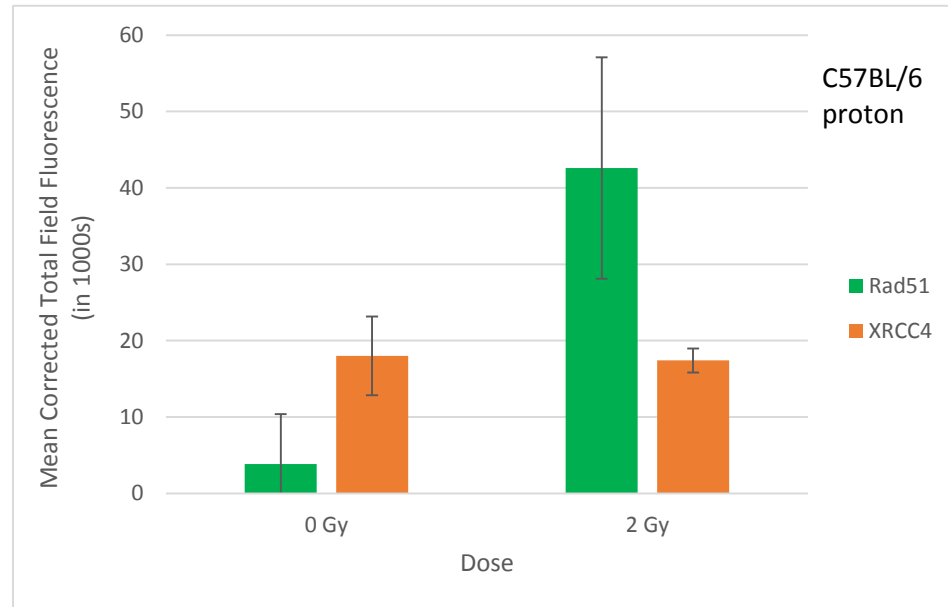
Figure 32:   DNA repair proteins in C57BL/6 mice after proton exposure. Groups were not significantly different in fluorescence.

protein expression by region of the crypt for the same set of animals. Expression of Rad51 was significantly increased in the upper region of the crypt after 2 Gy of radiation as compared to the 0 Gy upper region (p-value < 0.05). XRCC4 was significantly higher in the lower region of 2 Gy samples than the upper region of the same samples (p-value < 0.05). These results are counterintuitive to the idea that the stem cell region (lower portion) of crypts relies heavily on HR while the upper region uses NHEJ. However, as pointed out in Chapter 3, there is new evidence that supports this idea (Hua et al., 2012). BALB/c mice showed differences of significance in Rad51 expression between 2 Gy and 0 Gy samples (p-value < 0.01). XRCC4 in BALB/c mice was also present in greater
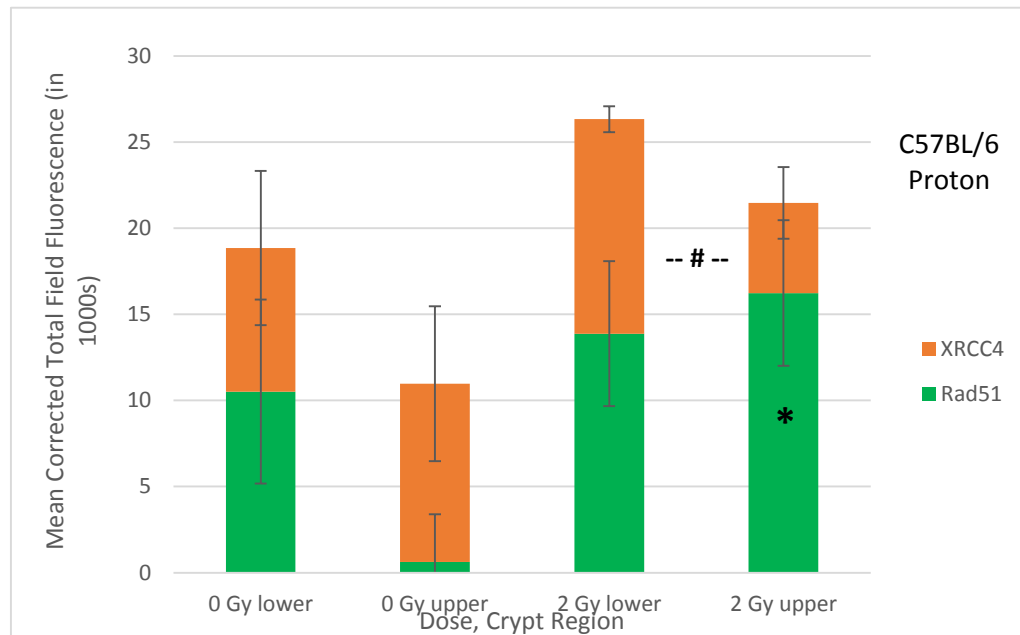
Figure 33:   DNA repair proteins in C57BL/6 mice by crypt region. *p-value < 0.05 when compared to Rad51 0 Gy upper. #p-value < 0.05 compared across regions for the same dose.

amounts than Rad51 in control samples (p-value < 0.05) (Figure 39). In analyzing Figure

34, it is important to point out to the reader the large negative values of Rad51 expression

in BALB/c mice for 0 Gy and 0.1 Gy animals. It is thought that this is a result of high

background staining of Rad51. However, the program used to quantify the fluorescence

of these images has a method built in which separates color channels and eliminates some

background. Additionally, the user must take sample areas from around the image in

order to first eliminate background before measuring area of fluorescent regions. The

background is subtracted from the fluorescent area before a quantity is provided.

Nonetheless, skepticism should be used in drawing conclusions about these values.
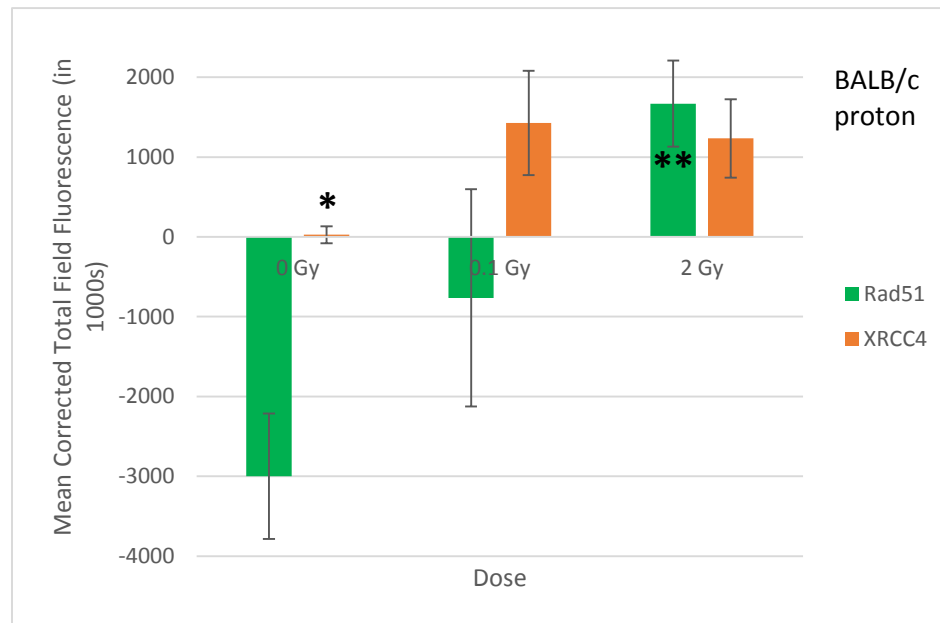
Figure 34:   DNA repair proteins in BALB/c mice after proton exposure. *p-value < 0.05, **p-value < 0.01, both when compared to Rad51 0 Gy.

BALB/c samples were separated by crypt region and quantified similarly to the C57BL/6 samples (Figure 35). For Rad51, the upper region in controls and the lower regions in both irradiated groups were significantly different from the lower region of control samples (p-value < 0.01 irradiated, p-value < 0.05 control). XRCC4 was present in greater amounts than Rad51 in control samples in both regions (p-value < 0.005 lower, p-value < 0.05 upper). This data supports the theory that HR is active in the lower regions of the crypts as an increase in expression in those regions was shown for Rad51 after irradiation.
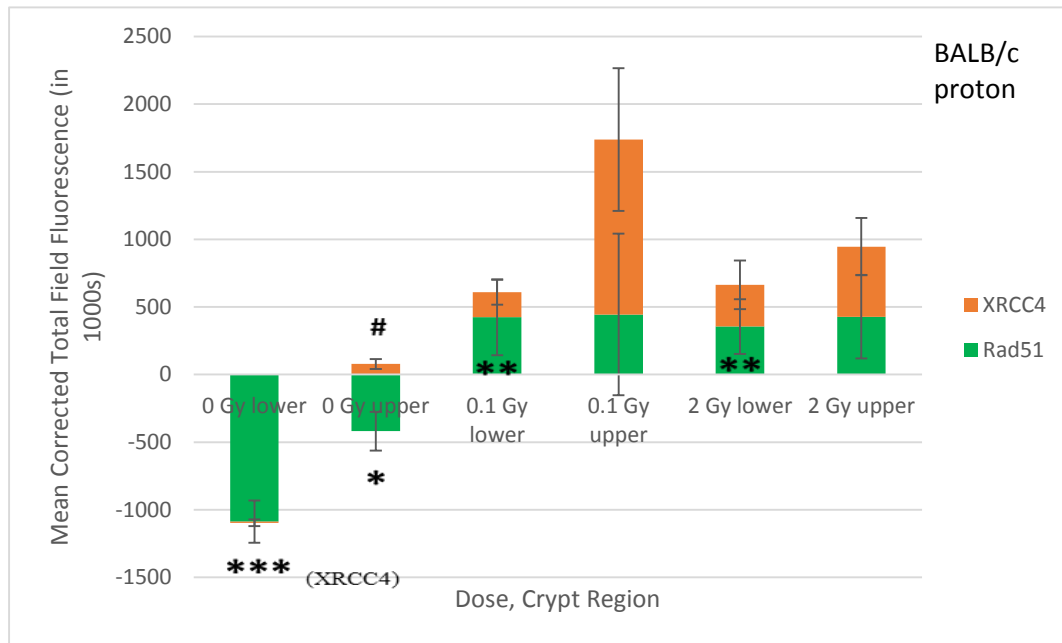
Figure 35: DNA repair proteins in BALB/c mice by crypt region. *p-value < 0.05, **p-value < 0.01, ***p-value < 0.005, all when compared to Rad51 0 Gy lower region. #p-value < 0.05 when compared to Rad51 0 Gy upper region.

Figure 36 compares C57BL/6 mice directly to BALB/c mice after charged particle exposures of 0 Gy and 2 Gy. BALB/c mice were shown to have significantly less expression of Rad51 than C57BL/6 mice in both control and irradiated samples (p-value < 0.05). This was not expected. In fact, a difference of expression in XRCC4 between strains would have made much more sense. BALB/c mice have two SNPs which make them deficient in expression of DNA-PKcs (Fabre et al., 2011). DNA-PKcs are known to be upstream in function of XRCC4 during NHEJ and so it would be logical to expect that a difference would be seen in XRCC4 expression between the two strains before Rad51. Evidence has been shown though that DNA-PKcs are not necessarily required for the
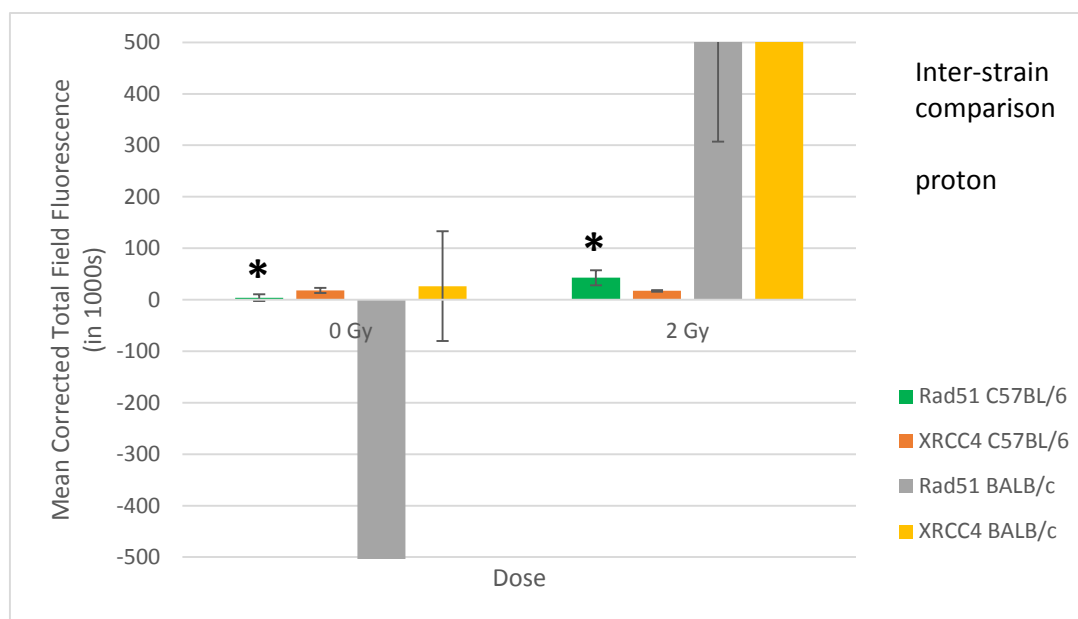
Figure 36: Inter-strain comparison of DNA repair proteins after proton exposure. *p-value < 0.05 compared to Rad51 BALB/c in same dose.

recruitment of XRCC4 to sites of DNA damage, but that does not change the surprise of this result (Mahaney et al., 2009). This could again be due to the high background of staining and that should be noted. When compared by crypt region, Rad51 in BALB/c mice was found to be significantly different from Rad51 in C57BL/6 mice in controls for both regions (p-value < 0.05) (Figure 37).

Overall, the most striking result was the observation of Rad51 being increased in expression following irradiation in lower regions of the crypts in BALB/c mice. The significant expression in C57BL/6 of Rad51 in the upper region after 2 Gy and XRCC4 being higher in the lower region after 2 Gy were also important. Based upon the intense apoptosis that is observed in the lower crypt regions due to the rapid proliferation rates of

93
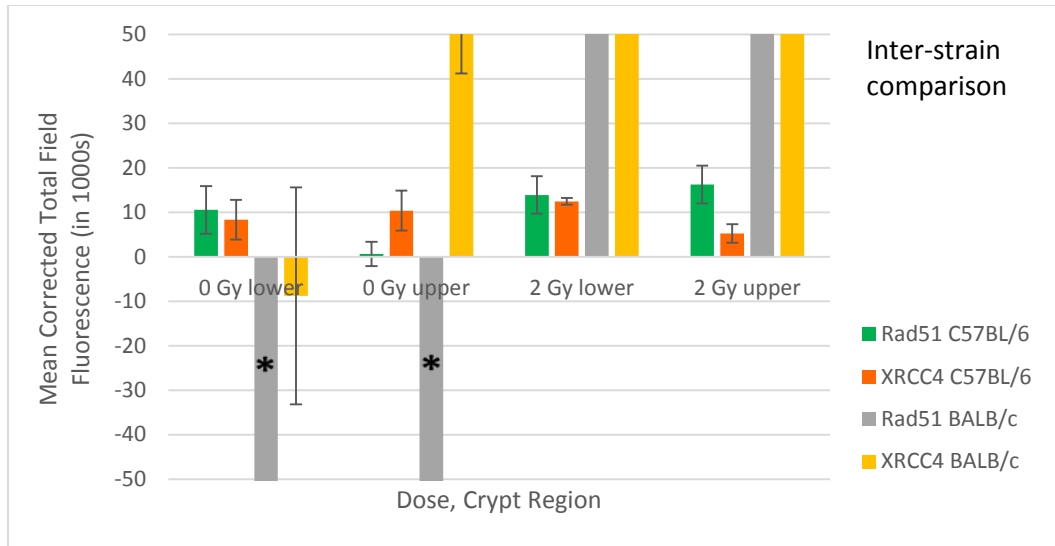
Figure 37: Inter-strain comparison of DNA repair proteins by crypt region. *p-value < 0.05 as compared to C57BL/6 same region and protein.

the cells there, it was hypothesized that HR would be the primary DNA repair pathway in those regions and that NHEJ would dominate any DNA repair processes occurring in the higher areas of transient cells. The staining of DNA shown here partially supports these concepts, but actually shows that both proteins are significantly present in both regions after irradiation. There seemed to be a large increase in Rad51 in BALB/c mice after 2 Gy proton exposure. Finally, at 0 Gy, there seemed to be more XRRC4 present in BALB/c and more Rad51 present in C57BL/6 at "rest' states. Together these results show that HR and NHEJ pathways are not limited to particular regions of the small intestinal crypts. This supports the notion that apoptosis is in fact a protective measure in the small intestine and is not a default process due to lack sufficient DNA repair moieties (Potten and Booth, 1997). BALB/c mice may utilize the HR pathway more than NHEJ in intestinal crypts following higher doses of radiation exposure relevant to space flight.

BALB/c expressed no significant changes in HR or NHEJ protein presence after the lower dose of 0.1 Gy. This supports the idea that divergent responses exist in low dose tissue exposures as compared to high dose exposures in terms of molecular mechanisms and DNA repair process in particular.

C57BL/6 mice were observed for the same DNA repair proteins but in the colon instead of the small intestine. Comparing the 2 Gy samples to controls yielded no differences between groups (Figure 38). In the colon, the mismatch repair DNA repair
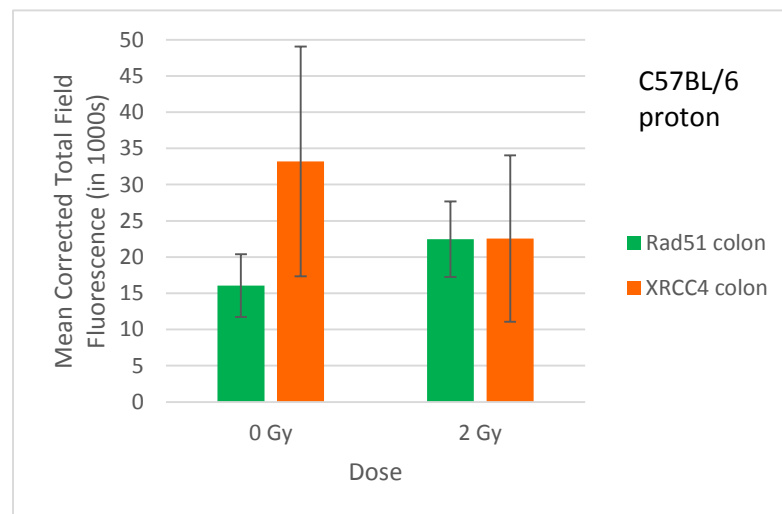
Figure 38:   DNA repair proteins in C57BL/6 colon. No significant differences between doses were observed

system is often utilized and mutations are sometimes present in that repair pathway in colon cancers depending on the type of carcinogenesis (Martin et al., 2010). It was still decided to study the DSB pathway proteins due to their critical nature in the radiation response. In thinking about why there were no differences in DNA repair protein

response between doses in the colon and between the colon and small intestine, it is possible that the two organs simply both rely on a mixed use of the two DSB repair pathways. The staining here indicated that is the case for the small intestine. Also, the compartment of the colon may be quite dependent for observing processes like apoptosis and DNA repair. In the small intestine, apopotosis, accumulation of p53 and expression of DNA repair proteins occurs the most at the stem cell compartment. In the colon, this is not the case and in fact apoptosis occurs away from the stem cell compartment. The stem cell compartment of the colon was measured here to keep the experiment consistent. Work was published which did show the importance of the particular location within colonic tissue of DNA damage and repair mechanisms after high-LET radiation (Roig et al., 2009). Further study of DSB repair in these organs should be completed, especially in tandem with apoptotic induction in the small intestine to determine mechanistically why the lesions may linger at 4 hour levels as late as 3 days.

4.2.2   Gene Expression

In studying gene expression, experiments were fortunately able to be performed on 6 different sets of animal samples in order to provide a broad depth of information addressing radiation quality, mouse strain, time and dose of exposure. Two different types of pathways were used to explore this project further: oxidative stress and apoptosis. Apoptosis was chosen to look at genes that may be directly influencing the damage assay from Chapter 3. Oxidative stress was chosen due to the broad group of genes that description represents and the many different pathways those genes overlap with in order to provide a more comprehensive inquiry. Oxidative stress is a very

important molecular process with regards to radiation exposures. One of the main ways that radiation causes damage to tissues is by interaction with water in cells when depositing energy which in turn generates DNA-damaging free radicals (Hall and Giaccia, 2006). It should be noted that presentation of this data is quite cumbersome as it is multitudes and multitudes of numbers. The best approaches have tried to be taken to make it easier on the reader.

4.2.2.1 Oxidative Stress Pathways

The mouse oxidative stress array plate from Qiagen (Valencia, CA) was utilized to study expression of genes whose function is pertinent to oxidative stress. Table 1 below displays the genes that were studied as part of these PCR arrays. The samples studied were C57BL/6 mice exposed to protons and sacrificed four hours later. The other samples were also C57BL/6 mice but exposed to gamma rays not protons. The sacrifice time points of these mice were 4 hours, 24 hours or 7 days. The organ studied was the duodenum of the small intestine. The first comparison analyzed in these pathways was a direct comparison of the C57BL/6 proton with the C57BL/6 gamma. Significant gene changes were teased out from a data set like that shown below (Figure 39). Significant changes were genes exhibiting fold change up or down 2 with a p-value less than 0.05. Next, a heat map was produced in order to aid in identifying important differences between the entire dataset and between multiple examples (Figure 40). For Figure 40, six data sets were included, all C57BL/6: 0 Gy gamma, 0 Gy proton, 5 cGy gamma, 5 cGy proton, 6 gy gamma, 6 Gy proton. A row tree listing the gene relationships on the heat map was used to identify those genes that were responsible for generating the color

97

Table 1:   Genes related to oxidative stress studied using a pathway-specific PCR

array for mouse oxidative stress.

Gene	Description	Gene	Description
Gpx8	Glutathione peroxidase 8 (putative)	Gpx4	Glutathione peroxidase 4
Aass	Aminoadipate-semialdehyde synthase	Gpx5	Glutathione peroxidase 5
Als2	Amyotrophic lateral sclerosis 2 (juvenile) homolog (human)	Gpx6	Glutathione peroxidase 6
Apc	Adenomatosis polyposis coli	Gpx7	Glutathione peroxidase 7
Apoe	Apolipoprotein E	Gsr	Glutathione reductase
Aqr	Aquarius	Gstk1	Glutathione S-transferase kappa 1
Atr	Ataxia telangiectasia and rad3 related	Hbq1	Hemoglobin, theta 1
Cat	Catalase	Idh1	Isocitrate dehydrogenase 1 (NADP+), soluble
Ccs	Copper chaperone for superoxide dismutase	Ift172	Intraflagellar transport 172 homolog (Chlamydomonas)
Xirp1	Xin actin-binding repeat containing 1	Il19	Interleukin 19
Ctsb	Cathepsin B	Il22	Interleukin 22
Cyba	Cytochrome b-245, alpha polypeptide	Kif9	Kinesin family member 9
Cygb	Cytoglobin	Lpo	Lactoperoxidase
Dnm2	Dynamin 2	Mb	Myoglobin
Duox1	Dual oxidase 1	Mpo	Myeloperoxidase
Ehd2	EH-domain containing 2	Mpp4	Membrane protein, palmitoylated 4 (MAGUK p55 subfamily member 4)
Epx	Eosinophil peroxidase		
Ercc2	Excision repair cross-complementing rodent repair deficiency, complementation group 2	Ncf2	Neutrophil cytosolic factor 2
		Ngb	Neuroglobin
Ercc6	Excision repair cross-complementing rodent repair deficiency, complementation group 6	Nos2	Nitric oxide synthase 2, inducible
		Nox1	NADPH oxidase 1
		Nox4	NADPH oxidase 4
Fancc	Fanconi anemia, complementation group C	Noxa1	NADPH oxidase activator 1
		Noxo1	NADPH oxidase organizer 1
Fmo2	Flavin containing monooxygenase 2	Nqo1	NAD(P)H dehydrogenase, quinone 1
Gab1	Growth factor receptor bound protein 2-associated protein 1	Nudt15	Nudix (nucleoside diphosphate linked moiety X)-type motif 15
Gpx1	Glutathione peroxidase 1	Nxn	Nucleoredoxin
Gpx2	Glutathione peroxidase 2	Park7	Parkinson disease (autosomal recessive, early onset) 7
Gpx3	Glutathione peroxidase 3		

Ppp1r15b	Protein phosphatase 1, regulatory (inhibitor) subunit 15b
Prdx1	Peroxiredoxin 1
Prdx2	Peroxiredoxin 2
Prdx3	Peroxiredoxin 3
Prdx4	Peroxiredoxin 4
Prdx5	Peroxiredoxin 5
Prdx6	Peroxiredoxin 6
Prdx6-rs1	Peroxiredoxin 6, related sequence 1
Prnp	Prion protein
Psmb5	Proteasome (prosome, macropain) subunit, beta type 5
Ptgs1	Prostaglandin-endoperoxide synthase 1
Ptgs2	Prostaglandin-endoperoxide synthase 2
Rag2	Recombination activating gene 2
Recql4	RecQ protein-like 4
Scd1	Stearoyl-Coenzyme A desaturase 1
Serpinb1b	Serine (or cysteine) peptidase inhibitor, clade B, member 1b

Slc38a1	Solute carrier family 38, member 1
Slc41a3	Solute carrier family 41, member 3
Sod1	Superoxide dismutase 1, soluble
Sod2	Superoxide dismutase 2, mitochondrial
Sod3	Superoxide dismutase 3, extracellular
Srxn1	Sulfiredoxin 1 homolog (S. cerevisiae)
Tmod1	Tropomodulin 1
Tpo	Thyroid peroxidase
Txnip	Thioredoxin interacting protein

patterns on the map. Finally, pathways were drawn based upon two things: one pathway was drawn using significant changes across at least two samples from the PCR array only. A second pathway(s) were drawn based upon patterns in the heat map and identified genes in those heat maps. In this case, three pathways were drawn; one pathway for significant gene changes and two for two different patterns found in the heat map. The pathways drawn use an online database which identifies only genes, enzymes, molecules, etc. which have been experimentally proven to express the relationship depicted in the pathways. The pathways are shown in Figures 41, 42 and 43.

The second comparison analyzed in these oxidative stress pathways was a direct comparison of the C57BL/6 gamma of 4 hours with the other time points of 24 hours and 7 days in order to provide a panel of genes significant over time. Significant gene changes were teased out as before. Significant changes were genes exhibiting fold change up or down 2 with a p-value less than 0.05. Next, a heat map was produced in order to aid in identifying important differences between the entire dataset and between multiple examples. None were found in this heat map. 9 data sets were included, all C57BL/6 gamma irradiation: 0 Gy, 5 cGy and 6 Gy for 4 hours, the same three doses for 24 hours and the same three doses for 7 days. Finally, a pathway was drawn based upon significant changes across at least two samples from the PCR array only. The pathways drawn using an online database which identifies only genes, enzymes, molecules, etc. which have been experimentally proven to express the relationship depicted in the pathways. The pathways are shown in Figure 44.
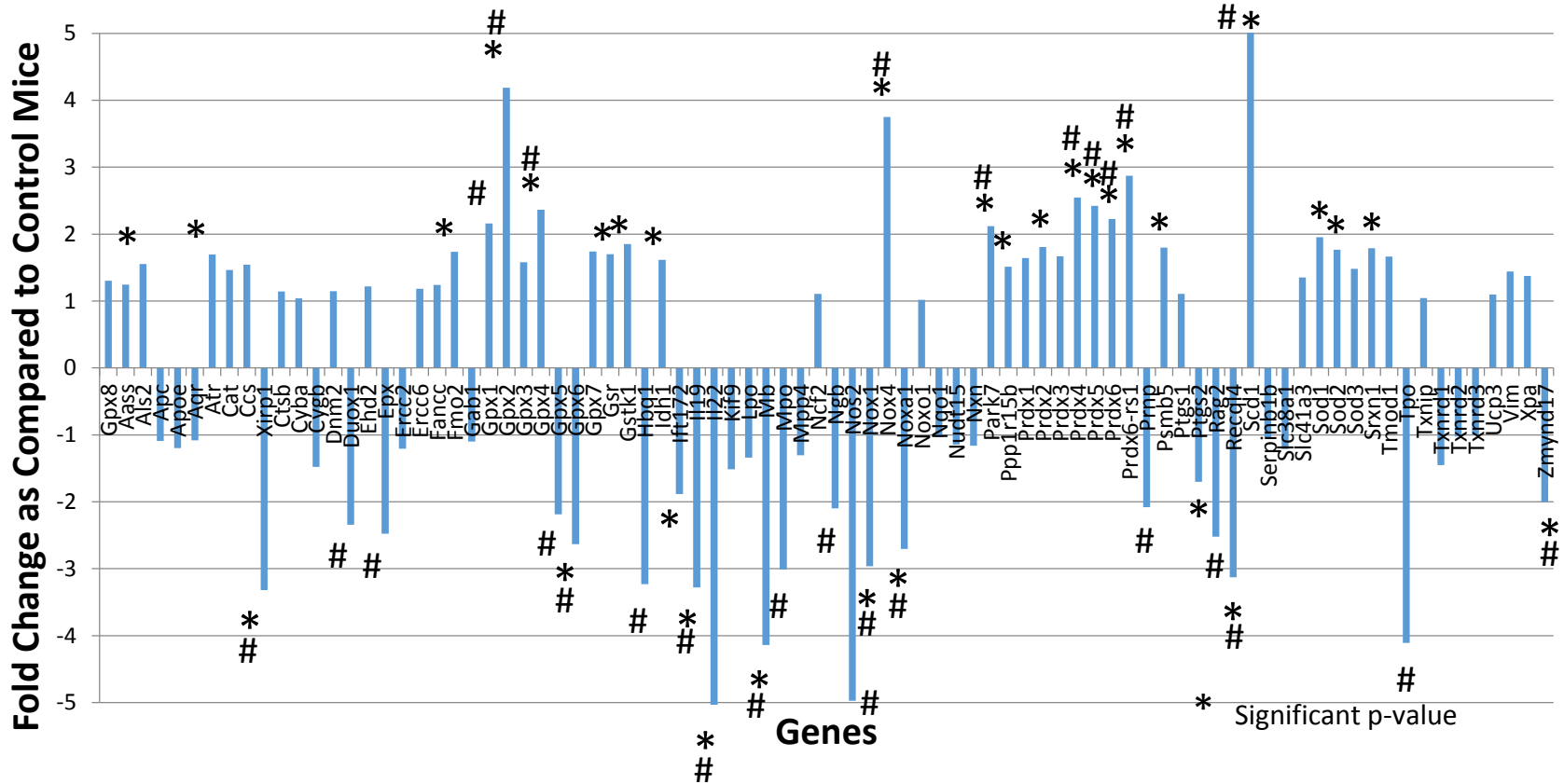
Figure 39: Example of significant genes from one PCR array. 84 genes are tested in every array.
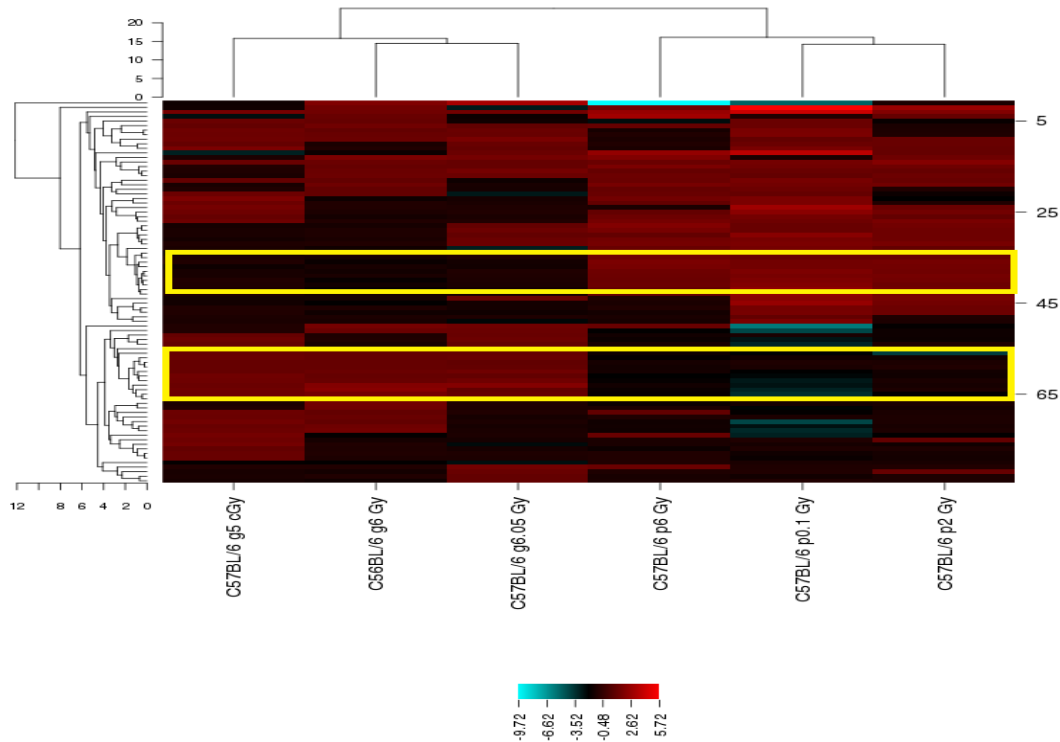
Figure 40: Heat map generated of PCR array gene expression changes in 6 C67BL/6 gene data sets. The yellow boxes were overlaid to identify regions of color patters across the entire heat map. This heat map compares three gamma irradiated samples against three proton irradiated samples.
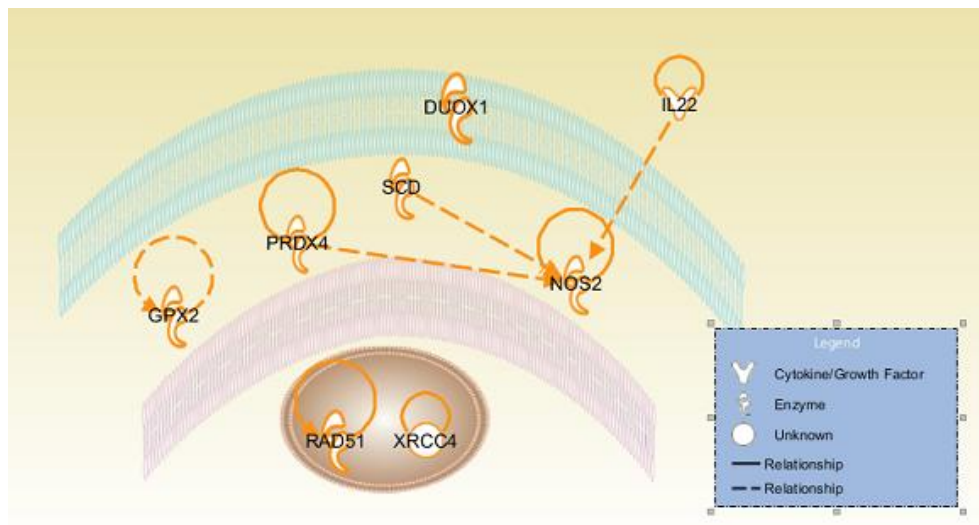
Figure 41: Pathway drawn by author using IPA to create a potential molecular mechanism. This pathway consists of significant gene changes across at least two samples between C57BL/6 mice exposed to gamma rays or protons.

102
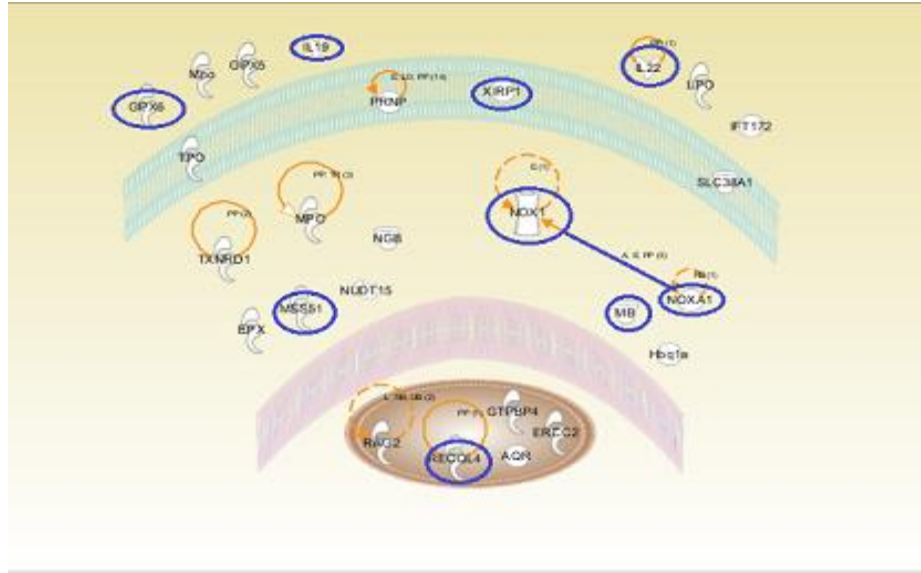
Figure 42: Pathway comparing genes in C57BL/6 mice with significantly down-folded expression as identified by a heat map after irradiation with varying radiation qualities. Please refer to the legend in Figure 41.
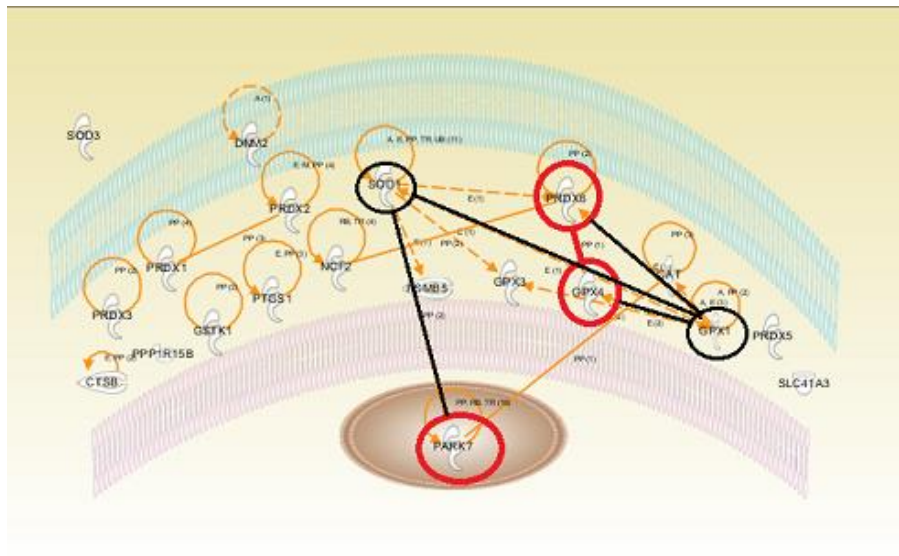
Figure 43: Pathways of genes identified in a heat map of being related. The genes are from C57BL/6 mice exposed to gamma rays or protons. Please refer to legend in Figure 41. The red is indicative of significantly altered genes while the black is pathway connections not significant but experimentally proven in the literature.
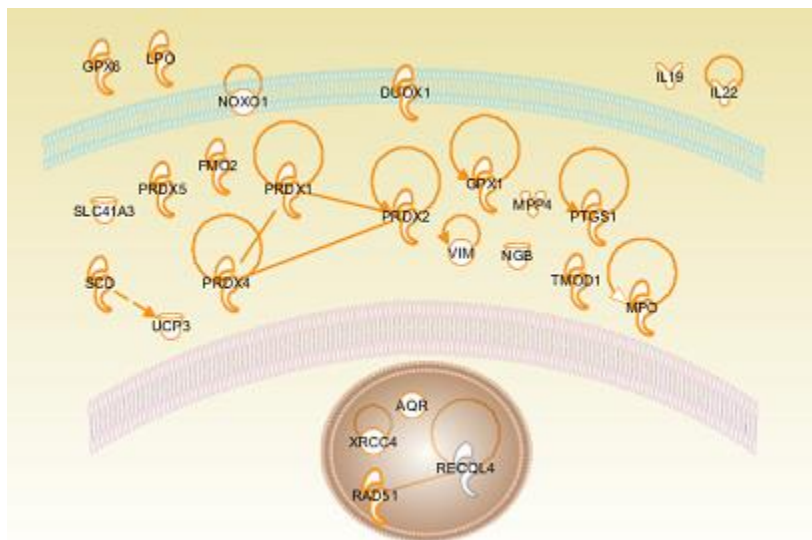
Figure 44: Pathway of significant gene changes across two strains of mice both exposed to protons. Please refer to the legend in Figure 41.

4.2.2.2 Apoptotic Pathways

The mouse apoptosis array plate from Qiagen (Valencia, CA) was utilized to study expression of genes whose function is specific to apoptosis. The samples studied were BALB/c and C57BL/6 mice exposed to protons and sacrificed four hours later. The organ studied was the duodenum of the small intestine. Table 2 below displays the genes that were studied as part of these PCR arrays.

The first and only comparison analyzed in these pathways was a direct comparison of the C57BL/6 proton with the BALB/c proton. Significant gene changes were teased out from a data set as shown before. Significant changes were genes exhibiting fold change up or down 2 with a p-value less than 0.05. Next, a heat map was produced in order to aid in identifying important differences between the entire dataset

and between multiple examples (Figure 45). For Figure 45, six data sets were included,

three BALB/c and three C57BL/6: 0 Gy proton, 0.1 Gy proton, 2 Gy proton. A row tree

listing the gene relationships on the heat map was used to identify those genes that were

responsible for generating the color patterns on the map. Finally, pathways were drawn

based upon two things: one pathway was drawn using significant changes across at least

two samples from the PCR arrays only. A second pathway was drawn based upon

patterns in the heat map and identified genes in those heat maps. In this case, two

pathways were drawn; one pathway for significant gene changes and one for a pattern
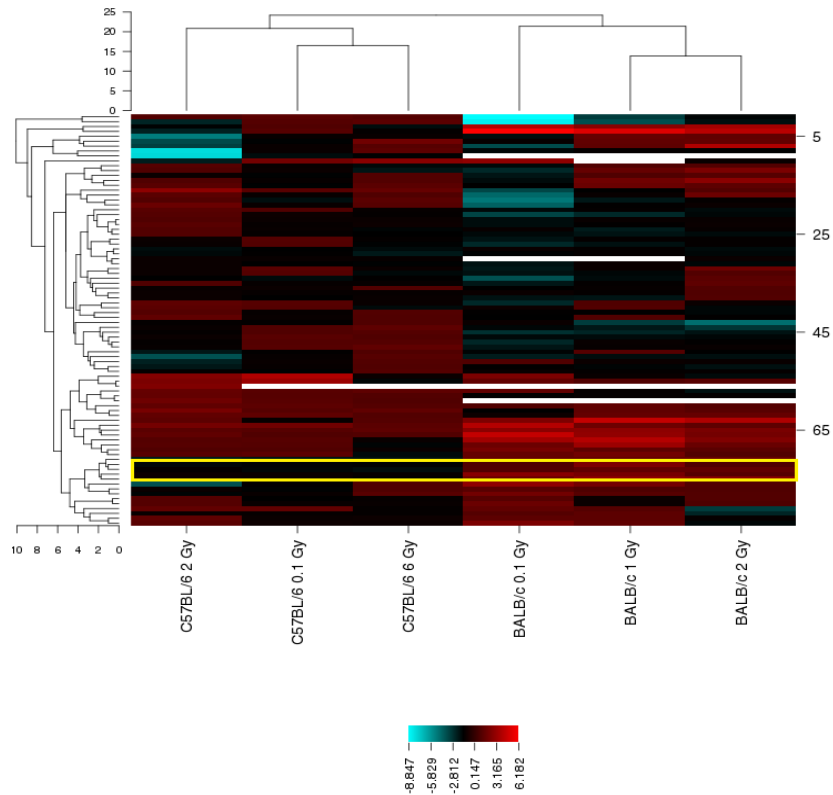
Figure 45: Heat map comparing gene expression data in C57BL/6 vs. BALB/c mice exposed to protons. The yellow overlay points out a color pattern across the map.

found in the heat map. The pathways drawn use an online database which identifies only genes, enzymes, molecules, etc. which have been experimentally proven to express the relationship depicted in the pathways. The pathways are shown in Figures 46 and 47.
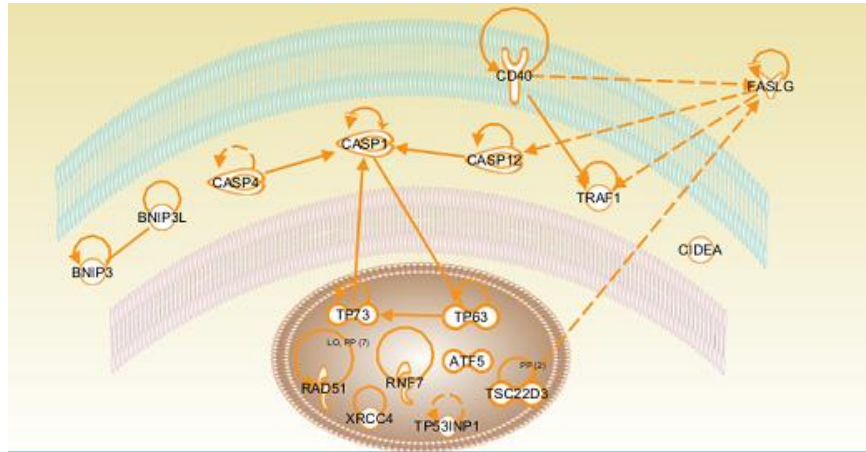

Figure 46: Pathway of significant gene changes between BALB/c and C57BL/6 mice after proton exposure. Please refer to the legend in Figure 41.
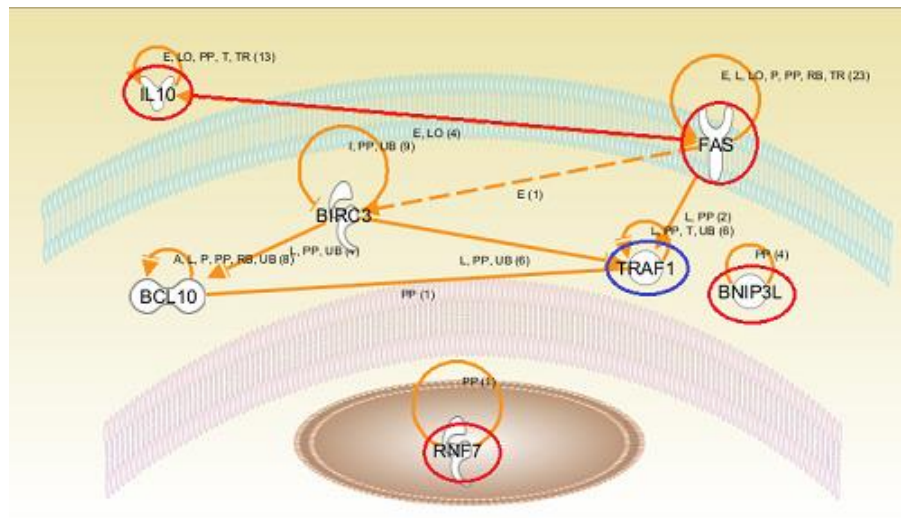
Figure 47: Pathway of genes identified in heat map as related between C57BL/6 and BALB/c mice exposed to protons. Please refer to the legend in Figure 41. Red indicates significant up-regulation while blue indicates significant down-regulation.

106

Table 2: Apoptotic genes in a PCR array used to study the mouse apoptosis pathway.

Akt1	Thymoma viral proto-oncogene 1	Bok	BCL2-related ovarian killer protein
Apaf1	Apoptotic peptidase activating factor 1	Card10	Caspase recruitment domain family, member 10
Api5	Apoptosis inhibitor 5	Nod1	Nucleotide-binding oligomerization domain containing 1
Atf5	Activating transcription factor 5	Card6	Caspase recruitment domain family, member 6
Bad	BCL2-associated agonist of cell death	Casp1	Caspase 1
Bag1	Bcl2-associated athanogene 1	Casp12	Caspase 12
Bag3	Bcl2-associated athanogene 3	Casp14	Caspase 14
Bak1	BCL2-antagonist/killer 1	Casp2	Caspase 2
Bax	Bcl2-associated X protein	Casp3	Caspase 3
Bcl10	B-cell leukemia/lymphoma 10	Casp4	Caspase 4, apoptosis-related cysteine peptidase
Bcl2	B-cell leukemia/lymphoma 2	Casp6	Caspase 6
Bcl2l1	Bcl2-like 1	Casp7	Caspase 7
Bcl2l10	Bcl2-like 10	Casp8	Caspase 8
Bcl2l2	Bcl2-like 2	Casp9	Caspase 9
Bid	BH3 interacting domain death agonist	Cflar	CASP8 and FADD-like apoptosis regulator
Naip1	NLR family, apoptosis inhibitory protein 1	Cidea	Cell death-inducing DNA fragmentation factor, alpha subunit-like effector A
Naip2	NLR family, apoptosis inhibitory protein 2	Cideb	Cell death-inducing DNA fragmentation factor, alpha subunit-like effector B
Birc2	Baculoviral IAP repeat-containing 2	Cradd	CASP2 and RIPK1 domain containing adaptor with death domain
Birc3	Baculoviral IAP repeat-containing 3	Dad1	Defender against cell death 1
Xiap	X-linked inhibitor of apoptosis	Dapk1	Death associated protein kinase 1
Birc5	Baculoviral IAP repeat-containing 5	Dffa	DNA fragmentation factor, alpha subunit
Bnip2	BCL2/adenovirus E1B interacting protein 2	Dffb	DNA fragmentation factor, beta subunit
Bnip3	BCL2/adenovirus E1B interacting protein 3	Tsc22d3	TSC22 domain family, member 3
Bnip3l	BCL2/adenovirus E1B interacting protein 3-like	Fadd	Fas (TNFRSF6)-associated via death domain

Fas+D51:E70D51:E89	Fas (TNF receptor superfamily member 6)	Pycard	PYD and CARD domain containing
Fasl	Fas ligand (TNF superfamily, member 6)	Ripk1	Receptor (TNFRSF)-interacting serine-threonine kinase 1
Hells	Helicase, lymphoid specific	Rnf7	Ring finger protein 7
Il10	Interleukin 10	Sphk2	Sphingosine kinase 2
Lhx4	LIM homeobox protein 4	Tnf	Tumor necrosis factor
Ltbr	Lymphotoxin B receptor	Tnfrsf10b	Tumor necrosis factor receptor superfamily, member 10b
Mcl1	Myeloid cell leukemia sequence 1	Tnfrsf11b	Tumor necrosis factor receptor superfamily, member 11b (osteoprotegerin)
Nfkb1	Nuclear factor of kappa light polypeptide gene enhancer in B-cells 1, p105	Tnfrsf1a	Tumor necrosis factor receptor superfamily, member 1a
Nme5	Non-metastatic cells 5, protein expressed in (nucleoside-diphosphate kinase)	Cd40	CD40 antigen
Nol3	Nucleolar protein 3 (apoptosis repressor with CARD domain)	Tnfsf10	Tumor necrosis factor (ligand) superfamily, member 10
Pak7	P21 (CDKN1A)-activated kinase 7	Tnfsf12	Tumor necrosis factor (ligand) superfamily, member 12
Pim2	Proviral integration site 2	Cd40lg	CD40 ligand
Polb	Polymerase (DNA directed), beta	Cd70	CD70 antigen
Prdx2	Peroxiredoxin 2	Traf1	Tnf receptor-associated factor 1

Traf2	Tnf receptor-associated factor 2	Hsp90ab1	Heat shock protein 90 alpha (cytosolic), class B member 1
Traf3	Tnf receptor-associated factor 3	Gapdh	Glyceraldehyde-3-phosphate dehydrogenase
Trp53	Transformation related protein 53		
Trp53bp2	Transformation related protein 53 binding protein 2	Actb	Actin, beta
		MGDC	Mouse Genomic DNA Contamination
Trp53inp1	Transformation related protein 53 inducible nuclear protein 1	RTC	Reverse Transcription Control
Trp63	Transformation related protein 63	RTC	Reverse Transcription Control
Trp73	Transformation related protein 73	RTC	Reverse Transcription Control
Zc3hc1	Zinc finger, C3HC type 1	PPC	Positive PCR Control
		PPC	Positive PCR Control
Gusb	Glucuronidase, beta	PPC	Positive PCR Control
Hprt1	Hypoxanthine guanine phosphoribosyl transferase 1		

4.2.3   HDAC Assay

An important component of this dissertation was to provide data relevant to carcinogenesis and therapeutic modalities that occur on Earth as a small translational piece of information. HDAC inhibitors are being investigated by many in combination with radiation oncology treatments as there has been evidence that their inhibition leads to enhanced cell killing by radiation (Konsoula et al., 2011). HDAC was measured in colon samples obtained from C57BL/6 mice after proton exposure. At the time of writing, there is no information available on HDAC activity after proton exposure for any organ. As mentioned previously, however, there is information available on HDAC inhibition serving as a radio-sensitizer in other qualities of radiotherapy for cancer. It was

hoped to address endogenous levels of HDAC after charged particle exposure. 24 hours

after doses of 0.1 Gy or 2 Gy protons, HDAC activity was suppressed as compared to

control samples in the C57BL/6 colon (Figure 48). However, no significant differences

were statistically identified between groups. Between 4 hours and 24 hours of exposure,

the data did show a decrease in HDAC activity after a dose of 0.1 Gy. However, a slight

increase was observed following the dose of 2 Gy.
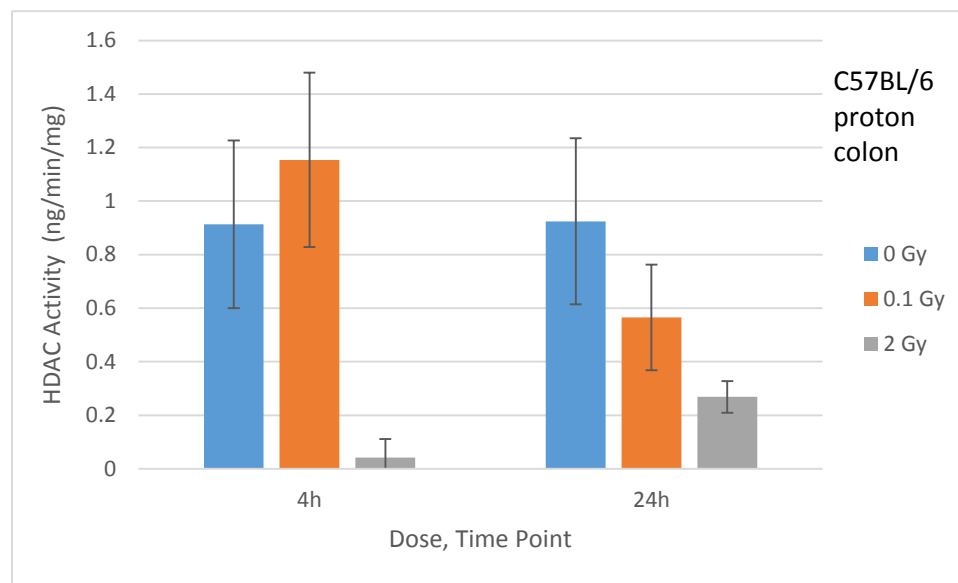
Figure 48:   HDAC activity in C57BL/6 colon after proton exposure. No significant
differences were found between groups.

The current literature available on this topic is very pertinent to tissue-targeted,

high doses for radiotherapy (as high as 60 Gy), or doses used experimentally that are

higher than 2 Gy (approximately 4 Gy or higher), and does not generally describe

differences in dose response with lows doses such as 0.1 Gy regarding HDAC activity

(Adimoolam et al., 2007; Shabason et al., 2011). With that in mind, and due to the lack of

significance in our findings, a detailed conclusion cannot be accurately provided

regarding endogenous levels of HDAC in the colon after proton exposures. Further study is needed to investigate this problem.

4.3 DISCUSSION

The DNA repair protein data provided in this study is extremely relevant to both colon carcinogenesis and acute effects in the entire GI tract. The most important finding from this staining was the presence of both strands of DSB repair, NHEJ and HR, in both regions of the crypts. This provides evidence that the very high levels of apoptosis seen in the small intestine may indeed be a protective measure and that apotosis is not a pathway chosen due to lack of repair mechanisms. There are multiple studies which support the theory that the apoptosis in the small intestine after radiological and other toxicants is a form of genome preservation and, mostly, functional preservation of the tissue (Potten et al., 1994; Merritt et al., 1997). Figure 33 did display that Rad51, or the HR repair pathway, might be the primary repair pathway for cells in any stage, both proliferation that occurs low in the crypts or the more mature cells in the higher region. However, it should be noted that there was a high background staining present in the lower regions as compared to the higher areas where cells are not actively proliferating. The possible priority of HR proteins over NHEJ-specific repair supports the idea that apoptosis could be a protective safeguard in the intestine after radiation exposure. Since NHEJ pathways typically occur earlier in the cell cycle, the presence of less NHEJ proteins (present but less than HR proteins) may indicate that cells which are in earlier phases of the cell cycle still undergo apoptosis instead of repair mechanisms. It is possible that less NHEJ proteins are naturally found because apoptosis is the dominant pathway after radiation.

Analyzing the pathways provided after gene expression was a process of searching the literature to further look into the relationships provided. The DNA repair proteins observed in this work were included to look for any relationships involving their functions with the significantly altered genes. The inter-quality radiation, proton vs. gamma, comparison in C57BL/6 mice (Figures 41, 42 and 43) is mostly associated with processes of free radical scavenging and cell proliferation when observing the functions of all the significantly altered genes. Interestingly, a study of proton gene expression profiles compared to electron radiation gene expression profiles showed similar expression to this network, namely IL22 and Prdx4 (Gridley et al., 2011). Prdx4 is known to interact with NF-kB and after observing many of the gene expression changes in this work, it is probable that several of our pathways are dependent on major molecules like p53 and NF-kB. These were not included in the pathway analysis, but based on the literature relationships can be identified. The BALB/c gene data, for example, seems to be divided between two possible mechanisms: one dependent upon p53 and one dependent upon NFkB.

Counterintuitive to what we saw with the lesions present in the BALB/c intestinal tissue being greatest after 2 Gy of proton-irradiation, the largest number of gene expression alterations occurred at the lowest dose of exposure, 0.1 Gy. Several genes, including CASP1, CASP4 and Trp53inp1, were found to be up-regulated for all three doses in this group. Trp53inp1, or transformation related protein 53 inducible nuclear protein 1, is an alternatively spliced gene encoding two nuclear protein isoforms

(TP53INP1alpha and TP53INP1beta), whose transcription is activated by p53. When overexpressed, both isoforms induce cell cycle arrest in G1 and enhance p53-mediated apoptosis (Tomasini et al., 2005). Together with the activation of CASP1, our data suggest that apoptosis is induced from both low and high doses of protons in a p53-dependent manner.

Several genes, however, were up- or down-regulated in only either the low or high dose samples. Atf5, or activating transcription factor 5, was down-regulated significantly after 0.1 Gy proton exposures. Atf5 suppresses the transactivational activity of p53 and blocks p53-dependent apoptosis induced by ionizing radiation (Nishioka et al., 2009). A dominant-negative AtfX mutant has also been shown to induce apoptosis of cells cultured in the presence of growth factors (Persengiev et al., 2002). In the present study, NF-kB1, a subunit of NF-kB, was also down-regulated in the 0.1 Gy samples. Inhibition of NF-kB nuclear translocation has been shown to enhance apoptotic killing by radiation in tumor cells (Wang et al., 1996). Our expression profiles of pro-apoptotic genes suggested that enhanced p53 activation and suppressed NF-kB activities may result in the high radiosensitivity of the small intestine at low doses of proton exposures.

The differences that we have shown in gene expression and the network analysis that followed among low versus high doses of proton-irradiation may indeed offer insight into the mechanism of damage underlying each. The network analysis performed with an input of genes whose expression level was changed after a 0.1 Gy proton exposure show two pathways with statistical significance: an anti-apoptotic pathway mediated by

external signals via NF-kB and an apoptotic pathway through death domain receptors and caspases. Only the pathway of apoptosis via domain receptors and caspases appeared in the analysis for 1 and 2 Gy protons. The role of p53 in the induction of radiation-induced apoptosis in the small intestine has been widely investigated (Wilson et al., 1998; Komarova et al., 2000; Inagaki-Ohara et al., 2001; Jee et al., 2005). Although apoptosis that appeared at 24 hours or later may follow a p53-independent pathway, apoptotic lesions that are detected within several hours post-irradiation is p53-dependent and is completely absent in p53 knockout mice (Merritt et al., 1994). Our present network analysis suggests that apoptosis from exposures to low and high doses of protons follows a similar p53-dependent pathway due to damages to the DNA by protons. An interesting finding from the network analysis is the suggestion of anti-apoptotic mechanism mediated by NF-kB for only the 0.1 Gy protons. The protective role of NF-kB in radiation-induced apoptosis in the small intestine has also been proposed (Fan et al., 2002; Egan et al., 2004; Wang et al., 2004). Activation of NF-kB in radioprotection may be unique for the small intestine, as the protective property was not found in the liver, heart and several other organs (Wang et al., 2004). NF-kB is known to respond to radiation damage and other stress factors (Dent et al., 2003). On the other hand, inhibition of NF-kB nuclear translocation has been shown to enhance apoptotic killing by radiation in tumor cells (Wang et al., 1996). Determining whether the NF-kB response is unique in the small intestine, whether it plays a protective or enhanced cell-killing role, and how NF-kB influences the supra-linear dose response requires further investigation.

114

It is widely thought that HDAC inhibition not only allows for the acetylation of cancer cells which contributes to their radio-sensitization, but that it also contributes to transcriptional regulation of genes associated with cancer and may even increase reactive oxygen species (ROS) leading to apoptosis (Chung et al., 2009; Robert and Rassool, 2012). HDAC inhibition also limits DNA repair processes (Shabason et al., 2011). Specifically, it has been hypothesized that DSB repair is limited after HDAC inhibition (Shabason et al., 2011). This has been supported experimentally by the delayed disappearance of gamma-H2AX foci, the diminished activity of Rad51 and a general decrease in HR activity (Adimoolam et al., 2007). Conversely, however, the literature also shows HDAC inhibition as a radio-protectant in some instances. Studies have shown HDAC inhibition to limit negative symptoms for patients undergoing radiotherapy by mitigating damage to the epidermis and even increasing DNA repair ability in normal fibroblast cell lines (Chung et al., 2004; Chung et al., 2009). Furthermore, healthy animals undergoing WBI had improved survival rates after irradiation and HDAC inhibition and structural damages to the intestine were attenuated in those animals (Brown et al., 2008; Konsoula et al., 2011). One difference to explain this disparity, at least between healthy versus cancerous tissues, is simply that HDACs are manifested in excess in tumor cells generally and are not in normal cells (Delcuve et al., 2013). It is therefore conceivable that HDAC inhibition can be of even greater benefit in radiotherapy, aiding in the death of tumor cells and the protection of healthy cells (Paoluzzi and Figg, 2004). The data shown here also involved WBI on healthy animals. No conclusive evidence about HDAC activity after irradiation in our colon samples can be drawn due to differing increase or decrease in response both across doses and time

115

points. However, what the data can suggest is that HDAC activity after radiation in the colon, or after proton exposure, may be variable between individuals depending on dose. As the data did not show a definitive increase or decrease in HDAC activity over doses or times, and given relatively low doses, it is only appropriate to speculate that colonic tissue exposed to radiation of protons or other qualities may exhibit radio-sensitization with the concurrent use of an HDAC inhibitor as HDAC levels were not suppressed by proton radiation and evidence exists for radio-sensitization after HDAC inhibition.

Most HDAC classes are found to be up-regulated in colon cancer (Stypula-Cyrus et al., 2013). Mechanistically, there is evidence which suggests that in colon cancer, HDAC inhibition enhances cell death induced by radiation in a p53-dependent manner (Flatmark et al., 2006; Chen et al., 2009). Therefore, future studies of this type of work should consider measuring radio-sensitivity in the colon with and without HDAC inhibition in p53-wild type and p53-knock out mice.

Chapter 5: Closing Remarks

In this work, there were two major findings collected from all of the data which have implications beyond that of the bench science field. The first is that DNA repair pathways are not limited in the small intestine to regions associated with cell death processes. This finding means that the colon, due to its carcinogenic nature, must be explored further for details in how it is *different* than the small intestine. The small intestine does not exhibit cancer often in human beings and this data points out that this is not due to deficiencies in DNA repair mechanisms. Perhaps the processes after radiation exposure are helpful in the small intestine for the organ's stability. Which leads in to the second point which is that apoptosis may be a protective mechanism for this organ. The damage data here followed general time courses for the most part indicating an order to the endpoints being observed. The apoptotic process must be broken down further molecularly to identify the elements that are not present in tissues such as the colon. Potten, the father of studying radiation on the small instestine, said it best in his work that "nature knows best" (Potten and Booth, 1997).

Low dose radiation is a much more common exposure in daily life and for astronauts in flight as opposed to high doses. It is pertinent to learn more about the effects of low dose radiation to better determine the risks of exposure for both astronauts and the general public. Radio-adaptation has been studied for 25 years now and provides evidence that the consequences of low dose radiation may not follow a linear damage effect and perhaps some low dose exposure can even be beneficial to the body. Of

particular relevance are astronauts traveling on long duration missions in the future as

they will be at risk of exposure to SPE's containing high doses of protons and,

consequently, increased risk for severe negative health effects. Learning more about

proton-mediated effects can potentially reduce the biological threats of these

unpredictable exposures. Underlying molecular mechanisms of the charge-particle

response are not well understood but could provide important insight into the complexity

of responses to low dose radiation exposure. The three strategies proposed here took

advantage of an *in vivo* model to better extrapolate awareness of the biological

consequences of low dose radiation exposure to the space flight and public health settings

and determine at the genetic level how the damage caused by protons and gamma rays

actually occurs. Potential molecular connections between signaling pathways were able

to be determined from this work and provide a new crop of researchable questions to be

asked and answered. The applicability of this work lies in physicians and scientists using

this information to better provide advice to astronauts on the risks of space travel. In

particular, the villous morphometry data provided in this dissertation demonstrates that

astronauts, as early as a few hours and even weeks after a radiation exposure, may exhibit

symptoms consistent with ARS that can be detrimental to a mission's success or timely

completion. With regard to patient care, the work given in this document shows that there

is much we still need to learn regarding colon cancer, both disease initiation and

prognosis, and HDAC enzyme activity as it relates to radiation exposure and radiation

therapy. The HDAC enzyme activity data shown here did not provide any definitive

conclusions. It was shown here, too, that DNA repair proteins and apoptotic damage in

the small intestine might be indicative of a natural and protective effort of the body to

induce apoptosis after irradiation. Using the genetic data accumulated in this work, such as the possible p53 versus NF-kB pathways, scientists can study why the small intestine is able to possibly induce a protective apoptotic wave on the molecular level and what differences exist in the colon since the large intestine does not exhibit that same apoptotic response after a radiological insult. The significance of this study is provided in that the knowledge obtained here can be used to better select low dose radiation exposure limits, discover effective counter-measures against the harmful effects of radiation, and potentially even find novel and favorable uses of radiation for humans. This can ultimately benefit the general public and especially astronauts in flight.

References

Adimoolam S, Sirisawad M, Chen J, Thiemann P, Ford JM, Buggy JJ (2007) HDAC inhibitor PCI-24781 decreases RAD51 expression and inhibits homologous recombination. Proc Natl Acad Sci U S A 104:19482-19487.

Baluchamy S, Ravichandran P, Periyakaruppan A, Ramesh V, Hall JC, Zhang Y, Jejelowo O, Gridley DS, Wu H, Ramesh GT (2010a) Induction of cell death through alteration of oxidants and antioxidants in lung epithelial cells exposed to high energy protons. J Biol Chem 285:24769-24774.

Baluchamy S, Zhang Y, Ravichandran P, Ramesh V, Sodipe A, Hall JC, Jejelowo O, Gridley DS, Wu H, Ramesh GT (2010b) Differential oxidative stress gene expression profile in mouse brain after proton exposure. In Vitro Cell Dev Biol Anim 46:718-725.

Baluchamy S, Zhang Y, Ravichandran P, Ramesh V, Sodipe A, Hall JC, Jejelowo O, Gridley DS, Wu H, Ramesh GT (2010c) Expression profile of DNA damage signaling genes in 2 Gy proton exposed mouse brain. Mol Cell Biochem 341:207-215.

Bhanja P, Saha S, Kabarriti R, Liu L, Roy-Chowdhury N, Roy-Chowdhury J, Sellers RS, Alfieri AA, Guha C (2009) Protective role of R-spondin1, an intestinal stem cell growth factor, against radiation-induced gastrointestinal syndrome in mice. PLoS One 4:e8014.

Blakely EA, Kleiman NJ, Neriishi K, Chodick G, Chylack LT, Cucinotta FA, Minamoto A, Nakashima E, Kumagami T, Kitaoka T, Kanamoto T, Kiuchi Y, Chang P, Fujii

N, Shore RE (2010) Radiation cataractogenesis: epidemiology and biology. Radiat Res 173:709-717.

Brada M, Pijls-Johannesma M, De Ruysscher D (2009) Current clinical evidence for proton therapy. Cancer J 15:319-324.

Brennan PC, Carr KE, Seed T, McCullough JS (1998) Acute and protracted radiation effects on small intestinal morphological parameters. Int J Radiat Biol 73:691-698.

Brenner D, Sachs R (2006) Estimating radiation-induced cancer risks at very low doses: rationale for using a linear no-threshold approach. Radiat Environ Biophys 44:253-256.

Brenner D, Doll R, Goodhead D, Hall E, Land C, Little J, Lubin J, Preston D, Preston R, Puskin J, Ron E, Sachs R, Samet J, Setlow R, Zaider M (2003) Cancer risks attributable to low doses of ionizing radiation: assessing what we really know. Proc Natl Acad Sci U S A 100:13761-13766.

Brown SL, Kolozsvary A, Liu J, Ryu S, Kim JH (2008) Histone deacetylase inhibitors protect against and mitigate the lethality of total-body irradiation in mice. Radiat Res 169:474-478.

Calabrese E (2009) Getting the dose-response wrong: why hormesis became marginalized and the threshold model accepted. Arch Toxicol 83:227-247.

Calabrese E, Stanek Er, Nascarella M, Hoffmann G (2008) Hormesis predicts low-dose responses better than threshold models. Int J Toxicol 27:369-378.

Carr KE, Toner PG (1972) Surface studies of acute radiation injury in the mouse intestine. Virchows Arch B Cell Pathol 11:201-210.

Carr KE, Bullock C, Ryan SS, McAlinden MG, Boyle FC (1991) Radioprotectant effects of atropine on small intestinal villous shape. J Submicrosc Cytol Pathol 23:569-577.

Casteleyn C, Van den Broeck W, Simoens P (2007) Histological characteristics and stereological volume assessment of the ovine tonsils. Vet Immunol Immunopathol 120:124-135.

Casteleyn C, Rekecki A, Van der Aa A, Simoens P, Van den Broeck W (2010) Surface area assessment of the murine intestinal tract as a prerequisite for oral dose translation from mouse to man. Lab Anim 44:176-183.

Chen X, Wong P, Radany E, Wong JY (2009) HDAC inhibitor, valproic acid, induces p53-dependent radiosensitization of colon cancer cells. Cancer Biother Radiopharm 24:689-699.

Chung YL, Wang AJ, Yao LF (2004) Antitumor histone deacetylase inhibitors suppress cutaneous radiation syndrome: Implications for increasing therapeutic gain in cancer radiotherapy. Mol Cancer Ther 3:317-325.

Chung YL, Lee MY, Pui NN (2009) Epigenetic therapy using the histone deacetylase inhibitor for increasing therapeutic gain in oral cancer: prevention of radiation-induced oral mucositis and inhibition of chemical-induced oral carcinogenesis. Carcinogenesis 30:1387-1397.

Chylack LT, Peterson LE, Feiveson AH, Wear ML, Manuel FK, Tung WH, Hardy DS, Marak LJ, Cucinotta FA (2009) NASA study of cataract in astronauts (NASCA). Report 1: Cross-sectional study of the relationship of exposure to space radiation and risk of lens opacity. Radiat Res 172:10-20.

Cummins AG, Alexander BG, Chung A, Teo E, Woenig JA, Field JB, Thompson FM, Roberts-Thomson IC (2011) Morphometric evaluation of duodenal biopsies in celiac disease. Am J Gastroenterol 106:145-150.

Delcuve GP, Khan DH, Davie JR (2013) Targeting class I histone deacetylases in cancer therapy. Expert Opin Ther Targets 17:29-41.

Dent P, Yacoub A, Contessa J, Caron R, Amorino G, Valerie K, Hagan MP, Grant S, Schmidt-Ullrich R (2003) Stress and radiation-induced activation of multiple intracellular signaling pathways. Radiat Res 159:283-300.

Ding L, Shingyoji M, Chen F, Hwang J, Burma S, Lee C, Cheng J, Chen D (2005) Gene expression profiles of normal human fibroblasts after exposure to ionizing radiation: a comparative study of low and high doses. Radiat Res 164:17-26.

Donnelly EH, Nemhauser JB, Smith JM, Kazzi ZN, Farfán EB, Chang AS, Naeem SF (2010) Acute radiation syndrome: assessment and management. South Med J 103:541-546.

Dörr H, Meineke V (2011) Acute radiation syndrome caused by accidental radiation exposure - therapeutic principles. BMC Med 9:126.

Egan LJ, Eckmann L, Greten FR, Chae S, Li ZW, Myhre GM, Robine S, Karin M, Kagnoff MF (2004) IkappaB-kinasebeta-dependent NF-kappaB activation provides radioprotection to the intestinal epithelium. Proc Natl Acad Sci U S A 101:2452-2457.

Fabre KM, Ramaiah L, Dregalla RC, Desaintes C, Weil MM, Bailey SM, Ullrich RL (2011) Murine Prkdc polymorphisms impact DNA-PKcs function. Radiat Res 175:493-500.

Fan C, Yang J, Engelhardt JF (2002) Temporal pattern of NFkappaB activation influences apoptotic cell fate in a stimuli-dependent fashion. J Cell Sci 115:4843-4853.

Finnberg N, Wambi C, Kennedy AR, El-Deiry WS (2013) The effects of antioxidants on gene expression following gamma-radiation (GR) and proton radiation (PR) in mice in vivo. Cell Cycle 12.

Finnberg N, Wambi C, Ware JH, Kennedy AR, El-Deiry WS (2008) Gamma-radiation (GR) triggers a unique gene expression profile associated with cell death compared to proton radiation (PR) in mice in vivo. Cancer Biol Ther 7:2023-2033.

Flatmark K, Nome RV, Folkvord S, Bratland A, Rasmussen H, Ellefsen MS, Fodstad Ø, Ree AH (2006) Radiosensitization of colorectal carcinoma cell lines by histone deacetylase inhibition. Radiat Oncol 1:25.

Gerweck LE, Kozin SV (1999) Relative biological effectiveness of proton beams in clinical therapy. Radiother Oncol 50:135-142.

Goetz W, Morgan MN, Baulch JE (2011) The effect of radiation quality on genomic DNA methylation profiles in irradiated human cell lines. Radiat Res 175:575-587.

Gridley DS, Freeman TL, Makinde AY, Wroe AJ, Luo-Owen X, Tian J, Mao XW, Rightnar S, Kennedy AR, Slater JM, Pecaut MJ (2011) Comparison of proton and electron radiation effects on biological responses in liver, spleen and blood. Int J Radiat Biol 87:1173-1181.

Group GaB (1997-present) CIMminer. Besthesda, MD: Laboratory of Molecular Pharmacology, Center for Cancer Research.

Hall EJ, Giaccia AJ (2006) Radiobiology for the Radiologist. In, Sixth Edition, p 135. Philadelphia, PA: Lippincott Williams & Wilkins.

Hamasaki K, Imai K, Hayashi T, Nakachi K, Kusunoki Y (2007) Radiation sensitivity and genomic instability in the hematopoietic system: Frequencies of micronucleated reticulocytes in whole-body X-irradiated BALB/c and C57BL/6 mice. Cancer Sci 98:1840-1844.

Harfouche G, Martin MT (2010) Response of normal stem cells to ionizing radiation: a balance between homeostasis and genomic stability. Mutat Res 704:167-174.

Hartlerode AJ, Scully R (2009) Mechanisms of double-strand break repair in somatic mammalian cells. Biochem J 423:157-168.

Hendry JH, West CM (1997) Apoptosis and mitotic cell death: their relative contributions to normal-tissue and tumour radiation response. Int J Radiat Biol 71:709-719.

Hendry JH, Potten CS, Merritt A (1995) Apoptosis induced by high- and low-LET radiations. Radiat Environ Biophys 34:59-62.

Higson D (2005) BEIR VII-2. J Radiol Prot 25:324-325.

Horie K, Kubo K, Yonezawa M (2002) p53 dependency of radio-adaptive responses in endogenous spleen colonies and peripheral blood-cell counts in C57BL mice. J Radiat Res 43:353-360.

Hornsey S (1973) The effectiveness of fast neutrons compared with low LET radiation on cell survival measured in the mouse jejunum. Radiat Res 55:58-68.

Hua G, Thin TH, Feldman R, Haimovitz-Friedman A, Clevers H, Fuks Z, Kolesnick R (2012) Crypt base columnar stem cells in small intestines of mice are radioresistant. Gastroenterology 143:1266-1276.

Ijiri K (1989) Cell death (apoptosis) in mouse intestine after continuous irradiation with

  gamma rays and with beta rays from tritiated water. Radiat Res 118:180-191.

Ijiri K, Potten CS (1983) Response of intestinal cells of differing topographical and

  hierarchical status to ten cytotoxic drugs and five sources of radiation. Br J

  Cancer 47:175-185.

Inagaki-Ohara K, Yada S, Takamura N, Reaves M, Yu X, Liu E, Rooney I, Nicholas S,

  Castro A, Ware CF, Green DR, Lin T (2001) p53-dependent radiation-induced

  crypt intestinal epithelial cells apoptosis is mediated in part through TNF-TNFR1

  system. Oncogene 20:812-818.

Indran M, Carr KE, Gilmore RS, Boyle FC (1991) Mucosal changes in mouse duodenum

  after gamma-irradiation or reserpine treatment. J Submicrosc Cytol Pathol

  23:267-278.

Ingenuity Systems I (2013) IPA. Redwood City, CA: Ingenuity Systems, Inc.

Ito M, Shibamoto Y, Ayakawa S, Tomita N, Sugie C, Ogino H (2007) Low-dose whole-

  body irradiation induced radioadaptive response in C57BL/6 mice. J Radiat Res

  (Tokyo) 48:455-460.

Jee YH, Jeong WI, Kim TH, Hwang IS, Ahn MJ, Joo HG, Hong SH, Jeong KS (2005)

  p53 and cell-cycle-regulated protein expression in small intestinal cells after fast-

  neutron irradiation in mice. Mol Cell Biochem 270:21-28.

Jeggo PA (2009) Risks from low dose/dose rate radiation: what an understanding of

  DNA damage response mechanisms can tell us. Health Phys 97:416-425.

Jia D, Koonce NA, Griffin RJ, Jackson C, Corry PM (2010) Prevention and mitigation of acute death of mice after abdominal irradiation by the antioxidant N-acetyl-cysteine (NAC). Radiat Res 173:579-589.

Kamel HM, Hume SP, Carr KE, Marigold JC, Michalowski A (1988) Development of villous damage in mouse small intestine after local hyperthermia or irradiation. J Submicrosc Cytol Pathol 20:185-193.

Karatzas T, Scopa S, Tsoni I, Panagopoulos K, Spiliopoulou I, Moschos S, Vagianos K, Kalfarentzos F (1991) Effect of glutamine on intestinal mucosal integrity and bacterial translocation after abdominal radiation. Clin Nutr 10:199-205.

Kerr JF, Wyllie AH, Currie AR (1972) Apoptosis: a basic biological phenomenon with wide-ranging implications in tissue kinetics. Br J Cancer 26:239-257.

Kim JS, Ryoo SB, Heo K, Kim JG, Son TG, Moon C, Yang K (2012) Attenuating effects of granulocyte-colony stimulating factor (G-CSF) in radiation induced intestinal injury in mice. Food Chem Toxicol 50:3174-3180.

Komarova EA, Christov K, Faerman AI, Gudkov AV (2000) Different impact of p53 and p21 on the radiation response of mouse tissues. Oncogene 19:3791-3798.

Konsoula Z, Velena A, Lee R, Dritschilo A, Jung M (2011) Histone deacetylase inhibitor: antineoplastic agent and radiation modulator. Adv Exp Med Biol 720:171-179.

Langell J, Jennings R, Clark J, Ward JJ (2008a) Pharmacological agents for the prevention and treatment of toxic radiation exposure in spaceflight. Aviat Space Environ Med 79:651-660.

Langell J, Jennings R, Clark J, Ward JB (2008b) Pharmacological agents for the

    prevention and treatment of toxic radiation exposure in spaceflight. Aviat Space

    Environ Med 79:651-660.

Leibowitz BJ, Qiu W, Liu H, Cheng T, Zhang L, Yu J (2011) Uncoupling p53 functions

    in radiation-induced intestinal damage via PUMA and p21. Mol Cancer Res

    9:616-625.

MacVittie TJ, Farese AM, Bennett A, Gelfond D, Shea-Donohue T, Tudor G, Booth C,

    McFarland E, Jackson W (2012) The acute gastrointestinal subsyndrome of the

    acute radiation syndrome: a rhesus macaque model. Health Phys 103:411-426.

Mahaney BL, Meek K, Lees-Miller SP (2009) Repair of ionizing radiation-induced DNA

    double-strand breaks by non-homologous end-joining. Biochem J 417:639-650.

Martin SA, Lord CJ, Ashworth A (2010) Therapeutic targeting of the DNA mismatch

    repair pathway. Clin Cancer Res 16:5107-5113.

Mason KA, Gillin MT, Mohan R, Cox JD (2007) Preclinical biologic assessment of

    proton beam relative biologic effectiveness at Proton Therapy Center Houston. Int

    J Radiat Oncol Biol Phys 68:968-970.

Merchant TE (2009) Proton beam therapy in pediatric oncology. Cancer J 15:298-305.

Merritt AJ, Allen TD, Potten CS, Hickman JA (1997) Apoptosis in small intestinal

    epithelial from p53-null mice: evidence for a delayed, p53-independent G2/M-

    associated cell death after gamma-irradiation. Oncogene 14:2759-2766.

Merritt AJ, Potten CS, Kemp CJ, Hickman JA, Balmain A, Lane DP, Hall PA (1994) The

    role of p53 in spontaneous and radiation-induced apoptosis in the gastrointestinal

    tract of normal and p53-deficient mice. Cancer Res 54:614-617.

Meyn RE, Milas L, Ang KK (2009) The role of apoptosis in radiation oncology. Int J
Radiat Biol 85:107-115.

Miyoshi-Imamura T, Kakinuma S, Kaminishi M, Okamoto M, Takabatake T, Nishimura
Y, Imaoka T, Nishimura M, Murakami-Murofushi K, Shimada Y (2010) Unique
characteristics of radiation-induced apoptosis in the postnatally developing small
intestine and colon of mice. Radiat Res 173:310-318.

Morris GM (1996) Review article: effects of radiation on the cell proliferation kinetics of
epithelial tissues--therapeutic implications. Br J Radiol 69:795-803.

Nishioka T, Miyai Y, Haga H, Kawabata K, Shirato H, Homma A, Shibata K, Yasuda M
(2009) Novel function of transcription factor ATF5: blockade of p53-dependent
apoptosis induced by ionizing irradiation. Cell Struct Funct 34:17-22.

Oh H, Seong J, Kim W, Park S, Koom WS, Cho NH, Song M (2010) Recombinant
human epidermal growth factor (rhEGF) protects radiation-induced intestine
injury in murine system. J Radiat Res 51:535-541.

Paoluzzi L, Figg WD (2004) Histone deacetylase inhibitors are potent radiation
protectants. Cancer Biol Ther 3:612-613.

Persengiev SP, Devireddy LR, Green MR (2002) Inhibition of apoptosis by ATFx: a
novel role for a member of the ATF/CREB family of mammalian bZIP
transcription factors. Genes Dev 16:1806-1814.

Ponnaiya B, Cornforth MN, Ullrich RL (1997) Radiation-induced chromosomal
instability in BALB/c and C57BL/6 mice: the difference is as clear as black and
white. Radiat Res 147:121-125.

Potten C (2002) Apoptosis induced in small intestinal crypts. International Congress Series/Excerpta Medica 1236:407-413.

Potten CS (1977) Extreme sensitivity of some intestinal crypt cells to X and gamma irradiation. Nature 269:518-521.

Potten CS (1991) Regeneration in epithelial proliferative units as exemplified by small intestinal crypts. Ciba Found Symp 160:54-71; discussion 71-56.

Potten CS (2004) Radiation, the ideal cytotoxic agent for studying the cell biology of tissues such as the small intestine. Radiat Res 161:123-136.

Potten CS, Booth C (1997) The role of radiation-induced and spontaneous apoptosis in the homeostasis of the gastrointestinal epithelium: a brief review. Comp Biochem Physiol B Biochem Mol Biol 118:473-478.

Potten CS, Merritt A, Hickman J, Hall P, Faranda A (1994) Characterization of radiation-induced apoptosis in the small intestine and its biological implications. Int J Radiat Biol 65:71-78.

Ramachandran A, Madesh M, Balasubramanian KA (2000) Apoptosis in the intestinal epithelium: its relevance in normal and pathophysiological conditions. J Gastroenterol Hepatol 15:109-120.

Rao KR, Fritz-Niggli H (1988) Alterations in the length of jejunal villi in mice irradiated with graded doses of X rays. Br J Radiol 61:839-842.

Robert C, Rassool FV (2012) HDAC inhibitors: roles of DNA damage and repair. Adv Cancer Res 116:87-129.

Roderick TH (1963) The Response of Twenty-Seven Inbred Strains of Mice to Daily Doses of Whole-Body X-Irradiation. Radiat Res 20:631-639.

Rodgers BE, Chesser RK, Wickliffe JK, Phillips CJ, Baker RJ (2001) Subchronic
exposure of BALB/c and C57BL/6 strains of Mus musculus to the radioactive
environment of the Chornobyl, Ukraine exclusion zone. Environ Toxicol Chem
20:2830-2835.

Roig AI, Hight SK, Shay JW (2009) Two- and three-dimensional models for risk
assessment of radiation-enhanced colorectal tumorigenesis. Radiat Res 171:33-40.

Sarna SK, Otterson MF (1989) Small intestinal physiology and pathophysiology.
Gastroenterol Clin North Am 18:375-404.

Schuller BW, Binns PJ, Riley KJ, Ma L, Hawthorne MF, Coderre JA (2006) Selective
irradiation of the vascular endothelium has no effect on the survival of murine
intestinal crypt stem cells. Proc Natl Acad Sci U S A 103:3787-3792.

Schulz-Ertner D (2009) The clinical experience with particle therapy in adults. Cancer J
15:306-311.

Shabason JE, Tofilon PJ, Camphausen K (2011) Grand rounds at the National Institutes
of Health: HDAC inhibitors as radiation modifiers, from bench to clinic. J Cell
Mol Med 15:2735-2744.

Shadad AK, Sullivan FJ, Martin JD, Egan LJ (2013) Gastrointestinal radiation injury:
symptoms, risk factors and mechanisms. World J Gastroenterol 19:185-198.

Somosy Z, Horváth G, Telbisz A, Réz G, Pálfia Z (2002) Morphological aspects of
ionizing radiation response of small intestine. Micron 33:167-178.

Sorokina S, Markova E, Gursky J, Dobrovodsky J, Belyaev I (2013) Relative biological
efficiency of protons at low and therapeutic doses in induction of 53BP1/γH2AX
foci in lymphocytes from umbilical cord blood. Int J Radiat Biol 89: 716-723.

Stypula-Cyrus Y, Damania D, Kunte DP, Cruz MD, Subramanian H, Roy HK, Backman V (2013) HDAC Up-Regulation in Early Colon Field Carcinogenesis Is Involved in Cell Tumorigenicity through Regulation of Chromatin Structure. PLoS One 8:e64600.

Tariq MA, Soedipe A, Ramesh G, Wu H, Zhang Y, Shishodia S, Gridley DS, Pourmand N, Jejelowo O (2011) The effect of acute dose charge particle radiation on expression of DNA repair genes in mice. Mol Cell Biochem 349:213-218.

Terasawa T, Dvorak T, Ip S, Raman G, Lau J, Trikalinos TA (2009) Systematic review: charged-particle radiation therapy for cancer. Ann Intern Med 151:556-565.

Tomasini R, Seux M, Nowak J, Bontemps C, Carrier A, Dagorn JC, Pébusque MJ, Iovanna JL, Dusetti NJ (2005) TP53INP1 is a novel p73 target gene that induces cell cycle arrest and cell death by modulating p73 transcriptional activity. Oncogene 24:8093-8104.

Townsend LW (2005) Implications of the space radiation environment for human exploration in deep space. Radiat Prot Dosimetry 115:44-50.

United States Cancer Statistics Working Group (2013) *United States Cancer Statistics: 1999–2009 Incidence and Mortality Web-based Report*. Atlanta, GA: United States Department of Health and Human Services, Centers for Disease Control and Prevention and National Cancer Institute.

Vereecke L, Beyaert R, van Loo G (2011) Enterocyte death and intestinal barrier maintenance in homeostasis and disease. Trends Mol Med 17:584-593.

Wang CY, Mayo MW, Baldwin AS (1996) TNF- and cancer therapy-induced apoptosis: potentiation by inhibition of NF-kappaB. Science 274:784-787.

Wang Y, Meng A, Lang H, Brown SA, Konopa JL, Kindy MS, Schmiedt RA, Thompson JS, Zhou D (2004) Activation of nuclear factor kappaB In vivo selectively protects the murine small intestine against ionizing radiation-induced damage. Cancer Res 64:6240-6246.

Weber U, Kraft G (2009) Comparison of carbon ions versus protons. Cancer J 15:325-332.

Wilson JM, Sanzari JK, Diffenderfer ES, Yee SS, Seykora JT, Maks C, Ware JH, Litt HI, Reetz JA, McDonough J, Weissman D, Kennedy AR, Cengel KA (2011) Acute biological effects of simulating the whole-body radiation dose distribution from a solar particle event using a porcine model. Radiat Res 176:649-659.

Wilson JW, Pritchard DM, Hickman JA, Potten CS (1998) Radiation-induced p53 and p21WAF-1/CIP1 expression in the murine intestinal epithelium: apoptosis and cell cycle arrest. Am J Pathol 153:899-909.

Withers HR, Elkind MM (1970) Microcolony survival assay for cells of mouse intestinal mucosa exposed to radiation. Int J Radiat Biol Relat Stud Phys Chem Med 17:261-267.

Wolff S (1998) The adaptive response in radiobiology: evolving insights and implications. Environ Health Perspect 106 Suppl 1:277-283.

Wyllie AH (1997) Apoptosis: an overview. Br Med Bull 53:451-465.

Zhang Y, Rohde L, Emami K, Hammond D, Casey R, Mehta S, Jeevarajan A, Pierson D, Wu H (2008) Suppressed expression of non-DSB repair genes inhibits gamma-radiation-induced cytogenetic repair and cell cycle arrest. DNA Repair (Amst) 7:1835-1845.

Zhou T, Chou J, Simpson D, Zhou Y, Mullen T, Medeiros M, Bushel P, Paules R, Yang X, Hurban P, Lobenhofer E, Kaufmann W (2006) Profiles of global gene expression in ionizing-radiation-damaged human diploid fibroblasts reveal synchronization behind the G1 checkpoint in a G0-like state of quiescence. Environ Health Perspect 114:553-559.

VITA

Ashley Michele Purgason was born in Arlington, Texas on July 8, 1984 to Dr. Thomas and Michele Purgason. She attended Mansfield High School and graduated Summa Cum Laude in 2002. After attending New York University for one year, Ashley finished her Bachelor and Master of Science, both in Biology in 2006 and 2007, respectively, at The University of Texas at Arlington (UTA) where she was a National Collegiate Athletic Association athlete on the Women's Basketball team. Ashley performed research during her time as a Master's student in the field of evolutionary phylogenetics. After being admitted to and enrolling in the Population Health Sciences-Environmental Toxicology doctoral program at The University of Texas Medical Branch (UTMB), Ashley also was fortunate to form a research collaboration working for Dr. Honglu Wu at the NASA Johnson Space Center. Her work in the Space Radiation Protection Element and Core Laboratories focused on the effects of charged particles of varying doses on the gastrointestinal tracts of varying mouse strains. Ashley was named a National Institute of Environmental Health Sciences Toxicology Scholar during her time at UTMB and was a teacher in a Toxicology course taught at Texas A&M University-Galveston for four years. She also attended the prestigious Space Radiation Summer School at the NASA Space Radiation Laboratory at Brookhaven National Laboratory in Upton, New York and was appointed as a visiting scientist at The University of Texas Health Science Center at Houston. Ashley also spent time volunteering as the Student Government President at UTMB and was appointed by the Texas Governor to be The University of Texas System Student Regent for one year in 2012-2013. She continues to be interested in space radiation and toxicology research as well as undergraduate research initiatives. Ashley will begin a job as an Assistant Dean for Undergraduate Research and Student Advancement and Assistant Professor of Practice within the College of Science at UTA in the Fall of 2013.

Ashley can be contacted at 2007 Misty Creek Drive, Arlington, Texas 76017.

Education

B.S., May 2006, The University of Texas at Arlington, Arlington, TX
M.S., December 2007, The University of Texas at Arlington, Arlington, TX

Publications

Articles Submitted to Peer-Reviewed Journals:

Purgason, A., Zhang, Y., Hamilton, S., Gridley, D., Sodipe, A., Jejelowo, O., Ramesh, G., and Wu, H. Molecular and Histopathological Changes in Mouse Intestinal Tissue after Proton Exposure. *Advances in Space Research*.

Abstracts:

Purgason, A., Zhang, Y., Hamilton, S., and Wu, H. Proton Exposure Causes Morphometric and Epigenetic Alterations in C57BL/6 Intestine and Colon. Presented at the Radiation Research Society Annual Meeting in Warsaw, Poland.

Purgason, A., Zhang, Y., Hamilton, S., and Wu, H. Molecular and Histopathological Changes in Mouse Intestinal Tissue Following Whole Body Proton- or Gamma-Irradiation. Presented at the 22nd Annual Space Radiation Investigators' Workshop in Houston, Texas (Third Place in Student Competition).

Xu, Y., Ruiz, J., **Purgason, A.**, and Boor, P.J. A Dissecting Aortic Aneurysm Model Induced by N-(2-Aminoethyl) Ethanolamine in Rat. Presented at 15th Annual Pathology Research Day (Winner of Edward S. Reynolds Award).